Fall 2022

Uncovering the Diverse Roles of the Human CST (CTC1-STN1-TEN1) Complex in Resolving Genomic Stress

Percy Logan Schuck

UNCOVERING THE DIVERSE ROLES OF THE HUMAN CST (CTC1-STN1-TEN1) COMPLEX IN RESOLVING GENOMIC STRESS

by

Percy Logan Schuck

Bachelor of Science
Virginia Polytechnic Institute and State University, 2014

Submitted in Partial Fulfillment of the Requirements

For the Degree of Doctor in Philosophy in

Biological Sciences

College of Arts and Sciences

University of South Carolina

2022

Accepted by:

Jason Stewart, Major Professor

Alan Waldman, Committee Member

Lydia Matesic, Committee Member

Maria Majorette Pena, Committee Member

Michael Stutman, Committee Member

Cheryl L. Addy, Interim Vice Provost and Dean of the Graduate School

DEDICATION

This work is dedicated to my family and friends. Thanks for all your help and moral support on this long journey.

ACKNOWLEDGEMENTS

I would like to first thank my advisor, Dr. Jason Stewart first for all the patience, support and mentoring he has provided over the years. Your guidance was monumental to getting me to this point. Your tenacity and drive have honestly been inspiring and the way to lead by example.

Many thanks to my committee members, Dr. Waldman, Dr. Matesic, Dr. Pena and Dr. Shtutman for your advice and feedback as well as patience. I have appreciated your varied opinions and different ways of looking at my projects that helped me to get through stalls and pushing me to do more.

Thanks to Dr. Ackerson, I mean Steph, for putting up with another stressed out graduate student when you yourself were going through it. You will always be the lab's "Flow Queen". We each had our skills and have helped each other with our weaknesses.

Much thanks to the post docs Dr. Yilin Wang and Dr. Ali Naqi for optimizing techniques for the lab and sharing your knowledge from creating new cell lines to purifying proteins.

Thanks to every undergraduate that worked in the lab and helped tremendously by being and extra set of hands and making sure lab conversations were always lively. Special thanks to those I mentored, Maggie, Ross, Anna. Also Carlan though I know you were a post-bac.

Thanks to my family and friends for helping me deal with graduate school these past 6 years. Dr. Nik Dopkins for being my roommate and going through it with me. Duncan, Christy and Dorian for being there all the time.

Finally thank you to everyone at U of SC who helped over the years! Kristen and Drew Hogan, Olivia Spead, Sam Burnett, Niti Jani, Andy Schumpert, , Jake Massey, Lindsay Sanchez, Jake Swanson, Liza Joudeh, Nicole Reilly, Katie Monts, Grace Hollenbeck, Trevor Olsen, Irene Dalla Costa, Erin Anderson, Katelyn Rygel, Claire Hann, Chad Simmons, Tancia Bradshaw, Marj Peña, Fabienne Poulain, Deanna Smith, Shannon Davis, Amanda Zeigler, Chang-uk Lim, Garrett Faulk, Mike Wyatt, Doug Pittman, Alissa Armstrong, Chang-uk Lim, Carolyn Banister, Phil Buckhaults, and Elizabeth Thames, thank you for being a wonderful part of my graduate school experience. You all have been wonderful friends and colleagues.

ABSTRACT

The CST (CTC1-STN1-TEN1) complex is a heterotrimeric single-stranded DNA binding protein known to stimulate polymerase α-primase (Pol α) and promote telomere length regulation, genome-wide DNA replication and double strand break repair. However, much of its cellular function remains unknown. The focus of my dissertation work was to uncover novel roles of CST in DNA stress response pathways. In particular, my work relates to understanding the function of CST in sister chromatid cohesion (SCC) and base excision repair (BER) as well as characterizing CST protein interactions. SCC is established following DNA replication by loading of the cohesion complex, which encircles replicated chromatids to keep them joined until mitosis. Previous work suggested that, when replication forks stall, cohesin must be removed and re-established to prevent SCC loss. However, how this occurs is not well understood. Our findings indicate that CST interacts with the cohesion complex and helps to maintain/remodel cohesin at stalled replication forks. In addition to its role in DNA replication, CST stimulates DNA repair, particularly double strand break repair. Whether CST also participates in other repair pathways was unknown. Intriguingly, we found that CST interacts with and stimulates multiple proteins in the BER pathway, including DNA polymerase β, APE1, FEN1 and DNA ligase I. Furthermore, we demonstrated that loss of CST leads to increased oxidative damage. This work is the first to identify CST as a novel player in BER and oxidative DNA repair. Finally, we validated previously shown CST interactions in situ using the proximity ligation assay (PLA), confirming that CST

interacts with Pol α, the replication helicase MCM2-7, and the telomere protection protein POT1. Combined, these findings reveal the ability of CST to serve as a multifunctional protein designed to preserve genomic integrity

TABLE OF CONTENTS

LIST OF FIGURES

LIST OF ABBREVIATIONS

8-oxo-G 8-Oxoguanine

Ac ..... Acetylated

AND1 ..... Acidic Nucleoplasmic DNA-Binding Protein

AP ..... Apurinic/Apyrimidinic

APE1 ..... Apurinic/Apyrimidinic (AP) Endonuclease 1

APH ..... Aphidicolin

ATP ..... Adenosine 5′-Triphosphate

ATR ..... Ataxia Telangiectasia and Rad3-related Protein

BER ..... Base Excision Repair

Cas9 ..... CRISPR Associated Protein 9

CHK1 ..... Checkpoint Kinase 1

c-NHEJ ..... Classical Non-homologous End Joining

Co-IP ..... Co-Immunoprecipitation

CpG ..... 5'-C-Phosphate-G-3'

CPT ..... Camptothecin

CST CTC1-STN1-TEN1

CTC1 ..... Conserved Telomere Capping Protein 1

Ctf4 ..... Chromosome Transmission Fidelity 4

DAPI ..... 4’,6-diamino-2-phenylindole

dNTP ..... Deoxynucleoside triphosphate

Dox.....Doxycycline

dRP..... 5'-deoxyribose Phosphate

DSBs .....Double Strand Breaks

dsDNA .....Double Stranded DNA

DTT.....Dithiothreitol

EdU ..... 5-Ethynyl-2'-deoxyuridine

ESCO1/2 .....Establishment Of Sister Chromatid Cohesion N-Acetyltransferase 1/2

FEN1 ..... Flap Endonuclease 1

FISH.....Fluorescent In Situ Hybridization

G1.....Gap 1 Phase

G4..... G-Quadruplex

GFP .....Green Fluorescent Protein

H2B ..... Histone 2B

H_2O_2 ..... Hydrogen Peroxide

HU..... Hydroxyurea

IF .....Immunofluorescence

KD.....Knockdown

KO.....Knockout

LIGI..... DNA Ligase 1

LP-BER.....Long Patch Base Excision Repair

MAD2 .....Mitotic Arrest Deficient 2

MCM2-7 ..... Minichromosome maintenance protein 2-7

OB..... Oligonucleotide/Oligosaccharide-Binding

OGG1..... 8-oxoguanine DNA Glycosylase 1

p53.....Tumor Protein P53

PARP1 ..... Poly [ADP-ribose] Polymerase 1

PBS ..... Phosphate-Buffered Saline

PBST ..... Phosphate-Buffered Saline with Tween

PLA ..... Proximity Ligation Assay

Pol α ..... Polymerase α (alpha)

Pol β ..... Polymerase β (beta)

Pol ε ..... Polymerase ε (epsilon)

Pol δ ..... Polymerase δ (sigma)

POLA1 ..... DNA Polymerase α (alpha) Catalytic Subunit

POT1 ..... Protection of Telomeres Protein 1

Pyr ..... Pyridostatin

RAP1 ..... Repressor/Activator Protein 1

RFP ..... Red Fluorescent Protein

ROS ..... Reactive Oxygen Species

RPA ..... Replication Protein A

SA1/2 ..... Stromal Antigen 1/2

SCC ..... Sister Chromatid Cohesion

SCC1 ..... Sister Chromatid Cohesion 1

sgRNA ..... Single Guide RNA

siRNA ..... Small Interfering RNA

shRNA ..... Short Hairpin RNA

SMC1A ..... Structural Maintenance of Chromosomes Protein 1A

SMC3 ..... Structural Maintenance of Chromosomes Protein 3

ssDNA ..... Single Stranded DNA

STN1 ..... Suppressor of Cdc Thirteen

TEN1 ..... Telomere Length Regulation Protein

TERC ..... Telomerase RNA Component

TERT ..... Telomerase Reverse Transcriptase

THF ..... Tetrahydrofuran

TIN2 ..... TERF1-Interacting Nuclear Factor 2

TPP1 ..... Tripeptidyl-Peptidase 1

TRF1/2 ..... TERF Telomeric Repeat Binding Factor 1/2

UT ..... Untreated

UV ..... Ultraviolet

WAPL ..... Wings Apart-like Protein Homolog

XRCC1 ..... X-ray Repair Cross-Complementing Protein 1

CHAPTER 1

INTRODUCTION

1.1 CST STRUCTURE AND FUNCTION

Human CST (CTC1-STN1-TEN1) is a heterotrimeric single-stranded DNA (ssDNA) binding protein complex that is conserved from yeast to humans. CST binds to ssDNA through multiple oligonucleotide/oligosaccharide-binding (OB)-folds, similar to the well-known DNA binding protein replication protein A (RPA) [1]. In total CST contains nine OB-folds, of which seven are found within the largest subunit, CTC1, while STN1 and TEN1 each contain a single OB-fold [2]. In contrast, RPA has a total of six OB-folds with four being on the largest RPA subunit, RPA70 [3] (Figure 1.1). CST has preference for G-rich ssDNA. It binds to short G-rich ssDNA sequences (18 nucleotides). While it is unable to bind to random or C-rich sequences of this length, this G-rich preference is lost as the length of ssDNA increases, likely due to the engagement of OB-folds that do not have preferences for G-rich DNA [4, 5]. For optimal binding, CST requires >36 nt ssDNA and binds with a K_d in the sub-nanomolar range. This G-rich preference differs from RPA, which has no nucleotide preference on long or short ssDNA substrates [6, 7]. As may be expected, CST is often found at G-rich regions of the genome, such as telomeres [1, 7, 8].

Telomeres are found at the end of chromosomes and are composed of highly repetitive G-rich sequences of DNA. In humans, telomeres range from 10-15 kb long and contain the repeat sequence 5'-TTAGGG-3' [9, 10]. Telomere ends usually end with a 50-300 bp G-overhang, which is used to create a telomeric-loop that protects the ends from recognition as double strand breaks [11, 12].

Telomeres are also bound by several protein complexes that protect and maintain telomeric DNA. In higher eukaryotes, the shelterin complex plays the primary function in

telomere end protection. Shelterin is composed of telomeric repeat-binding factor 1 and 2 (TRF1 and TRF2), TERF-interacting nuclear factor 2 (TIN2), repressor/activator protein 1 (RAP1), protection of telomeres protein 1 (POT1) and TPP1 (Figure 1.2). TPP1 is named after the first letter of each name given to it by the first three labs to characterize it, TINT1, PTOP and PIP1 [13]. TRF1 and TRF2 are both homodimers that bind telomeric dsDNA. The ends of telomeres are capped by a POT1-TPP1 heterodimer that binds the ssDNA G-overhang. TIN2 acts as a scaffold to connect POT-TPP1 with TRF1 and TRF2. RAP1 interacts with TRF2 [14]. Each shelterin subunit plays distinct functions in telomere end protection and maintenance [15]. In addition to shelterin, CST functions at telomeres to promote telomere replication, as discussed in more detail below. Telomeres are also transiently bound by various DNA replication and repair proteins that are used to regulate telomere replication and end protection [16].

Each replication cycle telomere ends shorten due to the end replication problem and once they become critically short senescence or apoptosis occurs [17, 18]. In order to combat replicative telomere shortening, a holoenzyme containing an RNA template extends the telomere through reverse transcription. This holoenzyme, named telomerase, is minimally composed of telomerase reverse transcriptase protein (TERT) and the telomerase RNA component (TERC). TERT is the enzyme responsible for adding telomeric sequence while TERC contains the RNA template used for reverse transcription [19]. In higher eukaryotes, telomerase is only expressed in germline and stem cells, restricting telomere extension in most somatic cells. Following telomere duplex replication, POT1 and TPP1 recruit telomerase and TPP1 stimulates the telomerase enzymatic activity [20-22]. Once telomerase has lengthened the telomere,

CST inhibits telomerase from over-extending the G-overhang by binding ssDNA and preventing telomerase re-association [23]. In a similar fashion, POT1 inhibits telomerase by binding to the G-overhang [24]. Following elongation of the G-overhang, the C-rich strand is filled in to convert most of the overhang to duplex DNA. CST aids in this process by stimulating polymerase α-primase (Pol α), leading to C-strand fill-in synthesis [1, 25-27].

In humans, telomere replication occurs throughout S-phase. The highly repetitive nature of telomeres can lead to stalls during replication of the duplex DNA that can devolve into breaks [28, 29]. Protective complexes, like shelterin, can also impede replication and require removal [30]. Once the most distal origin has fired the replisome must replicate the entire length of the telomere without another origin to rescue any stalled replication so fork collapse in this case can result in an un-replicated telomere end. Another barrier at the telomeres are G-quadraplexes (G4s) [7]. G4s are DNA secondary structures where G-rich ssDNA has folded in on itself and guanines form a series of G-quartets through non-traditional Hoogsteen base pairing that can block DNA polymerases, leading to replication fork stalling [6, 7, 31]. However, these also perform regulatory roles in transcription. G4s form in many gene promoter regions and function as transcriptional regulators [32, 33]. In yeast, G4s form a protective cap at the ends of telomeres and may play a similar role in humans [6, 7, 34]. Several helicases and ssDNA binding proteins can resolve G4s, including CST [7]. This ability, in addition to stimulating polymerase alpha-primase, makes CST well suited for C-strand fill in [35].

Outside telomeres, CST also plays several distinct roles in general DNA replication. For example, CST affects both origin licensing and dormant origin activation

[36-38]. Moreover, CST may promote DNA replication through the removal of G4s and loading of RAD51 at stalled replication forks to promote fork restart [7, 39, 40]. However, the role of CST during DNA replication is still not well understood. CTC1 has also been implicated as a regulator of the ATR-CHK1 DNA damage response pathway [41] and in protecting and repairing DSBs [42, 43].

The various roles CST plays in DNA replication and repair highlight its importance in preserving genomic integrity. When CST is absent there is an increase in the formation of anaphase bridges and micronuclei which can result from unresolved replication intermediates or telomere fusions can lead to DNA breaks and genomic rearrangements [3]. Knockdown or knockout of CST subunits results in both telomeric and non-telomeric replication defects, including telomere fragility, telomeric G-overhang elongation, increased anaphase bridges, micronuclei and defects in the licensing and firing of DNA replication origins [5, 36-38, 44].

Mutations in *CTC1* and *STN1* cause the genetic disorders Coats plus and dyskeratosis congenita, which manifest features such as premature aging, osteopenia, anemia, and brain calcifications. Both diseases usually result in premature death caused by gastrointestinal bleeding or bone marrow failure [45-50]. Stem cell depletion is thought to underlie the major symptoms of these CST related diseases. A common cause of stem cell depletion is telomere attrition, suggesting that stem cell loss following CST-dysfunction may be due to telomere loss. However, telomere attrition is not always observed in Coats plus patients, suggesting that non-telomere roles of CST may also play a role in disease progression [51]. CST-dependent genome stability may also contribute to the formation of cancer. Nucleotide polymorphisms in *STN1* have been correlated with

melanoma, lung cancer and ovarian cancer, while both *CTC1* and *STN1* polymorphisms have been correlated with chronic lymphocytic leukemia, osteosarcoma and neuroblastoma [52-57]. Low mRNA levels of *CTC1* or *STN1* are also linked to lower survival rates for individuals with breast, lung, and gastric cancers [58]. However, the mechanisms that lead to disease following CST dysfunction are still poorly understood.

1.2 DNA REPLICATION AND SISTER CHROMATID COHESION

Concurrent with DNA replication is the establishment of sister chromatid cohesion through the loading and acetylation of the cohesin complex. The cohesin complex is primarily composed of SMC3, SMC1 and SCC1. SMC3 and SMC1 are similar in that they both are primarily composed of a coiled coil domain, hinge domain and an ATPase head [59]. Cohesin creates a ring-like structure that can encircle the DNA to keep replicated chromatids together until mitosis. Cohesin is loaded onto the DNA in G1 prior to replication. This occurs concurrent with the loading of MCM2-7, the replicative helicase that is used to mark, or license, replication origins. During S-phase, cohesin must then be transferred from the unreplicated to replicated DNA. This process has been characterized in different organisms and appears to be well conserved, although several steps in the process are still not well understood.

During replication as the MCM2-7 helicase encounters DNA-bound cohesin, ESCO2, which travels with the replication machinery, acetylates the SMC3 subunit of cohesin. This allows sororin to interact with the cohesin complex and antagonize WAPL, leading to stably bound cohesin on the replicated sister chromatids [60, 61]. ESCO2 has been shown to bind MCM4 and MCM7, of MCM2-7, where it can acetylate cohesin as DNA synthesis occurs [60, 61]. Overall, the process of transferring cohesin onto the

replicated chromatids is known as cohesion establishment and leads to sister chromatid cohesion (SCC) (Figure 1.3).

The process of cohesin establishment is highly coordinated with DNA synthesis. During replication, the lagging strand is replicated discontinuously in small portions, called Okazaki fragments, which are protected by RPA prior to their replication [62]. The acetylation of cohesin by ESCO2 takes place after the replisome, near Okazaki fragments in budding yeast and most likely in humans as well [63]. Recent work in budding yeast suggests that cohesin is most likely loaded first onto dsDNA and then undergoes second strand capture of ssDNA on the lagging strand. This in-vitro work also showed that RPA impedes the ability of cohesion to embrace or capture the second ssDNA [64]. Following cohesion establishment during S-phase, cohesion is temporally regulated ensuring that cohesin is not removed until mitosis. Outside of SCC, cohesin is also loaded onto sister chromatids around DNA damage sites in response to DNA damage. However, in this case, it is acetylated by ESCO1 instead of ESCO2 [65].

During replication, the process of cohesion establishment and/or maintenance can be disrupted by replication stress that slows or stalls the replisome. Recent work suggests that replication fork stalling may require the removal and reloading or cohesin for replication fork protection and restart [66-68]. While it is known that replication stress contributes to cohesion loss, the way in which cohesion is maintained during replication stress is still unknown [66].

Once the cell reaches metaphase, cohesin must be removed to allow separation of the chromatids to the daughter cells. To facilitate this, sororin is phosphorylated along the chromosome arms allowing it to dissociate and cohesin can then be removed by WAPL.

At centromeres, cohesin is protected from removal by shugoshin until the metaphase-anaphase transition at which time the protease, seperase is released from securin. Seperase then cleaves SCC1 to release cohesin and allow separation of the chromatids [59]. At this point the sister chromatids move to their respective daughter cells. Defects in cohesin loading, establishment, maintenance or removal can have dire consequences on chromosome maintenance, with changes in cellular ploidy being the most common. Mutations in cohesion maintenance factors cause a class of diseases known as cohesionopathies and defects in SCC have been observed in many cancers.

1.3 BASE EXCISION REPAIR

DNA bases can become damaged due to a multitude of both endogenous and exogenous factors. A common form of DNA base damage comes in the form of free oxygen radicals that react with and damage DNA bases. Free oxygen radicals are created by radiation, such as UV and ionizing, and normal metabolic process [69, 70]. Oxidized bases are often highly mutagenic due to altered base pairing, which can create point mutations that lead to apoptosis or cancer formation. Due to its low redox potential compared to the other bases, the most common base affected by oxygen radicals is guanine, with the most common event being the formation of 8-oxo-guanines (8-oxo-G) [71-73]. If not repaired, 8-oxo-Gs can be converted to adenine, creating a potentially deleterious point mutation [74]. To repair 8-oxo-Gs and prevent these base substitutions, cells rely on the base excision repair (BER) pathway (Figure 1.4).

The BER pathway has evolved to recognize and remove many types of damaged bases as well as the removal of uracil that has been misincorporated into the DNA. To initiate the process, the damaged base is first identified by a DNA glycosylase that

recognizes and excises the damaged or mispaired base. There are several DNA glycosylases, with each being specialized to recognize a particular type of damage or misparing. In humans 8-oxoguanine DNA glycosylase 1 (OGG1) is used to recognize and remove 8-oxo-Gs [75]. Removal of the base leaves an abasic site, also called an apurinic/apyrimidinic (AP) site, where the phosphate backbone is intact but the base has been removed. The phosphate backbone at the AP site is then cut by an AP-endonuclease, the main one in humans being apurinic/apyrimidinic endonuclease 1 (APE1) [76]. This produces a 5′ deoxyribose-5-phosphate blocking group and a 3′ OH group [77]. Following APE1 cleavage, the repair process can proceed via the short or long-patch repair pathway. Pathway choice depends on when in the cell cycle BER is taking place, the type of lesion and even ATP levels [78-80].

Short patch BER is carried out by the multifunctional DNA polymerase β (Pol β) which uses its lyase activity to first remove the deoxyribo-5′-phosphate (dRP) created by the glycosylase before adding the correct nucleotide. Then DNA ligase III (LIG3) ligates the phosphodiester backbone to seal the DNA nick left by Pol β [80-82]. Additional factors aid in short patch repair, such as protein poly (ADPribose) polymerase 1 (PARP1) and X-ray repair cross-complementing protein 1 (XRCC1). PARP1 recruits XRCC1, which acts as a scaffold for other repair proteins in the process [83].

In long patch BER, the damaged base is displaced into a short DNA flap by a DNA polymerase and is then removed. In addition to using Pol β, long patch repair can be carried out by Pol δ [80]. Both polymerases have strand displacement activity and can efficiently polymerize a short tract of DNA. Following strand displacement, flap

endonuclease 1 (FEN1) cleaves the flap, and the newly replicated strand is then ligated by DNA ligase I (LIG1) [80].

Since guanines are highly suspectable to oxidation, G-rich regions of the genome show high levels of oxidative damage. Telomeres are particularly prone to oxidative damage due to their repetitive G-rich nature [84]. The shelterin components TRF1, TRF2 and POT1 stimulate BER. The strand displacement activity of Pol β is enhanced by TRF2, which suggest that long patch BER is preferred at telomeres [84-86]. Interestingly, the ability of TRF1 and TRF2 to bind telomeric DNA is disrupted by the presence of oxidative damage, suggesting that oxidative damage may disrupt telomere protection [87]. In line with this idea, studies have shown that oxidative stress accelerates telomere shortening [88].

Mutations in BER components are also thought to promote cancer. If BER is not initiated and the damaged base removed, then point mutations can accumulate, increasing the risk of developing cancer. Incomplete BER that results in AP-sites can also result in ssDNA breaks that can devolve into dsDNA breaks, further contributing to genome instability [89]. Polymorphisms in the BER components, such as the glycosylases, endonucleases, *XRCC1* and *Pol β*, promote cancer or lead to a worse prognosis [90]. Furthermore, the repair intermediates caused by the BER pathway are often more detrimental than the initial lesion, as an 8-oxo-G can lead to a base substitution but not lead to cell cycle arrest [90]. This makes BER proteins prime chemotherapeutic targets.

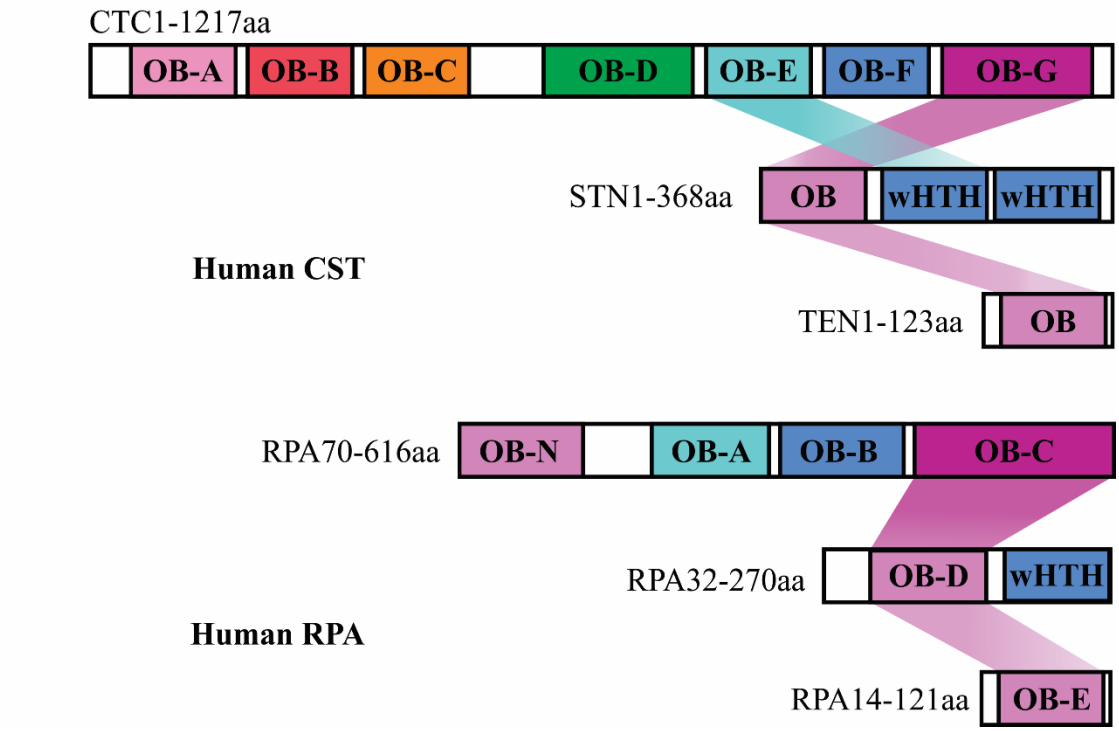

Figure 1.1 ***Comparison of human CST and RPA***. OB-folds and winged helix-turn-helix (wHTH) domains are based off published cryogenic electron microscopy, crystal structures, and structure predications [91]. Shaded areas between subunits denote interaction sites between CST or RPA subunits.

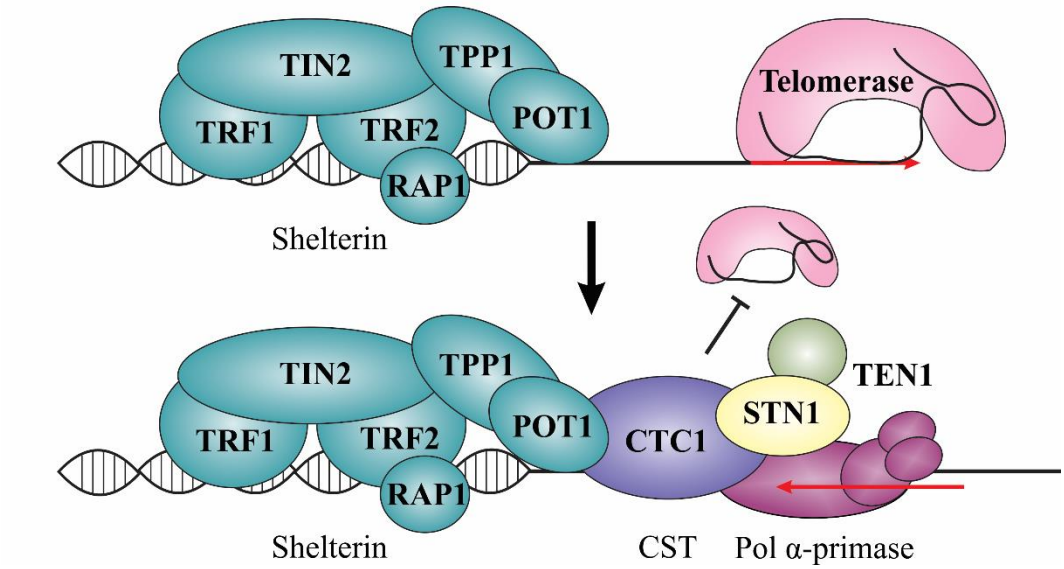

Figure 1.2 ***Telomere protein architecture, shelterin and CST.*** Structure of the shelterin complex at the telomere in blue. Telomerase in pink, extending the G-rich strand of the telomere. TPP1 recruits CST to the telomere to inhibit telomerase binding and to perform C-strand fill-in on the G-overhang by recruiting and stimulating Pol α.

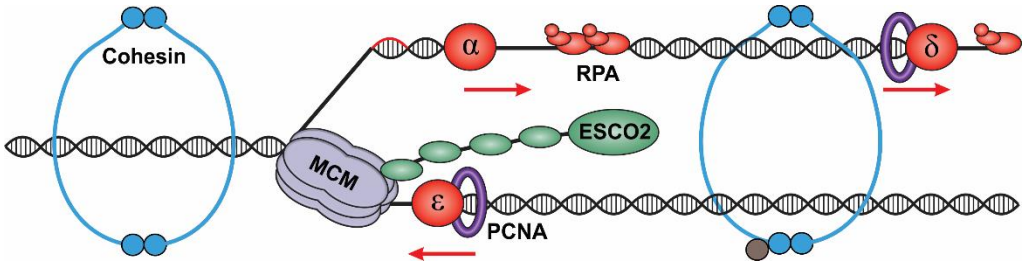

Figure 1.3 ***DNA replication fork and the replisome.*** The MCM2-7 helicase opens the dsDNA for replication by polymerases α, δ and ε (shown in red). PCNA (purple ring) keeps polymerase δ and ε associated with the DNA. During replication the cohesin ring (blue ring) encompasses the newly formed daughter DNA strands and becomes acetylated (grey circle) by ESCO2 (shown in green). RPA (red complexes) protects ssDNA until it is replicated.

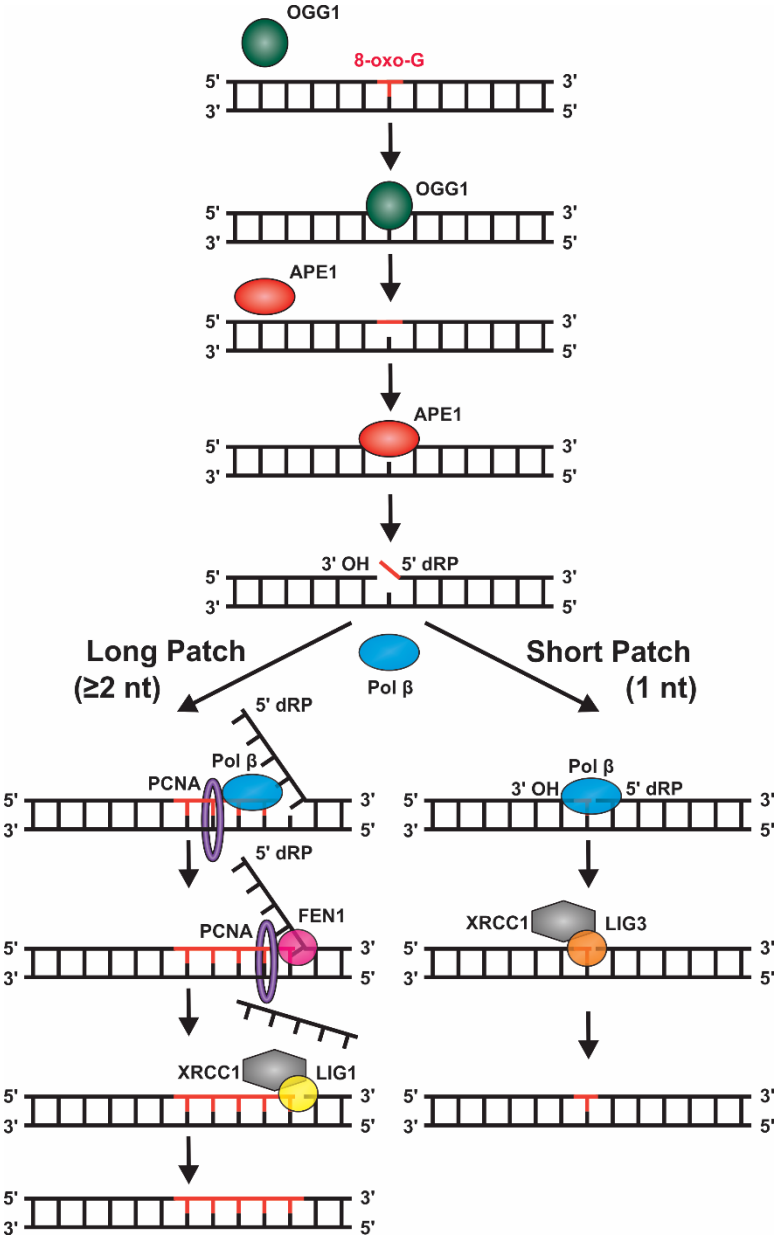

Figure 1.4 ***Base excision repair pathway***. The glycosylase OGG1(green circle) finds and excises 8-oxoguanine (red line) leaving the phosphate backbone intact. Upon identifying the absic site the apurinic/apyrimidinic endonuclease APE1 (red oval) cuts the phosphate backbone generating a nick with 3' hydroxyl and 5' dRP termini. Polymerase β (blue oval) can then begin long or short patch repair by either displacing the existing strand and synthesizing several nucleotides or inserting only the missing nucleotide. The processivity factor PCNA (purple ring) can aid Polymerase β in long patch repair. The endonuclease FEN1 (pink circle) then cleaves the displaced strand. The scaffolding protein XRCC1 (grey hexagon) along with ligase LIG1(yellow circle) or LIG3 (orange circle) ligates the phosphate backbone back together.

CHAPTER 2

ANALYSIS OF CST INTERACTIONS THROUGH PROXIMITY LIGATION ASSAY

2.1 INTRODUCTION

CTC1 and STN1 were originally discovered as interacting partners of Pol α and given the name alpha accessory factor (AAF) [25]. Interaction between CST and Pol α has been observed in multiple studies and is conserved from yeast to humans with CST stimulating Pol α enzymatic activity [26, 43, 92-94]. RPA plays a similar role in stimulating various proteins in DNA replication and repair [95-98]. More recent studies have uncovered additional CST interacting partners involved in DNA replication, DNA repair and cell cycle progression [39, 40, 99, 100]. This includes work showing that STN1 interacts with TPP1 and POT1, subunits of the shelterin complex and work from our lab showing that CST interacts components of the replisome, including with MCM2-7 and AND-1/Ctf4 [4, 36].

Many of the previous studies that analyzed CST interactions relied on co-immunoprecipitation (co-IP), which does not provide information about where the interaction takes place and how common it is in each cell. Additionally, CST is not very abundant so most studies utilized overexpression of epitope-tagged CST subunits to observe protein-protein interactions [1, 39]. Overexpression can potentially lead to interactions that may not occur under physiological conditions or not accurately predict the frequency of such interactions. To overcome these challenges, a technique was developed called the proximity ligation assay (PLA). This assay allows for the detection of two proteins in close proximity (< 40 nm) as a single foci [101]. Antibodies are used to target the proteins of interest, similar to traditional immunofluorescence, but instead of being conjugated to fluorophores the secondary antibodies are conjugated with a unique piece of ssDNA. If these proteins are in close proximity, then the DNA strands can

hybridize with a circular piece of DNA that is added after fixation and DNA amplified through rolling circle amplification. The generated DNA is then bound by fluorescent DNA probes at the site of interaction. This generates a detectable foci that can be observed by fluorescent microscopy.

Due to amplification of the signal, PLA can detect less abundant interactions that typically cannot be detected by traditional immunofluorescence. This can allow for the detection of endogenous protein-protein interactions and a greater understanding of what proteins are interacting under natural conditions (i.e., normal expression). This sensitivity theoretically allows detection of a single interaction.

Since CST is not highly abundant and most studies have used overexpression to characterize CST protein interacting partners, we used PLA to confirm that interaction of CST with key interacting partners and whether the well conserved interaction between CST and Pol α is affected by treatment with DNA replication inhibitors.

2.2 RESULTS

2.2.1 VALIDATION OF STN1 PLA FOCI IN STN1 KNOCKOUT CELLS

We wanted to validate our STN1 antibody in a conditional STN1 knockout (KO) cell line. This cell line was created by cloning a single guide RNA (sgRNA) to STN1 into the pLenti-sgRNA vector, which was then transduced into a previously created HeLa iCas9. This cell line has Cas9 under a doxycycline inducible promoter [102, 103]. Using this cell line (HeLa iCas9 sgSTN1), we determined whether STN1-Pol α PLA foci were dependent on STN1 expression. First, we confirmed KO of STN1 by Western blot (Figure 2.1). We then performed PLA following STN1 KO for STN1 and POLA1 (Figure 2.1). Compared to the control cell line, the number of PLA foci was reduced to near the

single antibody alone control for POLA1, indicating that the majority of PLA foci were dependent on STN1 expression.

Interestingly, the levels of extra nuclear foci were more abundant in the control (-Dox) than STN1 KO cells. It has previously been shown that Pol α shuttles CST into the nucleus and that CST nuclear localization is cell cycle regulated [93]. While we were unable to quantify these extra nuclear foci due to not having a marker of the cell membrane, a clear reduction in these foci was expected in the STN1 KO, suggesting that both nuclear and cytoplasmic foci are dependent on STN1 expression consistent with this previous study [93].

2.2.2 FORK STALLING DOES NOT INFLUENCE CST-POL α INTERACTION

Previous work indicates that CST promotes the rescue of stalled replication forks. Having confirmed the STN1 antibody by PLA, we next investigated whether their interaction was increased following replication stress. CST plays a role in DNA replication rescue by aiding in dormant origin firing, promoting replication through hard to replicate areas and recruiting RAD51. However, it is currently unknown whether these roles of CST require interaction between CST and Pol α.

Not all replication stalling events and the subsequent rescue are the same. DNA replication fork stalling can occur in numerous ways, such as nucleotide pool depletion, the inhibition of polymerase activity or barriers in front of the replisome that block the MCM2-7 helicase. In this study, we treated cells with different fork stalling agents that act in distinct ways to stall replication, including inhibition of the replicative DNA polymerases, the formation of protein-DNA crosslinks and the stabilization of DNA secondary structures, and then determined their effect on the interaction between STN1

and POLA1 through PLA. Below is a brief description of the mechanism by which these compounds lead to replication fork stalling.

The polymerase inhibitor aphidicolin (APH) stalls replication through the inhibition of the activity of the replicative DNA polymerases Pol α, Pol δ and Pol ϵ [104]. Interestingly, APH also blocks the firing of dormant replication origins, which are replication origins that are adjacent to the stall and can be fired to rescue the stall [105]. They are called "dormant" origins because they would not be fired, or activated, under normal conditions [106]. The replication inhibitor HU also leads to fork stalling but does so by inhibiting ribonucleotide reductase, which leads to the depletion of cellular nucleotide pools [107-109]. Both APH and HU cause replication stalling by stopping synthesis by the polymerases without creating a physical block. In fact, studies strongly suggest that the MCM2-7 helicase continues to unwind the DNA after the polymerase stalls, leading to an uncoupling of the replisome.

Like APH and HU, the polymerases can also be stalled by the presence of DNA secondary structures. This is particularly true in G-rich DNA, where the ssDNA can form G-quadruplexes (G4s). G4s are DNA secondary structures where G-rich ssDNA has folded in on itself and guanines form a series of G-quartets, a four stranded structure through non-traditional Hoogsteen base pairing [6, 7, 31]. These structures can form after unwinding by MCM2-7 and prior to DNA synthesis and perturb replisome dynamics, leading to fork stalling or slowing [110]. One way to increase G4 dependent fork stalling is the use of G4 stabilizers, such as pyridostatin and CX-5461 [111].

Unlike the compounds mentioned above, camptothecin (CPT), a topoisomerase inhibitor, creates a physical block in front of the replisome by crosslinking the

topoisomerase to the DNA. This inhibits the MCM2-7 helicase [112]. Topoisomerase I removes torsional stress in front of the replication fork by causing a single strand break allowing the broken strand to rotate around the intact DNA strand, thus removing the torsional stress. The DNA strands are then, re-ligated. When CPT is present it stabilizes the topoisomerase I cleavable complex with DNA, leaving a single strand break with topoisomerase I attached. This results in a stalling that can devolve into a double strand break [112, 113].

To test whether these compounds affected the interaction between CST and Pol α, cells were treated with each compound for the indicated time (see Methods), fixed and PLA performed as a readout of their interaction (Figure 2.2). While aphidicolin inhibits Pol α polymerase activity, it appears that aphidicolin does not greatly affect the interaction between STN1 and Pol α, leading to only a slight reduction in the frequency of the interaction (PLA foci per nucleus falls from 3.22 to 2.97) (Figure 2.2). Similarly, HU did not significantly affect the STN1-Pol α interaction leading only to a slight increase in PLA foci per nucleus (Figure 2.2).

Following treatment with CPT, the average number of PLA foci was 3.75 which is a bit higher than the 3.22 average for untreated cells. Interestingly, both pyridostatin and CX-5461 treatments led to a slight reduction in the number of PLA foci with 2.68 and 2.58 foci per nuclei respectively compared to the control of 3.22 (Figure 2.2). This reduction in interaction frequency between STN1 and Pol α could be caused by CST needing to aid in the resolution of stabilized G4s, which could require CST to disengage with Pol α. However, the decrease was minor and could also be caused by experimental variation. Overall, there were no large changes in the number of detected CST-Pol α

interactions with any treatment. This suggest that Pol α may be the main interaction partner of CST as CST is reliant on this interaction to enter the nucleus. Overall, these studies suggest that CST interaction with Pol α is not dependent on replication stress and that they are already in complex prior to their role in replication rescue.

2.2.3 CHARACTERIZING OTHERE KNOWN CST INITERACTION BY PLA

Our lab previously showed that STN1 interacts with MCM4 and MCM7 by co-IP and yeast two hybrid assays [36]. However, the interaction of endogenous CST and MCM had not been shown in human cells without the use of overexpression or interfering epitope tags. Therefore, we tested thee interaction between MCM7 and STN1 by PLA in HeLa cells. Consistent with previous work, we determined that endogenous MCM7 and STN1 interact in cells and that this interaction is mostly restricted to the nucleus (Figure 2.3).

Interaction between CST and POT1 was previously shown by co-IP and yeast-two-hybrid analysis [4, 114]. However, the co-IP experiments used a tagged version of the proteins and their interaction has not been verified in cells with antibodies to endogenous STN1 and POT1 [115-118]. Using PLA with antibodies to the endogenous proteins, we observed a significant increase in nuclear PLA foci, indicating an interaction between POT1 and STN1 (Figure 4.3). This interaction is quite weak or rare in comparison to other CST interactions observed by PLA. While various groups have shown that POT1 and CST both localize to the telomeres [115, 117, 119], these are the first experiments to confirm that POT1 and STN1 interact within cells.

2.3 DISCUSSION

In this chapter, we investigated CST interactions with various proteins and the dynamics of the STN1-Pol α interaction. We show that different forms of replication stress do not impact the STN1-Pol α interaction. In addition to Pol α, we demonstrated that endogenous STN1 interacts with MCM7 and the POT1 (Figure 2.2 and 2.3) [4, 36, 114]. This further confirms our earlier work showing that CST interacts with MCM2-7 [36]. While interaction between CST and POT1 has been shown, their co-localization *in vivo* has not, our work lends credence to the idea they interact within cells, most likely at the telomeres [120].

It has been shown that while overall levels of CST do not vary during the cell cycle their nuclear localization does, with the highest CST levels occurring during G1 and S-phase [93]. The cell cycle can have a profound influence on protein interactions by influencing the abundance of certain proteins as well as cell cycle-dependent modifications. We predict that CST interacts with the MCM2-7 complex in G1 and S-phase, due to its previously characterized roles in origin licensing and replication rescue. Furthermore, CST telomere localization is increased in late S/G2 phase so it is expected to interact with POT1 during this timeframe. Now that we have established that endogenous CST interacts with both MCM2-7 and POT1 through PLA, future experiments can be used to understand whether interactions between CST and MCM2-7 or POT1 are cell cycle regulated by using methods such as EdU incorporation and cell cycle synchronization combined with PLA.

In terms of CST-Pol α interaction, the recent discovery that Pol α is responsible for shuttling CST into the nucleus and that they function as a complex in double strand

break repair in G2 suggests that they remain complexed throughout the cell cycle either in the nucleus or cytoplasm [43, 93]. In order for CST to be transported to the nucleus it must stably interact with Pol α in the cytoplasm and thus they enter the nucleus as a complex. Our work suggest that they may remain in complex throughout the cell cycle. However, in our studies cells were asynchronous and no cell cycle markers were used to distinguish cell cycle phase, thus preventing the determination of when these interactions occur.

The replication inhibitors used in this study will have their greatest effect in S-phase but are still able to exhibit effects throughout the cell cycle. In HeLa cells, only approximately a third of the cells are in S-phase at a given time [121, 122]. More work is needed to elucidate whether CST-Pol α interaction is regulated in a cell cycle specific manner in response to replication stress. Moreover, the use of a dsDNA break causing agent could be used to assess whether interaction between CST- Pol α is more abundant in response to DSBs, where CST is known to require Pol α. Since CST and Pol α are complexed upon entering the nucleus, other CST interacting partners and/or post translational modifications of CST may dictate how CST is recruited to different DNA replication and repair scenarios within the nucleus. Overall, our data indicate that the interaction between CST and Pol α is quite robust consistent with previous results suggesting that Pol α is a predominant interaction partner of CST. Whether they remain in complex while CST interacts with other proteins, such as POT1 and MCM2-7 is still unclear and will require additional work, however, at DSBs, studies suggest that CST simultaneously interacts with both Pol α and the shieldin complex to counteract DNA resection.

2.4 EXPERIMENTAL PROCEDURES

2.4.1 CELL CULTURE

HeLa 1.2.11 cells were cultured in RPMI 1640 media and HeLa iCas9 in DMEM supplemented with 10% fetal bovine serum and 1% penicillin/streptomycin at 37 °C with 5% CO2. Cell lines were regularly checked for Mycoplasma contamination. HeLa iCas9 (inducible Cas9) cells were generously provided by Dr. Iain Cheeseman from Massachusetts Institute of Technology. STN1 inducible KO cell lines were constructed following the protocol outlined by McKinley [123], using the sgRNA (5' GGG GAC ACG ATC CGA GTC AGA 3') to STN1. The sgRNA was cloned into pLenti-sgRNA using the BsmB1 restriction site, lentivirus prepared and HeLa iCas9 cells transduced with the resultant virus. Clones were selected with puromycin and immunoblotting conducted to ensure successful KO. To induce the conditional gene KO of STN1, cells were incubated with 1 µg/ml Doxycycline to induce Cas9 expression for 3-4 days.

2.4.2 WHOLE-CELL LYSATE AND WESTERN BLOT ANALYSIS

These techniques were performed, as previously described [36].

2.4.3 ANTIBODIES AND CHEMICAL INHIBITORS

Primary antibodies: OBFC1 (STN1) (1:100 for PLA) (Novus Biologicals, NBP2-01006), α-actinin (Santa Cruz Biotechnology, SC17829), PolA1 (1:100 for PLA) (Bethyl Laboratories, A302-805A), MCM7 (1:500 for PLA) (Santa Cruz Biotechnology, sc22782) and POT1 (1:100 for PLA) (Abcam, ab124784).

Secondary antibodies: Thermo Fisher Scientific: anti-rabbit-HRP (32460), anti-mouse-HRP (32430), goat anti-rabbit Alexa Fluor 594 (A-11037).

Chemical inhibitors: Cells were treated with APH (1 μM, MilliporeSigma, 178273), HU (2 mM, MilliporeSigma, 400046), Pyridostatin (5 μM, Selleckchem, 1085412-37-8), CX-5461 (10 μM, Selleckchem, 1138549-36-6) or Hydrogen peroxide (200 μM) for 2 h or (S)-(+)-CPT (1 μM, MilliporeSigma, C9911) for 1 h.

2.4.4 PLA

HeLa 1.2.11 cells were fixed for 20 min at RT with 4% formaldehyde in 1× PBS followed by permeabilization with 100% methanol for 20 min at −20 °C. Subsequent steps were performed with the Duolink PLA kit (MilliporeSigma), as previously described [101], except the first wash after primary incubation was performed using wash buffer A, not 5% BSA in 1× PBS. The following primary antibodies were used: 1:100 mouse α-STN1, 1:100 rabbit α-PolA1, 1:500 rabbit α-MCM7 and 1:100 POT1.

2.4.5 IMAGE ANALYSIS AND STATISTICS

For PLA, images were taken on an EVOS FL microscope, using a 40× or 60× objective (Thermo Fisher Scientific). At minimum, ten images were scored per independent, biological experiment for each condition. Image analysis was performed with CellProfiler. All p-values were calculated by an unpaired, two-tailed t test.

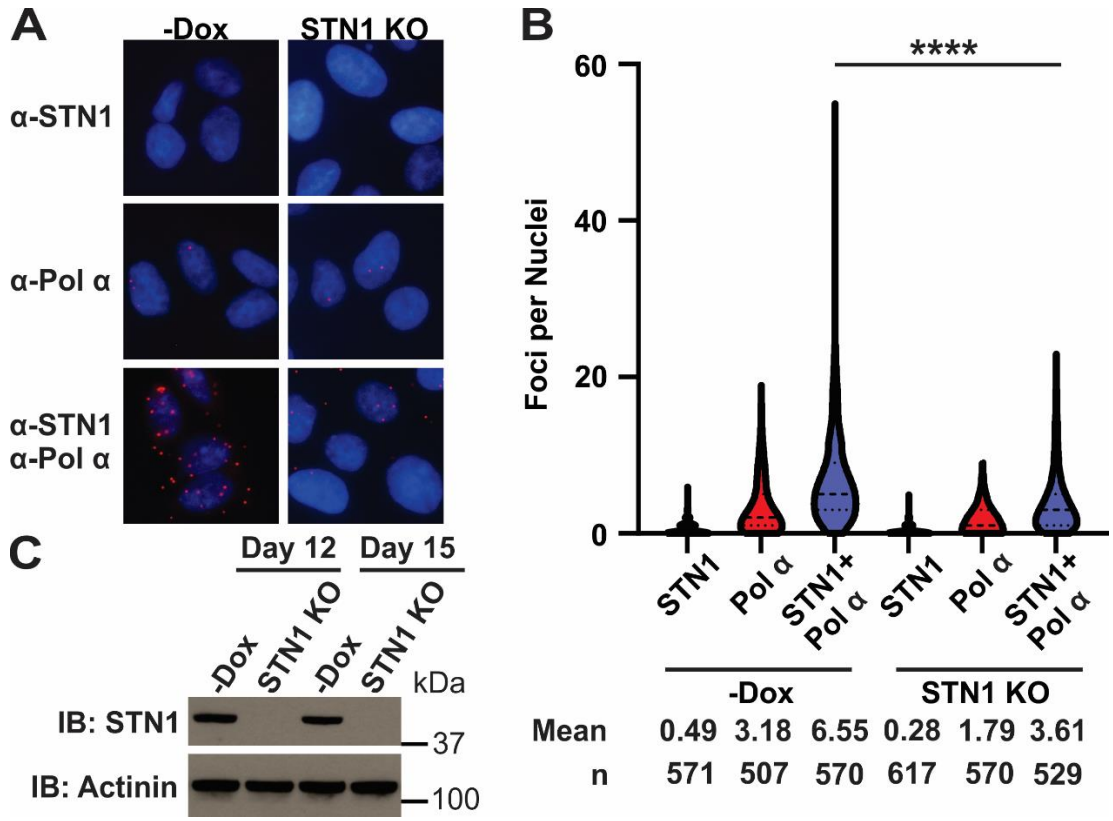

Figure 2.1 ***CST-Pol α interaction decreased in STN1 KO***. (A) Representative images of proximity ligation assay (PLA) performed in HeLa iCas9 sgSTN1 cells treated with or without doxycycline, with antibodies to STN1 or Pol α alone or in combination. Red represents PLA foci; blue represents DAPI. (B)Violin plot of PLA foci per nucleus. Results are representative of two independent, biological experiments. Bold dashed line represents the median, and dashed lines represent the first and third quartiles. (****p < 0.0001). (C)Western blot of STN1 knockout in HeLa iCas9 sgSTNT1 cells. Actinin was used as the loading control.

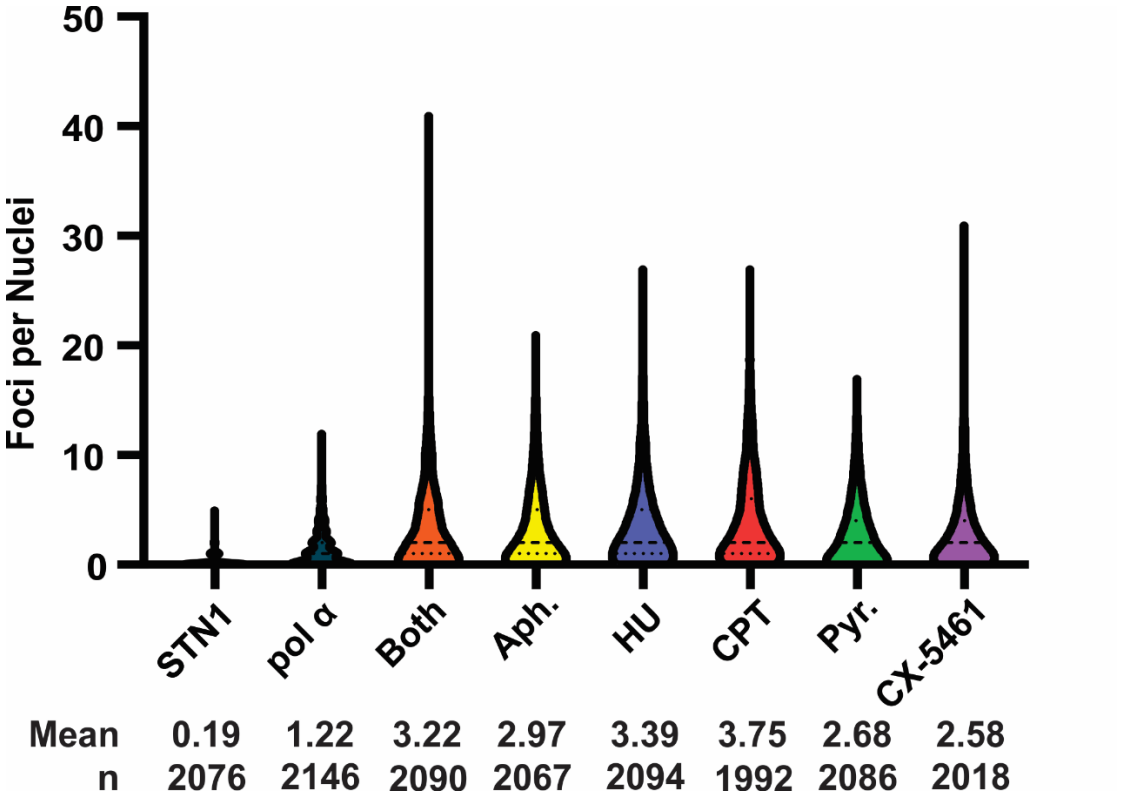

Figure 2.2 ***CST association with Pol α not affected by replication inhibitors***. Violin plot of nuclear PLA foci in HeLa cells after treatment with DNA replication inhibitors. Treatment: aphidicolin (APH), hydroxyurea (HU) pyridostatin (Pyr.) and CX-5461 for 2 h and camptothecin (CPT) for 1 h. The bold dashed line represents median and dashed lines the first and third quartiles. n = 5 independent, biological replicates.

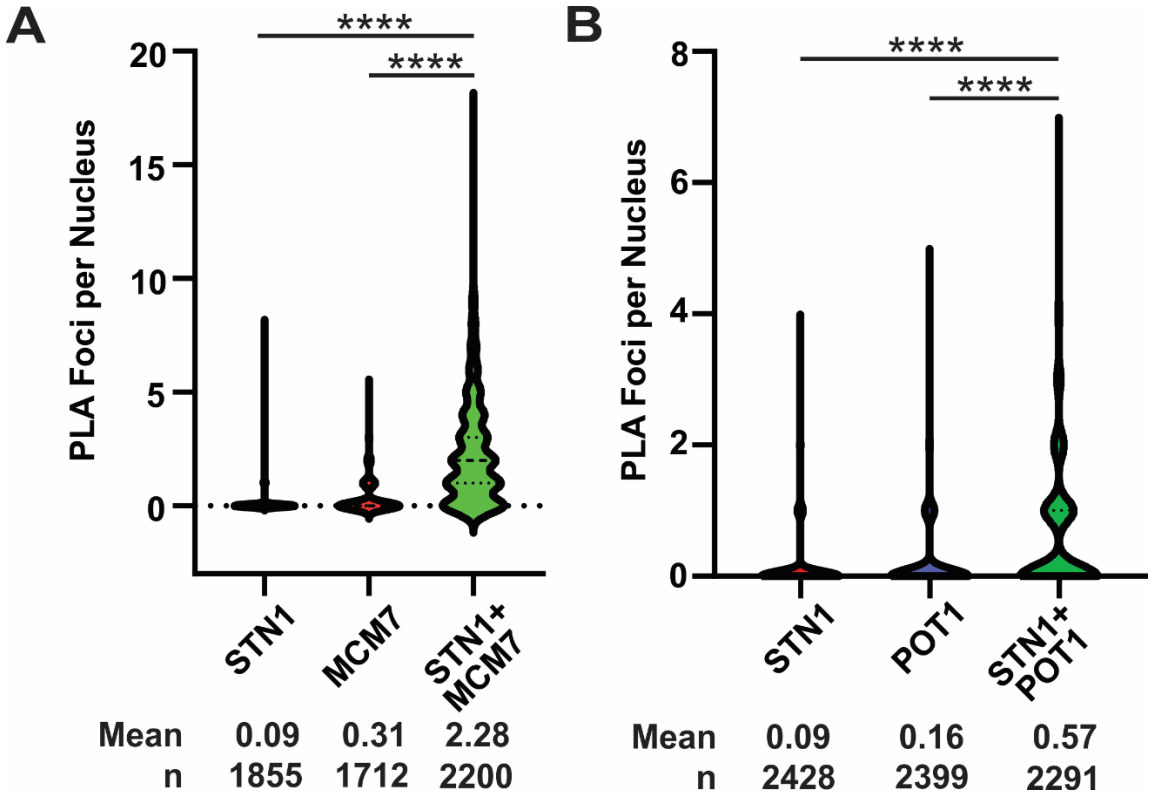

Figure 2.3 ***PLA demonstrating STN1 interaction MCM2-7 and POT1.*** (A) Proximity ligation assay (PLA) performed in HeLa cells with antibodies to STN1, MCM7 or in combination (STN1+ MCM7). (B) PLA was performed in HeLa cells as in (A) with antibodies to STN1 and POT1 (STN1+POT1). Violin plots of PLA foci per nucleus. Results for (A) and (B) are representative of two independent, biological experiments. Bold dashed line: median, dashed lines: first and third quartiles. (****P < 0.0001).

CHAPTER 3

HUMAN CST STIMULATES BASE EXCISION REPAIR TO PREVENT THE ACCUMULATION OF OXIDATIVE DNA DAMAGE

3.1 ABSTRACT

CTC1-STN1-TEN1 (CST) is an RPA-like single-stranded DNA binding protein vital for telomere length maintenance. CST also has additional genome-wide roles in regulating DNA replication and repair. While CST was previously shown to function in double-strand break repair and promote replication restart, it is currently unclear whether it also has specialized roles in other DNA repair pathways. Proper and efficient repair of DNA is critical to protecting genome integrity. Telomeres and other G-rich regions are strongly predisposed to oxidative DNA damage in the form of 8-oxoguanine. These oxidative lesions are repaired by the base-excision repair (BER) pathway. Previous work has implicated components of shelterin, the primary telomere protection complex, in mediating BER, suggesting accessory factors may be used at G-rich DNA to aid BER. CST interacts with and stimulates several DNA replication and repair factors and appears to facilitate the replication and repair of G-rich DNA. Therefore, we tested whether CST stimulated BER. Here, we show that CST robustly stimulates proteins involved in BER, including Pol β, APE1, and LIGI, on both telomeric and non-telomeric DNA substrates. Biochemical reconstitution indicates that CST stimulates BER. Moreover, the absence of STN1 leads to increased levels of 8-oxoguanine, suggesting defective BER in the absence of CST. Combined, our results define an undiscovered function of CST in BER, where it acts as a stimulatory factor to promote efficient repair.

3.2 INTRODUCTION

The generation of reactive oxygen species (ROS) is an unintended consequence of cellular metabolism, which triggers progressive oxidative damage to the genome and, ultimately cell death. Efficient repair of the damage generated by ROS is crucial to

prevent mutagenesis and maintain genome stability. Guanine bases are particularly prone to oxidative damage due to having a low redox potential. Therefore, G-rich regions, such as telomeres and CpG islands, are especially prone to oxidative damage in the form of 8-dihydro-2'-deoxyguanine (8-oxoG). 8-oxoG is the most common DNA lesion, and estimates are that 1.5 x 105 spontaneous 8-oxoGs are formed in the genome each day due to normal metabolic processes [124].

Exposure to harmful ultraviolet light, ionizing radiation, inflammation and environmental pollutants such as chemical carcinogens and tobacco smoke can significantly compound the volume of ROS and, thus, 8-oxoGs produced in the cell [125]. When 8-oxoGs are not repaired, they are highly mutagenic and can lead to the development of cancer and other aging disorders. Furthermore, high amounts of oxidative stress can accelerate the rate of telomere shortening, which can contribute to telomere biology disorders [88]. High amounts of oxidative damage at telomeres are also linked to the onset of diabetes and cancer [126, 127].

Consequently, it is imperative that oxidative lesions are correctly repaired. The most significant pathway used to repair single base lesions is base excision repair (BER) [128]. BER is initiated through the action of DNA glycosylases, which locate and remove oxidized, deaminated, or other inappropriate bases [129]. The resulting abasic site is then cleaved by AP endonuclease 1 (APE1) to form a single-strand nick that can then be repaired via DNA polymerase β (Pol β) through one of two pathways: short patch BER [SP-BER] (in which a single nucleotide gets replaced) [130-132] or long patch BER [LP-BER] (in which approximately 2-13 nucleotides are replaced) [132-135]. Typically, the LP-BER pathway is employed when the 5'-deoxyribose-5-phosphate (dRP) moiety in

itself is either oxidized or reduced, thereby inhibiting the lyase activity of Pol β. The polymerase then performs strand displacement synthesis to create a displaced flap which is cleaved by flap endonuclease (FEN1) to remove the modified dRP moiety.

While the basic mechanisms of BER have been characterized, whether additional accessory factors are required in response to different DNA structures/sequences and chromatin environments is still not well understood. Intriguingly, the shelterin complex, a six-membered protein complex essential for telomere protection, has been implicated in stimulating the BER pathway via several mechanisms including the stimulation of Pol β [85, 136]. In this study, we tested whether another telomere-associated complex, CTC1-STN1-TEN1 (CST), also stimulates BER.

CST is a single-stranded DNA (ssDNA) binding protein, which shares structural similarity to Replication Protein A (RPA) [2, 3, 12]. It primarily functions in the replication and maintenance of telomeres, where it coordinates telomere duplex replication and telomerase-dependent telomere elongation [12]. CST also functions in various aspects of DNA replication and repair, including origin licensing, the rescue of stalled replication, and double-strand break repair [3, 137, 138]. Mutations in CST are associated with the telomere biology disorders dyskeratosis congenita, Coats plus, and idiopathic pulmonary fibrosis as well as increased risk of various cancers [3]. However, the cellular functions of CST remain incompletely characterized.

Previous work demonstrated that CST primarily localizes to G-rich DNA, such as telomeres and CpG islands, and can resolve DNA secondary structures called G-quadruplexes (G4s) that form in G-rich DNA [6, 39]. Like RPA, CST localizes and/or stimulates specific protein factors to facilitate replication or repair. A well-known

function of CST across species is its ability to interact with and stimulate the activity of DNA polymerase α-primase (Pol α) [26, 27, 91, 92, 139-141]. Therefore, we postulated that CST may also interact and regulate the activity the BER polymerase Pol β.

Consistent with our hypothesis, we find that CST interacts with Pol β and stimulates its various activities in vitro. Furthermore, individual components and the entire CST complex interacts with other BER components and stimulates multiple steps in the repair process. Biochemical reconstitution of the long patch BER pathway demonstrated that CST greatly stimulates BER in vitro. In line with these findings, deletion of the CST subunit STN1 leads to increased genomic 8-oxo-Gs, indicating a defect in BER. Overall, our findings strongly support a role for CST in the repair of oxidative DNA damage through BER.

3.3 RESULTS

3.3.1 STN1 INTERACTS WITH POL β AND OTHER BER COMPONENTS

Pol β plays a crucial role in maintaining fidelity of the genome through its function in BER, where it synthesizes new bases to replace those that were damaged [128]. To test whether CST and Pol β interact in cells, we performed proximity ligation assay (PLA) [101]. Antibodies to endogenous STN1 and Pol β were first used in the absence of exogenous oxidative stress. In comparison to single antibody controls, we observed a significant increase in the number of PLA foci with antibodies to STN1 and Pol β (Figure 3.1). Next, we treated cells with H_2O_2 to determine whether oxidative stress increased the association between CST and Pol β. Treatment with H_2O_2 led to an approximate 2-fold increase in PLA foci, suggesting that their interaction is linked to oxidative stress and potentially BER (Figure 3.1 B).

Since the primary role of Pol β is in BER, we hypothesized that CST interacts with Pol β to promote BER. If correct, we would expect that CST interacts or associates with other BER components. Therefore, PLA was performed with antibodies to other factors with roles in BER, including PARP1 and XRCC1. Like Pol β, STN1 associated with PARP1 and XRCC1 (Figure 3.2). As a control, we also performed PLA for Pol β - XRCC1, which showed a strong interaction as expected. Together, these findings strongly suggest a potential function of CST in BER.

3.3.2 CST STIMULATE POL β ACTIVITY

Since STN1 and Pol β showed increased interaction in the presence of H_2O_2-induced damage and CST stimulates Pol β [27, 139, 140], we next purified and tested the ability of the individual components as well as the entire CST complex to modulate Pol β's enzymatic activities (Figure 3.3 and 3.4). We first confirmed that purified CST was active by observing DNA binding on a ssDNA oligonucleotide (Figure 3.3 B). The apparent KD was 1.5 nM similar to previously reported values of CST binding [4, 6]. Consistent with previous studies [1, 142, 143], individual subunits also showed weak to undetectable binding in comparison to the full CST complex (Figure 3.3 C).

To study the impact of CST on Pol β, we first used a substrate containing a tetrahydrofuran (THF) residue next to a gap. The THF mimics an abasic (apurinic or apyrimidinic) site and the gap resembles a BER intermediate that has already been processed by APE1 (where the phosphodiester backbone has been cleaved at the abasic site) [144]. Using this substrate, we tested the ability of Pol β to fill in the gap either in the presence of increasing concentrations of individual CST components or the full CST complex. We observed that CTC1 and STN1 and the entire complex stimulated the gap-

filling activity of Pol β (Figure 3.4 A). Additionally, we observed increased strand displacement synthesis by Pol β in the presence of CTC1, STN1, and the entire CST complex. Synthesis traces are shown in Figure 3.4 B.

Pol β has previously been shown to possess processive gap-filling activity on substrates with containing gaps up to six nucleotides [145, 146]. Since we observed a stimulation in Pol β synthesis on a single-nt gapped THF substrate we next utilized a 6-nt gapped substrate to analyze the impact of CST on Pol β's synthesis and strand displacement synthesis activity. Due to CST's function at both telomeres and genome-wide, DNA synthesis and strand displacement were monitored on both a random sequence (Figure 3.5 A, B) and a telomeric sequence (Figure 3.5 C) containing substrate in the presence of increasing concentrations of the CST complex or individual subunits. Both CTC1 and STN1 were able to greatly improve the strand displacement activity of Pol β, with a calculated 3-fold increase in synthesis for both subunits. TEN1 and the CST complex were able to improve the strand-displacement activity of Pol β marginally, as evidenced by an increase in synthesis beyond the pause point, but not to the degree observed with CTC1 and STN1 (Figure 3.5 A). Synthesis traces on random (Figure 3.5 B) and telomere (Figure 3.5 C) substrates display increased strand displacement synthesis in the presence of CST, irrespective of the substrate sequence. On the telomere substrate, both CTC1 (red trace, Figure 3.5 C) and STN1 (purple trace, Figure 3.5 C) showed significant full-length synthesis when compared to synthesis by Pol β alone (black trace, Figure 3.5 C).

Unlike the replicative polymerases, Pol β does not synthesize over long stretches of a DNA template. However, since we observed varying levels of stimulation by the

individual components as well as the entire CST complex, we next tested the impact of CST stimulation on the gap-filling function of Pol β. Similar to its stimulation of Pol β synthesis [27, 139, 140], CST stimulated Pol β synthesis on a random sequence containing 66 nt gapped DNA substrate. Incubation with CTC1 (lanes 4, 5, 6, Figure 3.6 A) or STN1 (lanes 8, 9, 10, Figure 4A) alone even resulted in the robust accumulation of full-length product, which was not achieved using Pol β alone. Both CTC1 and STN1 were shown to stimulate Pol β DNA synthesis by ~7-fold, whereas TEN1 (lanes 12, 13, 14, Figure 3.6 A) or the entire CST complex (lanes 16, 17, 18, Figure 3.6 A) resulted in an ~3-fold increase in synthesis. This increase was both observable and quantifiable, as shown in the intensity traces for both the random (Figure 3.6 B) and telomere (Figure 3.6 C) substrates.

While the reason for the increased stimulation with the individual subunits alone versus the entire complex is not clear, it is possible that interacting regions are more exposed in CTC1 and STN1 when not within the full complex. Whether individual subunits are always together as a complex in cells is currently unclear. Regardless, these results indicate that CST interacts with Pol β and stimulates its synthesis and strand displacement activities. Additionally, this appears to be through direct interaction versus the DNA binding activity of CST since individual subunits stimulate Pol β but have little to no detectable DNA binding activity (Figure 3.3 C).

3.3.3 CST ENHANCES MULTIPLE STEPS IN BER IN VITRO

To better understand how CST may promote BER, we sought to characterize how CST affected the different steps of BER through biochemical reconstitution, using

purified proteins and DNA substrates that resemble the different intermediates of both SP- and LP-BER.

CST stimulates APE1 cleavage - During BER, APE1 cleaves the abasic site generated after a DNA glycosylase removes the oxidized or damaged base. APE1 is an indispensable player in BER, and its efficiency must be maximized for cells to cope with oxidative damage [147, 148]. Additionally, cleavage by APE1 is common between both SP and LP-BER. To assess how CST affected APE1 activity, the individual subunits or the full CST complex was incubated with APE1 and the endonuclease activity of APE1 was tested on a DNA substrate containing a THF residue, which resembles an abasic site. On a random THF substrate (Figure 3.7 A) APE1 endonuclease activity was modestly stimulated by the CST complex with a nearly 2.0-fold increase. CTC1 alone stimulated cleavage 2.7-fold and the addition of STN1 or TEN1 resulted in an approximately 1.2-fold increase (Figure 3.7 B). Similar patterns of stimulation were observed on a telomeric THF substrate (Figure 3.7 C).

CST stimulates Pol β lyase activity - In addition to DNA synthesis via its polymerization domain, Pol β also possesses a lyase domain, which removes the dRP residue that persists following APE1 cleavage of an abasic site. Previous studies suggested the dRP lyase activity of Pol β occurred after gap-filling synthesis by the polymerase [130, 149, 150]. A recent study has proposed an interlocked mechanism wherein the polymerase and dRP lyase function in tandem [151]. Irrespective of the sequence of events, without lyase activity, SP-BER cannot be completed. Therefore, we next examined the impact CST has on the lyase activity of Pol β.

To study the dRP lyase activity, we utilized a 55 nt duplex DNA substrate that contained an uracil residue. The uracil containing DNA was 3' end labeled with [α-32P]dCTP and then treated with Uracil DNA Glycosylase (UDG) to generate an abasic site. APE1 cleavage of this abasic site forms a 5'-dRP group which can be excised via the lyase activity of Pol β. Because this Pol β -incised product does not contain the sugar phosphate residue, it will migrate slightly faster when separated by gel electrophoresis. A schematic of the methodology used to generate the substrate and perform the assay is outlined in Figure 6A.

CST or individual subunits were incubated with the lyase substrate. Lyase activity was then assessed by denaturing polyacrylamide gel electrophoresis. The results demonstrated that the lyase activity of Pol β is improved in the presence of the full complex and individual subunits (Figure 3.8 B-C). There was an ~7.5-fold increase in Pol β lyase activity with CTC1, 8-fold by STN1, 1.5-fold with TEN1, and an ~10-fold increase with the full complex. These results provide further evidence that CST interacts with Pol β and mechanistically improves its catalytic functions during BER.

Individual subunits but not the CST complex stimulate FEN1 - Flap endonuclease 1 (FEN1) also plays an important role during LP-BER by excising the 5' DNA flaps that are formed [152]. Without functional or optimal FEN1, gap-filling stalls and the efficiency of long patch BER is significantly diminished [153].

To test whether CST regulates FEN1 nuclease activity, CST or individual subunits and FEN1 were incubated with a DNA substrate with a 30 nt 5' DNA flap. FEN1 cleavage was then measured (Figure 3.9 A). A 2.1-fold stimulation in FEN1 activity was observed in the presence of CTC1 and ~1.5-fold stimulation measured with STN1 or

TEN1 (Figure 3.9 B). However, minimal effect was observed in the presence of the full CST complex. Similar results were observed with a telomere-sequence containing substrate, except that TEN1 showed minimal stimulation similar to the full complex (Figure 3.9 C).

CST promotes ligase activity - LIGI is responsible for completing the final step of both SP-BER and LP-BER by sealing the nick between the DNA stands following Pol β gap filling [154]. The ligation efficiency of LIGI was assessed in the presence of CST or individual subunits on a nicked DNA substrate (Figure 3.10 A). CST, CTC1 or TEN1 increased the ligation activity of LIGI by ~2-fold, while STN1 showed no effect (Figure 8B). Similar results were observed with a nicked telomere-sequence containing substrate (Figure 3.10 C). These results demonstrate that CST improves the ligation activity of LIGI on nicked DNA.

3.3.4 CST ENHANCES LONG PATCH BER

Based on the ability of CST and individual components to stimulate multiple steps of BER, we sought to reconstitute the entire LP-BER pathway in vitro and characterize the impact that CST and individual subunits have on the overall repair efficiency. LP-BER is employed by the cell when the dRP lyase activity of Pol β is diminished or inhibited [155]. In this pathway, Pol β displaces the oxidized residue into a 2-10 nt flap which then gets cleaved by FEN1, and the resultant nick sealed by LIGI. Therefore, minimal reconstitution of LP-BER requires Pol β, APE1, FEN1, and LIGI.

The BER components were co-incubated in the presence of increasing concentrations of CST or individual subunits on both non-telomeric and telomeric THF-containing substrates, resembling an abasic site. Our results demonstrate the ability of the

full CST complex or individual subunits to stimulate the overall repair efficiency of LP-BER (Figure 3.11). On the random sequence substrate, there was a calculated fold increase in ligation efficiency of 2.2-fold for the entire complex, 2.0-fold for CTC1, and 2.5-fold for STN1 (Figure 3.11 B). However, TEN1 alone did not simulate BER in vitro. Similar results were observed on the telomeric substrate although to a lesser extent (Figure 3.11 C).

3.3.5 LOSS OF STN1 INCREASES CELLULAR 8-OXOGS

Our in vitro biochemical reconstitution experiments suggest that CST plays an undiscovered role in the repair of oxidative DNA damage through BER. Therefore, we hypothesized that cells lacking CST would be compromised in their ability to repair oxidized bases. Based on our in vitro work showing that CST stimulates Pol β, APE1, and LIG1, we predicted that there would be increased levels of abasic sites and/or ssDNA breaks due to incomplete BER in CST deficient cells. Therefore, alkaline comet assays were performed to detect both ssDNA breaks and abasic sites that devolve into breaks under alkaline conditions [156]. Conditional HeLa STN1 knockout (KO) cells (Figure 3.12 A) were treated with H_2O_2 for 1 hour and then cells were collected without release or with a 1, 2 or 4-hour release from H_2O_2 (Figure 3.12 B). Interestingly, the tail moments were not significantly different in the STN1 KO cells compared to the parental line, suggesting that ssDNA breaks and abasic sites were not increased following loss of STN1.

Since DNA breaks were not increased in the alkaline comet assay, we wondered whether CST promotes the recognition of oxidized DNA bases. As mentioned previously, 8-oxoG is the most common form of oxidative base damage and is highly mutagenic.

Accordingly, we tested whether cells lacking STN1 had increased levels of 8-oxoG. HeLa STN1 KO cells were treated with increasing concentrations of H_2O_2 (50, 100 or 200 μM) for 1 h. Cells were then washed and released into fresh media for 4 h prior to collection. Genomic DNA was then extracted and 8-oxoG content measured (Figure 3.12 C).

Intriguingly, even in the absence of exogenous oxidative stress, 8-oxoG levels in STN1 KO cells were approximately double that of the parental cells, indicating that CST aids in oxidative repair even in unstressed cells. In the presence of H_2O_2, there was also a corresponding increase in the percentage of 8-oxoGs (Figure 3.12 C & 3.13). These findings suggest that CST may aid in recognition of the oxidized base by a DNA glycosylase to initiate BER. As OGG1 is used to repair 8-oxoGs, we tested whether CST associated with OGG1 by PLA. Consistent with our hypothesis, we observed STN1-OGG1 foci, which were increased with H_2O_2 treatment (Figure 3.12 D). Taken together, these findings corroborate our in vitro studies that CST promotes BER to minimize oxidative DNA damage.

3.4 DISCUSSION

Human CST is a ssDNA binding protein that is essential for telomere maintenance with emerging roles in DNA replication and repair. Due to its role at telomeres [12], preference for G-rich DNA [39], and ability to stimulate another polymerase (i.e., Pol α) [27, 139, 140], we sought to characterize whether CST functions in BER by studying the biochemical interactions between CST and BER-associated proteins. Combined our results demonstrate that CST interacts with and stimulates the enzymatic activities of several BER-associated proteins, in particular the activities of Pol

β. Furthermore, full reconstitution of LP-BER showed a direct stimulation by CST in vitro. Finally, an assessment of cellular 8-oxo-G levels indicate that CST is needed to prevent the accumulation of basal endogenous and exogenously oxidative DNA damage. Combined, these studies provide a clear link between CST and oxidative DNA repair through the stimulation of BER.

The ability of CST to stimulate the DNA synthesis, strand-displacement, and dRP lyase activities of Pol β portends a possible direct interaction (Figure 3.1). This is further supported by data showing that individual CST subunits, which have little to no DNA binding activity, still stimulate Pol β. Considering that Pol β is the chief polymerase responsible for nucleotide synthesis during BER, our observed biochemical stimulation of Pol β by CST provides compelling evidence that CST promotes oxidative repair through the stimulation of Pol β. This agrees with past work indicating that human CST acts as a stimulatory factor for Pol β [26, 27, 139]. However, it is interesting to note that CST also stimulated the enzymatic activities of other proteins in the pathway, including APE1, FEN1, and LIG1. Therefore, CST may also act more generally to stimulate the entire process.

Initial characterization of mammalian CST focused on its ability to interact with and stimulate Pol β, a function conserved across eukaryotes [157]. However, more recent work has shown that CST can also stimulate the activities of RAD51 and MRE11 [40, 158]. These interactions are proposed facilitate the rescue of stalled replication forks. Thus, CST may act at several points to facilitate or stimulate this process. In like manner, our results suggest that CST acts at multiple points to stimulate BER and prevent the accumulation of oxidative DNA damage.

While further work will be required to determine the timing and mechanism of CST localization to oxidative DNA damage, the fact that loss of STN1 increased the levels of 8-oxoG, indicates that that CST must be required for efficient recognition and/or removal of damaged bases. We speculate that CST acts to localize or recruit BER factors to G-rich regions of the genome, such as telomeres and CpG islands, where oxidative DNA damage is common and CST is known to localize [39]. However, further work is required to test whether CST is necessary for oxidative repair in these regions.

CST could also be required to resolve G4s, which may affect the efficiency of 8-oxoG repair in this structural motif [7, 159]. As a result of their G-rich sequence, telomeres are particularly prone to both the formation of G4s and oxidative damage. The presence of G4s may make it difficult for BER-associated proteins to optimally function, as has been observed for other proteins. For example, it has been shown that DNA Pol δ synthesis is severely impeded by the presence of G4s [160]. Given that CST binds to G-rich telomeric sequences and can resolve G4 structures, CST is well-equipped to promote oxidative repair in G-rich DNA.

We propose that the ability of CST to stimulate the enzymatic activities of BER-associated proteins may help alleviate the inhibition these proteins may face in the presence of G4s. Yet, it is important to note that the stimulatory effects of CST on individual BER-associated proteins and full reconstitution of LP-BER was similar on both telomere and non-telomere substrates. Therefore, it is also possible that CST acts more generally in BER across the genome. Accordingly, further work will be required to fully understand how CST stimulates BER in the cellular context.

Overall, our biochemical results have identified previously unknown interactions between CST and BER-associated proteins and provide an important foundation for future studies seeking to understand how oxidative damaged DNA is repaired to maintain genome integrity and prevent disease.

3.5 MATERIALS AND METHODS

3.5.1 RECOMBINANT PROTEINS

Recombinant human Pol β [161], FEN1 [162], APE1 [163], and LIG1 [164], were purified as described previously. Constructs for purification of CST as well as the individual CTC1, STN1 or TEN1 subunits were kindly provided by Dr. Carolyn Price from the University of Cincinnati.

Human FLAG-CTC1 – The construct for full-length FLAG-tagged human CTC1 was previously generated by cloning the DNA sequence for the CTC1 gene into the pcDNA 3.1 vector. Transfection of pcDNA-FLAG-CTC1 plasmid DNA was performed in Expi293 cells using the ExpiFectamine kit according to manufacturer protocol (Thermo Fisher Scientific). Cells were harvested 72 hours after transfection.

Cell lysates were prepared by sonicating the thawed cell pellet with 5 second on/off pulses for 10 minutes at 35% amplitude in lysis buffer containing 25 mM Na-HEPES, pH 7.5, 75 mM NaCl, 0.5 mM EDTA, 0.5% Triton X-100, 10% glycerol, 0.5 mM DTT, 1 mM PMSF, and protease inhibitor cocktail tablet (Roche Applied Science). The clarified cell lysate was collected by centrifugation at 3000 x g for 20 minutes and incubated with 100 µL anti-FLAG M2 agarose beads (Sigma-Aldrich) for 2 hours on a LabQuake rotator. Anti-FLAG M2 agarose beads were prepared for use according to the protocol published by Gerace and Moazed [165].

After binding, the beads were washed thrice in buffer containing 25 mM Na-HEPES, pH 7.5, 75 mM NaCl, and 0.5 mM EDTA, 5% glycerol, and 1 mM PMSF. The elution step was performed by addition of elution buffer containing 200 µg 3X FLAG-peptide (MedChemExpress), 25 mM Na-HEPES, pH 7.5, 50 mM NaCl, and 1 mM PMSF. Peak fractions containing purified CTC1 protein were confirmed using SDS-PAGE and Western Blotting with α-FLAG (Sigma-Aldrich) and α-CTC1 [41] antibodies. CTC1 protein concentration was assessed using QuBit protein assay on a QuBit Fluorometer. The purified CTC1 fractions were supplemented with 25% glycerol and 0.5 mg/mL BSA, aliquoted, and kept frozen at -80°C. Due to stability concerns, aliquots of CTC1 were only thawed twice for use in functional assays. As shown in Figure S2A, repeated freeze-thaw cycles resulted in the degradation of the CTC1 protein.

Human GST-STN1 – Full-length GST-tagged human STN1 was cloned into the pGEX-6p-3 plasmid and purified as an N-terminal GST fusion via batch purification. The expression plasmid was introduced into E. coli strain BL21 (DE3) and allowed to grow at 25°C shaking for 220 RPM overnight following induction with 0.1 mM IPTG. Bacterial pellets were collected by centrifuging at 12,000 x g for 30 minutes. Pellets were then kept frozen at -80°C. Pellets from 1 L of culture were resuspended in 25 mL ice cold lysis buffer containing 10% glycerol, 1 mM PMSF, 1 mM 2-mercaptoethanol, 0.5 mg/mL lysozyme, and protease inhibitor cocktail tablet, and kept on ice for 20 minutes before sonicating using 30 second on/off pulses at 35% amplitude for 10 minutes. Lysates were diluted in 1X PBS buffer to 40 mL and clarified by centrifuging at 10,000 x g for 20 minutes. Glutathione sepharose resin (GE Healthcare) was equilibrated in 1X PBS buffer and allowed to incubate with the cleared lysate for 2 hours at 4°C. Beads were washed

3X with 20 mL 1X PBS buffer, and 1X with 10 mL wash buffer containing 50 mM Tris-HCl, pH 8.0, and 150 mM. Washed beads were resuspended in 2 mL of elution buffer containing 50 mM Tris-HCl, pH 8.0, 150 mM NaCl, and 20 mM L-glutathione reduced, pH 8.0, and allowed to rotate for 20 minutes at 4°C before fraction collection. The presence of purified GST-STN1 was confirmed by SDS-PAGE and the protein concentration assessed by the QuBit protein assay. Aliquoted fractions were frozen and stored at -80°C.

Human His-TEN1 – Full-length His-tagged human TEN1 was cloned into pET28a, cultured in BL21 (DE3) competent E. coli cells, and expressed at 37°C shaking overnight following induction with 0.1 mM IPTG. Cell pellets were collected via centrifugation at 12,000 x g and then kept frozen at -80°C. Pellets were resuspended in ice cold lysis buffer at the ratio of 1 mL buffer per 1 gram of pellet. The lysis buffer consisted of 20 mM Tris-HCl, pH 7.5, 0.5 M NaCl, 30 mM imidazole, pH 7.4, 1 mM DTT, 0.01% Igepal CA-630, 6 M guanidine-HCl, and 1 protease inhibitor cocktail tablet. Lysates were sonicated using 15 second on/off pulse cycles for 8 minutes at 40% amplitude and loaded onto a pre-equilibrated Ni-NTA agarose resin (Qiagen). Using an NGC chromatography system (Bio-Rad), the resin was washed using 10X column volumes of binding buffer containing 20 mM Tris-HCl, pH 7.5, 0.5 M NaCl, 30 mM imidazole, pH 7.4, 1 mM DTT, 0.01% Igepal CA-630, and a protease inhibitor cocktail tablet (Roche Applied Science). Purified TEN1 was collected after gradient elution in buffer containing 20 mM Tris-HCl, pH 7.5, 0.5 M NaCl, and 500 mM imidazole, pH 7.4. Peak fractions containing TEN1 were pooled and concentrated using Amicon Ultra

centrifugal filters, assessed by SDS-PAGE and QuBit Fluorometer. Aliquoted fractions were frozen and stored at -80°C.

Human CST complex – HEK293T cells were co-transfected with pcDNA3.1-FLAG-CTC1, pcDNA3.1-FLAG-STN1, and pcMV-Sport6-TEN1 in a ratio of 2:1:1, using polyethylenimine (PEI) (Polysciences). After 72 hours, cells were harvested, suspended in 1X PBS, pelleted via centrifugation at 2000 x g for 20 minutes, and then stored at -80°C. Cell pellets were lysed in NETN buffer (40 mM Tris-HCl, pH 8.0, 100 mM NaCl, 1 mM EDTA, 0.5% NP40, 1× protease inhibitors [1 μg/ml pepstatin A, 5 μg/ml leupeptin, 1 μg/ml E64, 2 μg/ml aprotinin, and 5 μg/ml antipain], and 1× phosphatase inhibitors [4 mM β-glycerophosphate, 4 mM sodium vanadate, and 20 mM sodium fluoride]). Cell lysates were centrifuged at 15,000 x g for 20 minutes at 4°C. The supernatant was run on a column of single-stranded DNA beads (Bethesda Research Laboratories, Inc.) followed by 5 column volume (CV) washes of NETN, 5 CV BC75 (20 mM Tris-HCl, pH 8.0, 75 mM NaCl, 0.2 mM EDTA, 10% glycerol) and BC200 (20 mM Tris-HCl, pH 8.0, 200 mM NaCl, 0.2 mM EDTA, 10% glycerol). CST was eluted with 3 CV BC500 (20 mM Tris-HCl, pH 8.0, 500 mM NaCl, 0.2 mM EDTA, 10% glycerol, 100 μg/mL BSA) and 3 CV BC1000 (20 mM Tris-HCl, pH 8.0, 1000 mM NaCl, 0.2 mM EDTA, 10% glycerol, 100 μg/mL BSA). DNA binding activity was checked by EMSA on a 48 nt substrate and elutions with active ssDNA binding activity were combined and incubated overnight with 1 ml of 50% M2 α-Flag (Sigma-Aldrich) agarose bead slurry. Beads were washed with at least 3 CV of NETN before eluting CST using storage buffer (20 mM Tris-HCl, pH 8.0, 50 mM NaCl, 0.5 mM EDTA, 0.25% NP40, 10% glycerol, 100 μg/mL BSA and 100 μg/mL 3x FLAG peptide [Sigma-Aldrich]).

3.5.2 SYNTHETIC OLIGONUCLEOTIDES

All custom synthetic oligonucleotides used for ¬in vitro experiments were designed and ordered from IDT (Integrated DNA Technologies, Coralville, IA), except the T1 oligonucleotide which was purchased and prepared by Midland Certified Reagent Company. The sequences are listed in Table S1. "Φ" denotes a tetrahydrofuran (THF) residue, and "p" represents a 5' phosphorylation modification. Upstream and downstream primer sequences are listed in the 5' – 3' direction, while the template sequences are shown in the 3' – 5' direction to help with orientation. Primers were labeled as denoted in the figures either at the 5' end using [γ-32P]ATP and T4 polynucleotide kinase (Roche Applied Science), or the 3' end using [α-32P]dCTP and the Klenow fragment of E. coli DNA polymerase I (Roche Applied Science). All radionucleotides were purchased from PerkinElmer Life Sciences. For 3'-end labeling, the primer was annealed to the template containing a G-overhang on the 5' end to facilitate the incorporation of [α-32P]dC TP by Klenow. The labeled primers were isolated and purified on a 15% polyacrylamide, 7 M urea denaturing gel. The DNA was then ethanol precipitated and quantified using a Beckman Coulter Liquid Scintillation Counter. Primers were annealed in a 1:2:4 ratio of upstream primer to template to downstream primer in nuclease-free duplex buffer (Integrated DNA Technologies) by heating at 95°C for 5 minutes, then cooling slowing to room temperature overnight. Substrates without a downstream sequence were annealed in a 1:2 ratio of upstream primer to template.

3.5.3 ENZYME ASSAYS

Enzymatic assays were performed by generating 20 µL reaction mixtures containing 5 nM 32P-radiolabeled DNA substrate and the enzyme of interest (Pol β,

APE1, LIG1, or FEN1) along with the addition of the full CST complex and/or individual subunits (CTC1, STN1, TEN1) at the concentrations listed in the figure legends. Reactions were incubated at 37°C for 10 minutes, unless otherwise noted. The Pol β reaction buffer consisted of 50 mM Tris-HCl, 2 mM DTT, 2 µg/mL BSA, 2 mM ATP 8 mM MgCl2, 25 nM NaCl, and 0.1 mM dNTP mixture (Roche Applied Science). The APE1/FEN1 reaction buffer consisted of 50 mM Tris-HCl, pH 8.0, 2 mM DTT, 0.25 mg/mL BSA, 30 mM NaCl, 5% glycerol, 8 mM MgCl2, and 2 mM ATP. The LIG1 reaction buffer consisted of the Pol β reaction buffer without dNTPs. Reactions were terminated using 2X termination loading dye consisting of 90% formamide (v/v), 10 mM EDTA, 0.1% bromophenol blue, and 0.1% xylene cyanole. After termination, reaction mixtures were boiled for 5 minutes at 95°C, loaded onto a pre-heated 12% polyacrylamide urea denaturing gel, and separated by electrophoresis at 80 Watts.

3.5.4 LYASE ACTIVITY ASSAY

The dRP lyase activity of Pol β was assessed by measuring the excision of the 5'-dRP residue on a duplex DNA substrate containing an uracil residue at position 20 (U5:T3). The 5'-dRP residue was enzymatically generated by treating 5 nM of substrate with 1 U of Uracil DNA Glycosylase enzyme (New England Biolabs, M0280S) in 1X UDG Reaction Buffer (New England Biolabs, M0280) for 30 minutes at 37°C. Next, the UDG cleaved substrate was incubated for 10 min at 37°C with APE1 (100 nM) in reaction buffer containing 50 mM Tris-HCl, 2 mM DTT, 2 µg/mL BSA, 2 mM ATP 8 mM MgCl2, and 25 nM NaCl. Pol β (0.25 nM) along with the CST complex (5, 15, 45 nM) or subunits CTC1/STN1/TEN1 (250, 750, 1500 nM) were then added to the APE1 cleaved DNA and allowed to incubate for 10 minutes at 37°C. Each reaction was 20 µL

total. Following incubation, 3.4 µL of 2 M $NaBH_4$ was added to each reaction to stabilize the dRP product, and the reactions were kept on ice for 30 minutes. Finally, each of the reaction samples were ethanol precipitated (this is essential to prevent smearing on the gel due to the $NaBH_4$), separated by electrophoresis for 2.5 hours on a 20% polyacrylamide gel at 80 W, dried and imaged via PhosphoImaging.

3.5.5 LP-BER ASSAY

The LP-BER pathway was reconstituted in vitro by incubating APE1, Pol β, FEN1, and LIG1 with 5nM of an abasic substrate containing a THF residue in buffer containing 50 mM Tris-HCl, 2 mM DTT, 2 µg/mL BSA, 2 mM ATP 8 mM $MgCl_2$, 25 nM NaCl, and 0.1 mM dNTP mixture (Roche Applied Science). Reactions were incubated at 37°C for 10 minutes and subsequently terminated samples were loaded onto a pre-heated 12% polyacrylamide urea denaturing gel and separated by electrophoresis at 80 Watts and ligation efficiency was monitored.

3.5.6 GEL ANALYSIS

Following electrophoresis, gels were transferred to Whatman filter paper, wrapped in plastic wrap, and dried for 1 hour on Bio-Rad vacuum gel drier. Reaction products were visualized by exposing the dried gels to phosphor screens overnight and scanning on a Typhoon 9500 phosphoimager (GE Healthcare). Gels displayed in figures are representative of at least three independent experiments and were analyzed using ImageQuant TL version 8.1. Quantitation of gels was performed using Image Studio version 5.2, and intensity traces were generated using ImageJ version 1.53, graphs were plotted using GraphPad Prism software.

3.5.7 CELL CULTURE

HeLa 1.2.11 cells were maintained in RPMI 1640 media and HeLa iCas9 and HEK 293T in DMEM at 37°C with 5% CO2. All cell lines were supplemented with 10% fetal bovine serum and 1% penicillin/ streptomycin. Cell lines were regularly checked for mycoplasma contamination. HeLa 1.2.11 cells were used for PLA analysis, HEK 293T cells for the purification of the full CST complex and HeLa iCas9 cells for 8-oxoG analysis. HeLa iCas9 (inducible Cas9) cells were generously provided by Dr. Iain Cheeseman from Massachusetts Institute of Technology. STN1 inducible KO cell lines were constructed following the protocol outlined by McKinley [123], using the sgRNA (5' GGG GAC ACG ATC CGA GTC AGA 3') to STN1. The sgRNA was cloned into pLenti-sgRNA using the BsmB1 restriction site, lentivirus prepared, and HeLa iCas9 cells transduced with the resultant virus. Clones were selected with puromycin and immunoblotting conducted to ensure successful KO. To induce the conditional gene KO of STN1, cells were incubated with 1 μg/ml Doxycycline (Dox) for 3-4 days.

3.5.8 WHOLE CELL PROTEIN EXTRACTION

Cell pellets were lysed, sonicated and nuclease-treated, as previously described [41]. The supernatant was collected, and protein concentration measured by BCA assay (Thermo Fisher Scientific). The samples were then mixed with SDS-PAGE loading buffer and analyzed by Western blot, as previously described [41]. Primary: OBFC1 (STN1) (Novus, NBP2-01006), β-Actinin (Santa Cruz, SC17829). Secondary: goat-anti-mouse-HRP (Thermo Scientific, 32430),

3.5.9 PROXIMITY LIGATION ASSAY (PLA)

HeLa 1.2.11 cells were fixed for 20 minutes at room temperature with 4% formaldehyde in 1X PBS followed by permeabilization with 100% methanol for 20 min at -20° C. H_2O_2 treated cells were incubated with 200 μM H_2O_2 for 2 hours prior to fixation. Subsequent steps were performed with the Duolink PLA kit (Millipore-Sigma) as previously described [101], except the first wash after primary incubation was performed using wash buffer A, not 5% B SA in 1x PBS. Primary antibodies: 1:100 mouse α-STN1 (Novus, NBP2-01006), 1:100 rabbit α-POLB (Abbexa, abx304879), 1:100 rabbit α-PolA1 (Bethyl Laboratories, A302-850A), 1:100 rabbit α-XRCC1 (Genetex, GTX111712), 1:100 mouse α-XRCC1 (Invitrogen, MA1-12640), 1:100 rabbit α-PARP1 (Proteintech, 6520-1-Ig), 1:100 rabbit α-OGG1 (Proteintech, 15125-1-AP). Images were taken on an EVOS FL microscope, using a 40× objective (Thermo Fisher Scientific). Ten images were scored per independent, biological experiment for each condition. Image analysis was performed with CellProfiler. Violin plots and p-values were generated with GraphPad Prism. All p-values were calculated by an unpaired, two-tailed t-test.

3.5.10 ALKALINE COMET ASSAY

HeLa iCas9 sgSTN1 cells (+/-Dox) were treated with 100 μM H_2O_2 for 1 h. Cells were then washed with three times with 1x PBS, fresh media added, and allowed to recover for 0, 1, 2, or 4 h, as indicated. Cells were then collected, washed, resuspended in ice-cold 1x PBS and counted, keeping samples on ice prior to embedding. Cells were then embedded into agarose by combining 1x105 cells/ml at a ratio of 1:10 (v/v) with molten agarose at 37°C. For the 0 h time point, cells were first collected, washed and

resuspended in ice-cold 1x PBS prior to the addition of H_2O_2. These cells were then incubated on ice for 1 h and collected without release. Subsequent steps and scoring were performed using the Trevigen CometAssay HT kit (#4252-040-K) and Trevigen CometAssay Analysis Software (#4260-000-CS), as previously described [166].

3.5.11 DETECTION OF 8-OXOGS

Genomic DNA from HeLa iCas9 sgSTN1 cells (CTRL – no Doxycycline, KO – Doxycycline treated) with or without H_2O_2 treatment was collected and analyzed for the level of 8-oxo-Gs. Cells were treated for 1 hour with the indicated amount of H_2O_2, washed three times with 1X PBS, and released into fresh media for 4 hours. Cells were then collected and genomic DNA isolated (Thermo Scientific, K0722). 8-oxoGs were then measured using EpiQuik 8-OHdG kit (Epigentek, P-6004-96), per manufacturer's instructions.

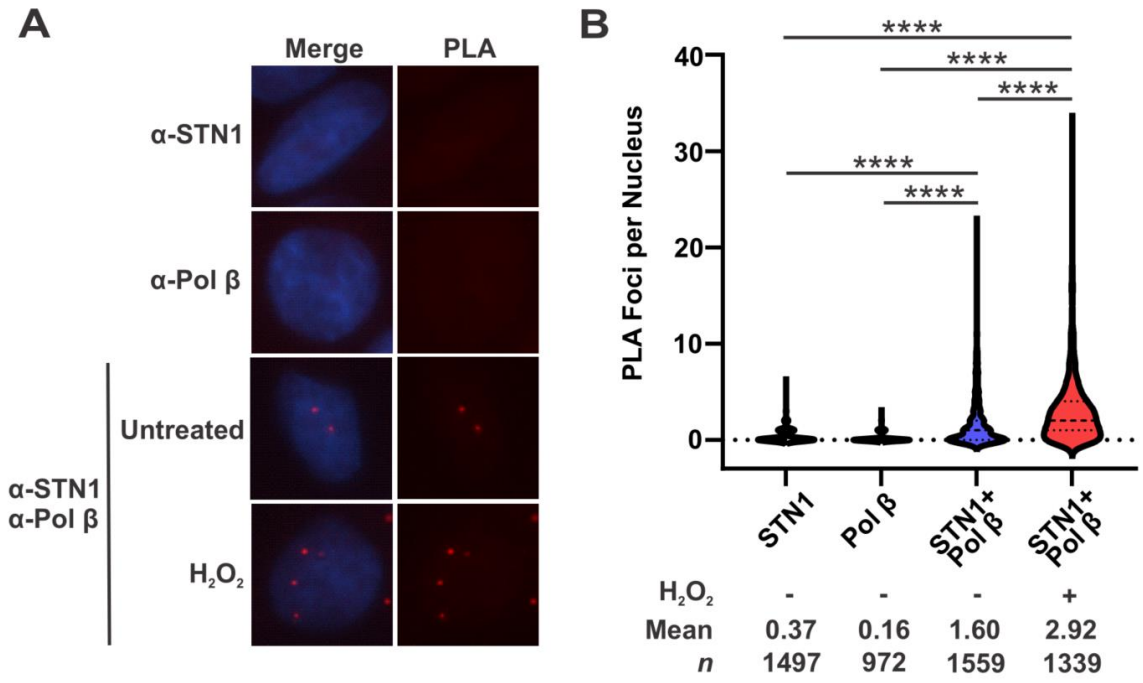

Figure 3.1 ***STN1 associates with Pol β.*** (A) Representative images of proximity ligation assay (PLA) performed in HeLa cells with antibodies to STN1 or Pol β alone or in combination with and without H_2O_2 treatment. Red, PLA foci; blue, DAPI. (B) Violin plot of PLA foci per nucleus. Results are representative of three independent, biological experiments. Bold dashed line represents the median, and dashed lines represent the first and third quartiles. (∗∗∗∗p < 0.0001).

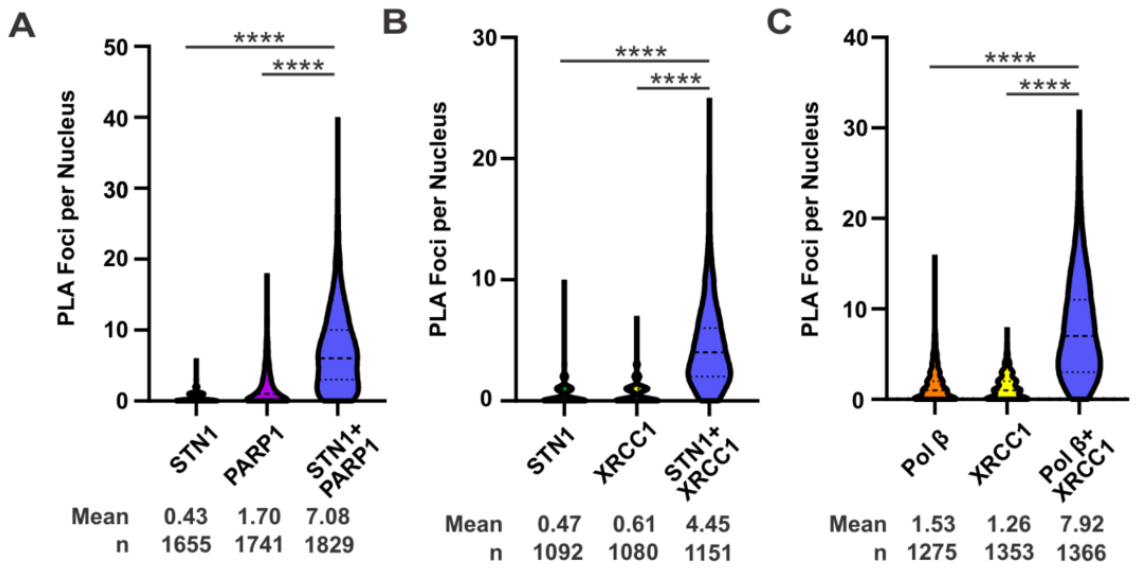

Figure 3.2 ***STN1 associates with PARP1 and XRCC1.*** (A) Proximity ligation assay (PLA) performed in HeLa cells with antibodies to STN1, PARP1 or in combination (STN1+ PARP1). (B) PLA was performed in HeLa cells as in (A) with antibodies to STN1 and OGG1 (STN1 + OGG1). (C) PLA was performed as in (A) with antibodies to Pol β and XRCC1. Violin plots of PLA foci per nucleus. Results for (A), (B) and (C) are representative of four independent, biological experiments. Bold dashed line: median, dashed lines: first and third quartiles. (****P < 0.0001).

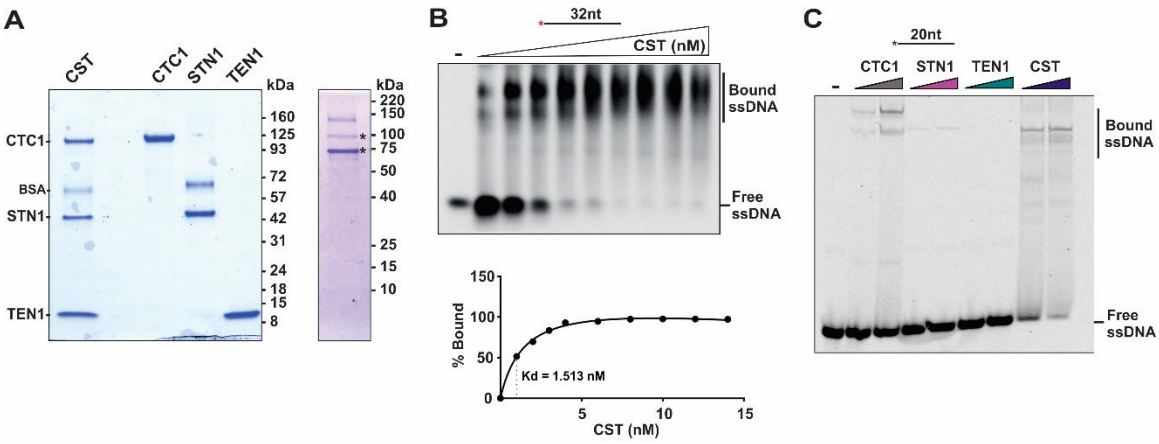

Figure 3.3 ***CST complex and subunit purification and DNA binding activity.*** Recombinant proteins were purified as described in Materials and Methods (A) Left, Coomassie blue stained SDS-PAGE gel (4-15% gradient gel) of purified recombinant proteins. Right, Coomassie blue stained SDS-PAGE gel (4-20% gradient gel) of purified CTC1 protein after repeated freeze-thaw cycles. * indicates CTC1 degradation products, which were confirmed using an anti-FLAG antibody. (B) Top, increasing concentrations of CST binding were incubated with 5 nM of a 32 nt (5' IR-label) substrate to determine the dissociation constant (Kd). Bottom, the K d was calculated using Graph Pad. (C) 5 nM of a 20 nt ssDNA substrate (5' IR-label) was bound with increasing concentrations (500 and 1000 nM) of CTC1, STN1 and TEN1 and (15 and 30nM of CST complex). Substrate bound products were separated by 6% native PAGE gel and analyzed. Substrate alone and protein-bound substrate are indicated on the gel.

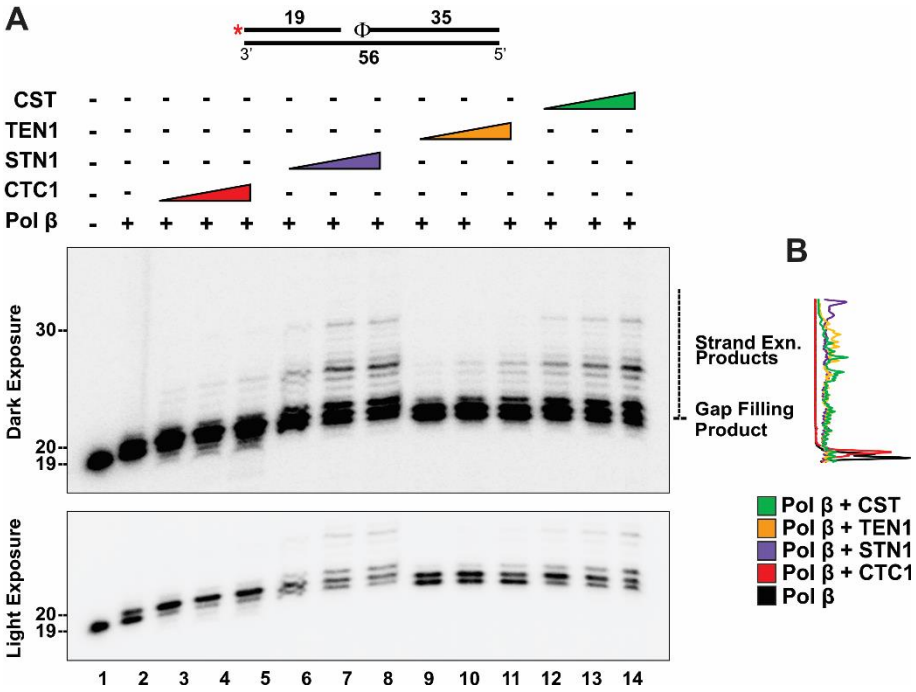

Figure 3.4 ***The CST complex and individual subunits stimulate DNA Pol β synthesis on a gap substrate containing an abasic site.*** Synthesis by DNA Pol β (2 nM) on a 1 nt gapped substrate (5 nM) containing an abasic site mimic (Φ denotes tetrahydrofuran [THF]) in the presence of increasing amounts of CTC1/STN1/TEN1 (100, 500, 1000 nM) or CST (5, 15, 30 nM) as denoted in the figure. The substrate was generated by annealing primers U1:T1:D1 in a 1:2:4 ratio. The red asterisk shown on the substrate represents the location of the 32P radiolabel. Gel shown is representative of at least three independent experiments. A darker exposure of the gel shows the strand displacement synthesis products. (B) The trace at the right of the gel depicts the signal intensity of the gap-filling and strand-displacement products in the lanes containing the highest concentration of CTC1(red trace)/STN1 (purple trace)/TEN1 (orange trace)/CST (green trace) [lanes 6, 10, 14, and 18] as compared to Pol β synthesis alone (black trace) [lane 2]. (Experiments performed by Brandon Wysong of the Balakrishnan lab).

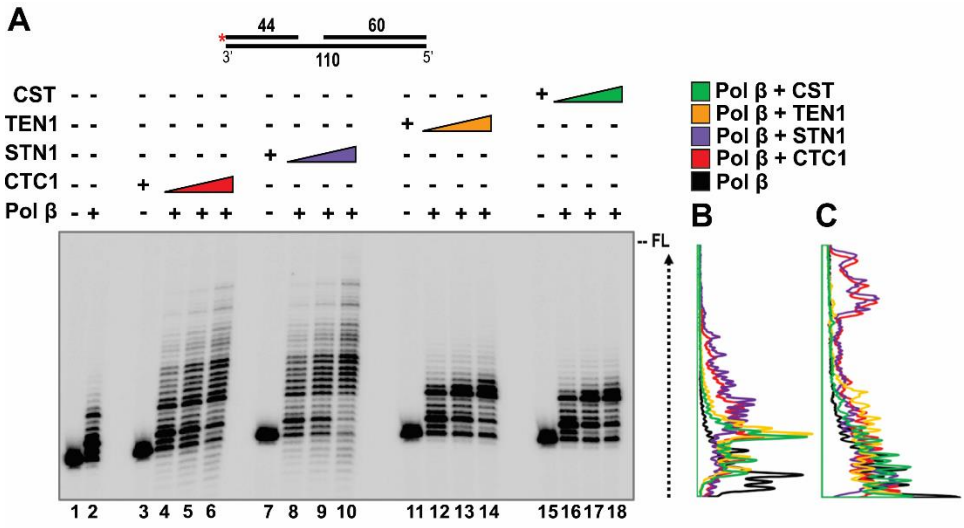

Figure 3.5 ***The CST complex and individual subunits stimulate DNA Pol β synthesis on a 6-nt gap substrate.*** (A) Synthesis by DNA Pol β (10 nM) on a 6 nt gap random sequence substrate (5 nM) in the presence of increasing amounts of CTC1/STN1/TEN1 (100, 500, 1000 nM) or CST (5, 15, 30 nM) as denoted in the figure. The red asterisk shown on the substrate in the figure represents the location of the 32P radiolabel. Gel shown is representative of at least three independent experiments. (B) The trace at the right of the gel depicts the signal intensity of the synthesis products in the lanes containing the highest concentration of CTC1(red trace)/STN1 (purple trace)/TEN1 (orange trace)/CST (green trace) [lanes 6, 10, 14, and 18] as compared to Pol β synthesis alone (black trace) [lane 2]. (C) Traces from a gel with a 6 nt gap telomere sequence substrate calculated as in (B). The random substrate (U2:T2:D2) and telomere substrate (U3:T3:D3) was generated by annealing primers in a 1:2:4 ratio (Experiments performed by Brandon Wysong of the Balakrishnan lab).

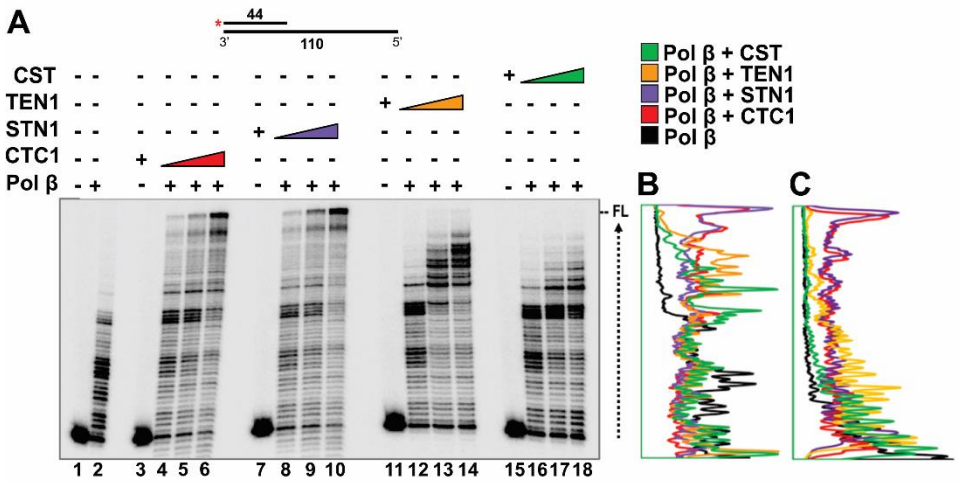

Figure 3.6 ***The CST complex and individual subunits stimulate DNA Pol β synthesis.*** (A) Synthesis by DNA Pol β (10 nM) on a synthesis substrate (5 nM) in the presence of increasing amounts of CTC1/STN1/TEN1 (100, 500, 1000 nM) or CST (5, 15, 30 nM) as denoted in the figure. The red asterisk shown on the substrate in the figure represents the location of the 32P radiolabel. Gel shown is representative of at least three independent experiments. (B) The trace at the right of the gel depicts the signal intensity of the synthesis products in the lanes containing the highest concentration of CTC1(red trace)/STN1 (purple trace)/TEN1 (orange trace)/CST (green trace) [lanes 6, 10, 14, and 18] as compared to Pol β synthesis alone (black trace) [lane 2]. (C) Traces from a gel with a telomere sequence substrate calculated as in (B).The random substrate (U2:T2:) and telomere substrate (U3:T3:) was generated by annealing primers in a 1:2 ratio (Experiments performed by Brandon Wysong of the Balakrishnan lab).

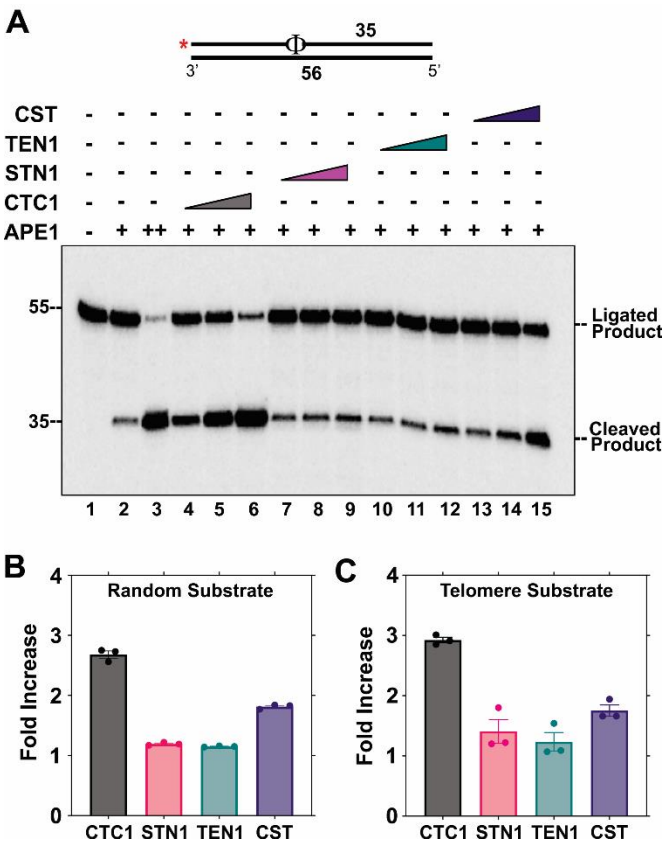

Figure 3.7 ***The CST complex and CTC1 enhance APE1 cleavage activity***. (A) APE1 (0.075 nM, lanes 2, 4-15; 100 nM, lane 2) cleavage activity was measured on a random sequence DNA substrate (5 nM) containing a THF residue in the presence of increasing concentrations of CTC1/STN1/TEN1 (250, 750, 1500 nM) or CST (5, 15, 60 nM) as denoted in the figure. The red asterisk shown on the substrate in the figure represents the location of the ^{32}P radiolabel and an Φ represents a THF residue. Gel shown is representative of at least three independent experiments. (B) Graph of the fold increase in APE1 cleavage activity for the lanes containing the highest concentration of the CST complex and individual subunits. (C) Graph of the fold increase in APE1 cleavage activity on a telomere substrate calculated as in (B). The error bars represent the standard error mean. The random substrate (U4:T1) and telomere substrate (U5:T4) was generated by annealing primers in a 1:2 ratio (Experiments performed by Brandon Wysong of the Balakrishnan lab).

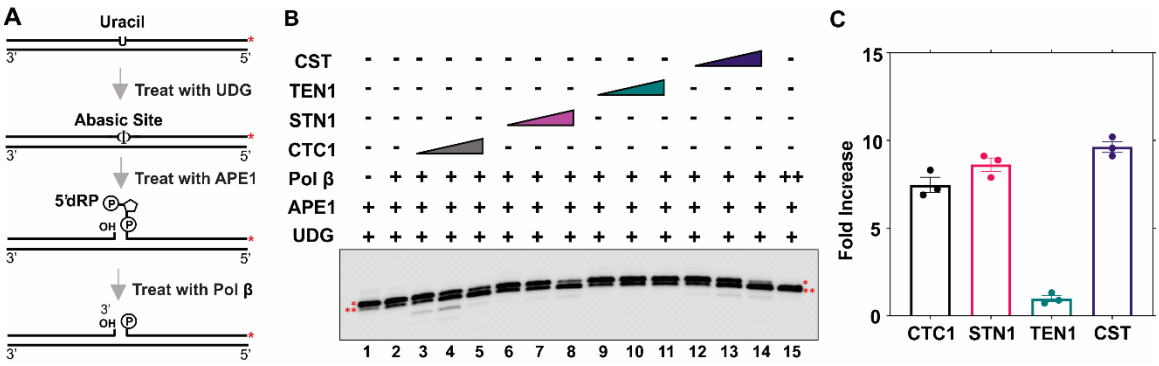

Figure 3.8 ***The CST complex, CTC1, and STN1 subunits stimulate dRP lyase activity of Pol β***. (A) Substrate (5 nM) was pre-treated with 1 U of UDG before the addition of 100 nM APE1 to generate the dRP substrate, as shown in the schematic and described in "Materials and Methods" (B) The lyase activity of POL β (0.25 nM, lanes 1-13; 5 nM, lane 14) was observed in the presence of increasing concentrations of CTC1/STN1/TEN1 (250, 750, 1500 nM) or CST (7.5, 15, 45 nM) as denoted in the figure. Gel shown is representative of at least three replicate experiments. (C) Graph of the fold increase in lyase activity for the lanes containing the highest concentration of CST proteins utilized. The error bars represent the standard error mean. * denotes the dRP lyase substrate; ** denotes the dRP lyase product. The substrate was generated by annealing primers U6:T1 in a 1:2 ratio. (Experiments performed by Brandon Wysong of the Balakrishnan lab).

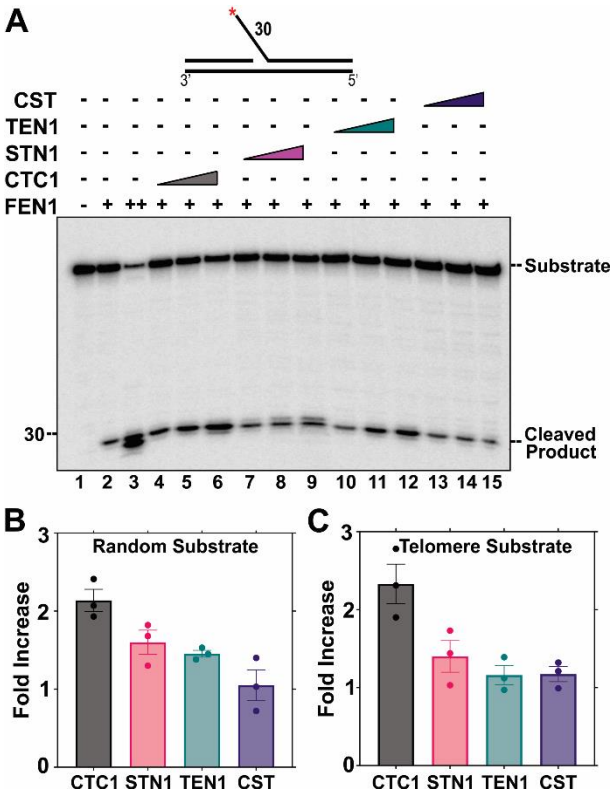

Figure 3.9 ***FEN1 cleavage activity is stimulated by CTC1 and STN1 but not the full CST complex*****.** FEN1 (0.025 nM, lanes 2, 4-15; 10 nM, lane 2) cleavage activity was measured on a random sequence 5' DNA flap DNA substrate (5 nM) in the presence of increasing concentrations of CTC1/STN1/TEN1 (250, 750, 1500 nM) or CST (5, 15, 60 nM) as denoted in the figure. The red asterisk shown on the substrate in the figure represents the location of the 32P radiolabel. Gel shown is representative of at least three independent experiments. (B) Graph of the fold increase in FEN1 cleavage activity for each of the lanes containing the highest concentration of CST proteins utilized. (C) Shows the fold increase in FEN1 cleavage activity on a telomere substrate calculated as in (B). The error bars represent the standard error mean. The random substrate (U7:T5:D4) and telomere substrate (U8:T6:D5) was generated by annealing primers in a 4:2:1 ratio (Experiments performed by Brandon Wysong of the Balakrishnan lab).

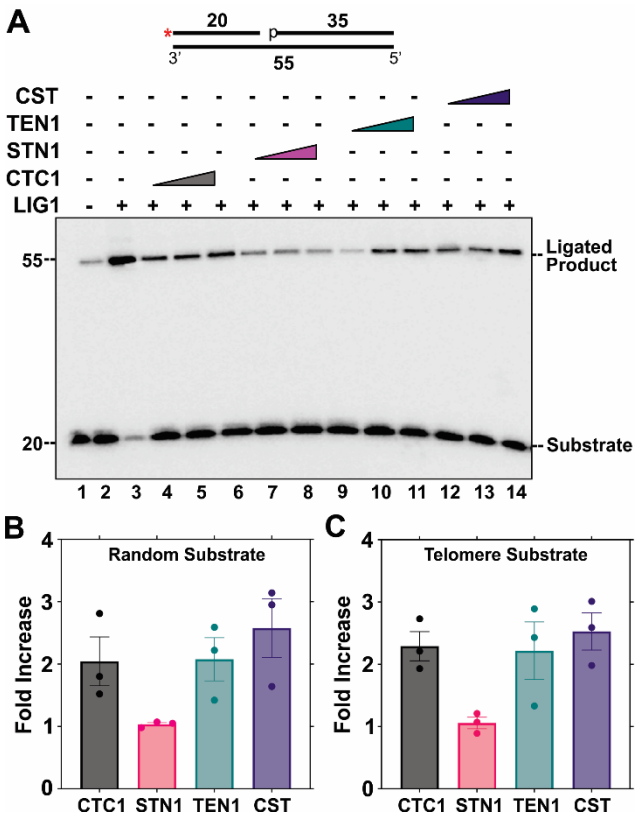

Figure 3.10 ***The CST complex, CTC1 and TEN1 stimulate ligation efficiency of LIGI.*** (A) LIGI (0.05 nM, lanes 2, 4-15; 100 nM, lane 3) ligation activity was measured on a nicked DNA substrate (5 nM) in the presence of increasing concentrations of CTC1/STN1/TEN1 (250, 750, 1500 nM) or CST (5, 15, 45 nM) as denoted. The red asterisk shown on the substrate in the figure represents the location of the 32P radiolabel. Gel shown is representative of at least three independent experiments. (B) Graph of the fold increase in LIGI ligation activity for the lanes containing the highest concentration of CST proteins utilized. (C) Shows the fold increase in LIGI ligation activity on a telomere substrate calculated as in (B). The error bars represent the standard error mean. The random substrate (U9:T1:D6) and telomere substrate (U10:T4:D7) was generated by annealing primers in a 1:2:4 ratio (Experiments performed by Brandon Wysong of the Balakrishnan lab).

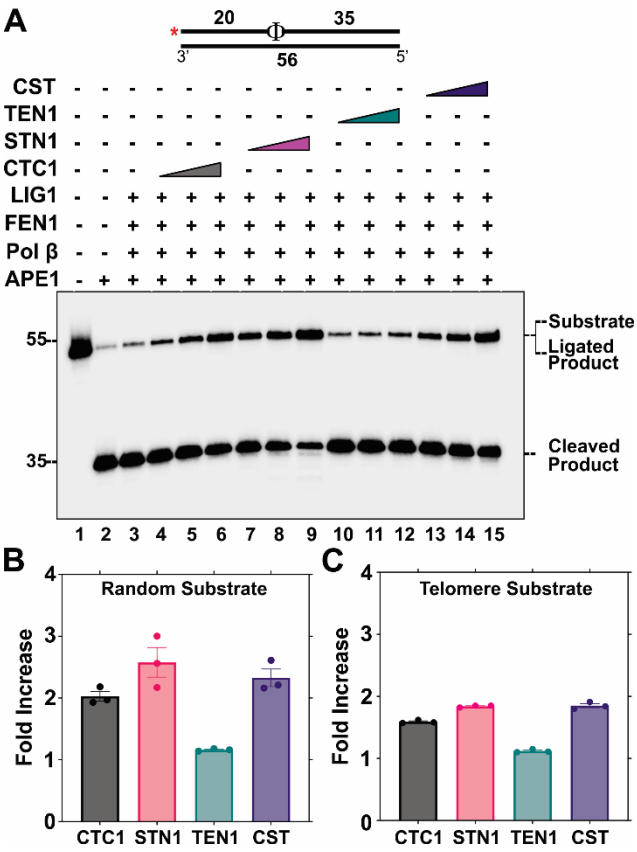

Figure 3.11 ***The CST complex, CTC1 and STN1 increase the efficiency of LP-BER.*** (A) The LP-BER pathway was reconstituted in vitro by combining APE1 (3 nM), Pol β (0.5 nM), FEN1 (0.01 nM), and LIGI (0.1 nM) on a random sequence abasic substrate containing a tetrahydrofuran (THF) residue (5 nM). An Φ represents a THF residue and a red asterisk represents the location of the 32P radiolabel on the substrate. The ligation efficiency was monitored following the addition of CTC1/STN1/TEN1 (100, 500, 1000 nM) or CST complex (14.75, 29.5, 59 nM) as denoted. Gel shown is representative of at least three replicate experiments. (B) Graph of the fold increase in ligation efficiency for the lanes containing the highest concentration of CST proteins utilized. (C) Shows the fold increase in ligation efficiency on a telomere substrate calculated as in (B). The error bars represent the standard error mean. The random substrate (U4:T1) and telomere substrate (U5:T4) was generated by annealing primers in a 1:2 ratio (Experiments performed by Brandon Wysong of the Balakrishnan lab).

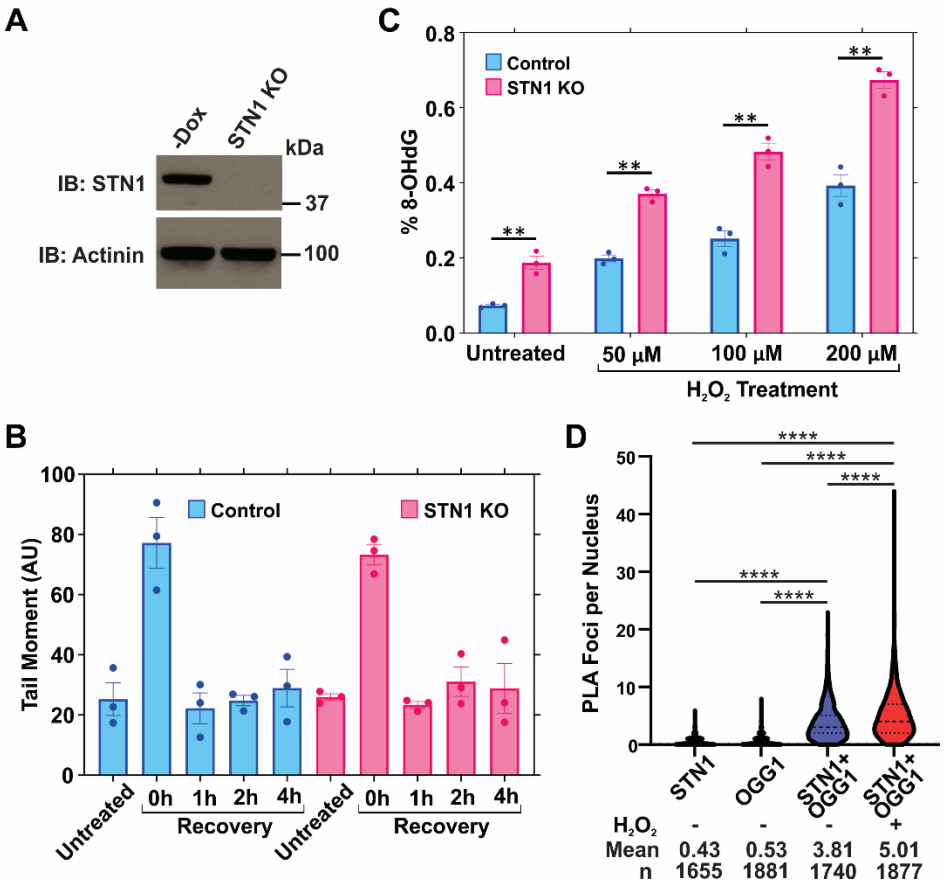

Figure 3.12 ***CST prevents the accumulation of genomic 8-oxo-Gs.*** (A) Western blot of STN1 levels in HeLa iCas9 sgSTN1 cells. Actinin serves as a loading control. +Dox indicates cells treated with doxycycline to induce Cas9 expression and STN1 gene disruption (STN1 KO). (B) Parental and STN1 KO cells were treated for 1 hour (h) with 100 μM H_2O_2 before being released for the either 0, 1, 2 or 4 h. Cells were then collected, an alkaline comet assay performed, and tail moments quantified. n = 3 independent, biological replicates. The error bars represent the standard error mean. (C) Parental and STN1 KO cells were treated with 0, 50, 100 or 200 μM H_2O_2 for 1 h before release and recover for 4 h. Cells were collected, and genomic DNA extracted and 8-oxoG levels measured. A representative trial of 3 independent biological trials is shown (see Figure S3 for additional trials). Circles represent three technical replicates. The error bars represent the standard error mean. (∗∗p < 0.01). (D) Proximity ligation assay (PLA) performed in HeLa cells with antibodies to STN1, OGG1, or in combination (STN1+ OGG1). n = 3 independent, biological experiments. Bold dashed line: median, dashed lines: first and third quartiles. (****p < 0.0001). (Comet assays were performed by Dr. Jacob Massey of the Wyatt lab).

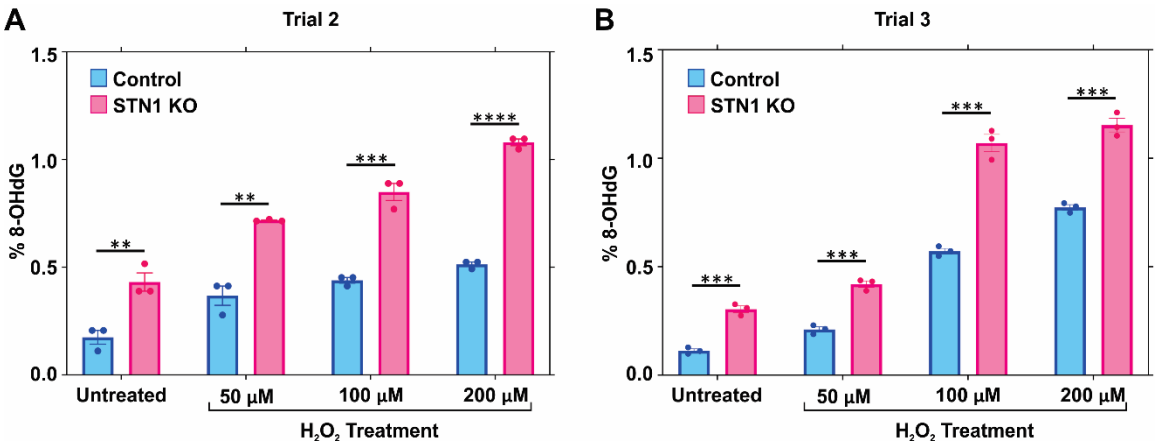

Figure 3.13 ***Additional trials of 8-oxoG levels in STN1 KO cells.*** Independent, biological replicates of 8-oxoG levels in parental and STN1 KO cells. Circles represent three technical replicates. See Figure 3.12 for additional details. (**P < 0.01 *** P < 0.001 ****P < 0.0001).

CHAPTER 4

THE DNA-BINDING PROTEIN CST ASSOCIATES WITH THE COHESIN COMPLEX AND PROMOTES CHROMOSOME COHESION

(Schuck, P.L., Ball, L.E., Stewart, J.A. (2021) *Journal of Biological Chemistry.* 297:101026)

4.1 ABSTRACT

Sister chromatid cohesion (SCC), the pairing of sister chromatids after DNA replication until mitosis, is established by loading of the cohesin complex on newly replicated chromatids. Cohesin must then be maintained until mitosis to prevent segregation defects and aneuploidy. However, how SCC is established and maintained until mitosis remains incompletely understood, and emerging evidence suggests that replication stress may lead to premature SCC loss. Here, we report that the ssDNA-binding protein CTC1-STN1-TEN1 (CST) aids in SCC. CST primarily functions in telomere length regulation but also has known roles in replication restart and DNA repair. After depletion of CST subunits, we observed an increase in the complete loss of SCC. In addition, we determined that CST associates with the cohesin complex. Unexpectedly, we did not find evidence of altered cohesin loading or mitotic progression in the absence of CST; however, we did find that treatment with various replication inhibitors increased the association between CST and cohesin. Because replication stress was recently shown to induce SCC loss, we hypothesized that CST may be required to maintain or remodel SCC after DNA replication fork stalling. In agreement with this idea, SCC loss was greatly increased in CST-depleted cells after exogenous replication stress. Based on our findings, we propose that CST aids in the maintenance of SCC at stalled replication forks to prevent premature cohesion loss.

4.2 INTRODUCTION

As DNA is replicated, the sister chromatids must be held together until mitosis to ensure chromosomes are properly segregated between daughter cells. This process, known as sister chromatid cohesion (SCC), is facilitated by the cohesin complex [59,

167]. In mammals, the cohesin complex is composed of a ring-like structure that encircles the DNA. The core structure is composed of SMC3, SMC1A, SCC1/RAD21, and SA1 or SA2. Cohesin loading and removal is tightly regulated during the cell cycle [168-170]. In G1 phase and early S phase, cohesin is loaded onto chromatin but not stably bound. As the DNA is replicated, cohesin is passaged to the replicated sister chromatids and becomes stably bound until mitosis when it is removed to allow segregation of the chromatids into daughter cells. In addition to its essential role in SCC, the cohesin complex is involved in organizing topologically associated domains for cellular processes such as DNA repair and gene expression [171]. Moreover, several recent studies found that replication stress causes perturbation in cohesin dynamics at stalled replication forks and premature SCC loss in human cells [66, 172, 173].

In this study, we present unexpected findings that human CTC1-STN1-TEN1 (CST) helps maintain SCC. CST is an replication protein A (RPA)-like, ssDNA-binding protein that is conserved from yeast to humans [3]. CST primarily functions in telomere length regulation; however, it has also been shown to function in DNA replication and repair [12, 174]. Although its role in DNA replication is still not well understood, it is proposed to aid in the replication of G-rich DNA sequences, such as telomeres, promote dormant origin firing, and negatively regulate origin licensing [7, 36, 37, 175]. CST also interacts with several components of the replication machinery, including DNA polymerase α-primase, the MCM2-7 helicase, and AND-1/Ctf4 [25, 27, 36]. Together, these findings provide strong evidence that CST is involved in DNA replication, presumably as a specialized versus general replication factor.

Here, we report that depletion of CST leads to premature SCC loss. Furthermore, we show that CST associates with the cohesin complex, suggesting that CST may directly influence SCC. Upon further investigation, we found that the association between cohesin and CST is increased after replication stress and CST prevents SCC loss after treatment with several replication inhibitors. Together, our findings identify CST as a new factor involved in preventing premature cohesion loss and suggest that it does so by stabilizing cohesion after replication fork stalling.

4.3 RESULTS

4.3.1 DEPLETION OF CST RESULTS IN SCC LOSS

While performing telomere-FISH in STN1 knockdown cells, we consistently observed metaphase spreads that had lost SCC. To determine whether depletion of STN1 increased cohesion loss, we quantified the number of metaphase spreads with SCC loss in HeLa cells with stable shRNA knockdown of STN1 (shSTN1) (Figure 4.1, A–C) [37]. Only metaphase spreads with at least 50% of the chromosomes having lost complete cohesion were scored as loss. By and large, these metaphase spreads had completely lost cohesion on all chromosomes, as shown in Figure 1B. In agreement with our observation, we observed a 2- to 4-fold increase in premature SCC loss in two separate shSTN1 clones, shSTN1-6 and shSTN1-7 (Figure 4.1 C and Figure A.1 C). Furthermore, this increase was largely rescued by stable expression of a Flag-tagged shRNA-resistant STN1 construct in shSTN1-7 cells (shSTN1-7 +Flag-STN1). Previous studies suggest that a common off-target effect of RNA interference is MAD2 depletion [101]. Loss of MAD2 also results in premature SCC loss. However, MAD2 levels were measured in the

shSTN1 cells, and no significant changes were observed compared with controls (Figure 4.1A).

To confirm our findings, we next performed mitotic shake-off to measure SCC loss after STN1 depletion. Processing of cells for standard metaphase spread analysis includes treatment with a hypotonic solution, which can release proteins from the chromatin [102]. If cohesion is only partially lost, this can exacerbate SCC loss. To address this possibility, mitotic cells were collected, fixed, and spun onto slides without hypotonic treatment. Unlike standard metaphase spread preparation, chromosomes from cytospun metaphase cells are not clearly separated. Therefore, a chromosome-specific probe to centromere 6 was used to assess SCC loss by FISH, as previously described [103]. Because HeLa cells are triploid for chromosome 6, three spots indicate the retention of SCC, whereas greater than three spots indicate loss. Consistent with metaphase spread analysis, knockdown of STN1 led to a significant increase in SCC loss (Figure 4.1 D and E and Figure A.1 C). However, the fold increase was less than that observed by standard metaphase spread analysis (Figure 4.1C). This may be due to weakened but not complete SCC loss in a subset of cells or differences between the methodologies used.

Next, we determined whether cohesion loss was specific to STN1 depletion or due to a general CST loss. siRNA knockdown of CTC1, STN1, or TEN1 was performed followed by metaphase spread analysis (Figure 4.1, F and G and Figure A.1 C). Like shSTN1 cells, transient siRNA knockdown of individual CST subunits resulted in increased SCC loss. Finally, we confirmed that this phenotype was not cell-type specific by demonstrating SCC loss in HCT116 cells with conditional CTC1 KO (Figure A.1 A

and B) and in both HCT116 and HEK293T cells with siRNA knockdown of STN1 (Figure A.1 D–F and J). Interestingly, the background percentage of loss in the HCT116 cells was significantly lower than in HeLa and HEK293T cells (Figure A.1 E and F). This is likely due to HCT116 cells having an intact p53 response (Figure A.1 G) [41]. In addition, CTC1 deletion [41] or STN1 depletion (Figure A.1 H) in the HCT116 cells increased the number of G2/M, subG1, and aneuploid (>4n) cells, whereas no cell cycle defects were observed in HeLa [37] or HEK293T (Figure A.1 I) cells after STN1 depletion. Like HeLa cells, HEK293T cells have a defective p53 response (Figure A.1 G). However, regardless of p53 status, depletion of CST subunits increased SCC loss, suggesting that this phenotype is independent of p53. Together, these results indicate that CST promotes SCC.

4.3.2 CST ASSOCIATES WITH THE COHESIN COMPLEX

We next addressed whether CST is associated with the cohesin complex by coimmunoprecipitation (co-IP) and proximity ligation assay (PLA) (Figure 4.2). IP of epitope-tagged CST pulled down both endogenous SMC3 and SMC1A (Figure 4.2A). To determine whether the association between cohesin and CST was through CTC1 or STN1, co-IP was performed with expression of Flag-CTC1 or Flag-STN1. STN1 alone pulled down SMC3, although at lower levels. Pulldown of CTC1 showed little to no association with SMC3 or SMC1A. This suggests that the entire CST complex, or at least multiple subunits, may be required for stable association with cohesin. As further confirmation of CST–cohesin association, we identified both SMC1A and SMC3 by MS after IP of Flag-STN1 in cells overexpressing all three CST subunits (Figure A.2). Furthermore, PLA was performed using antibodies to endogenous STN1 and SMC3 to

detect their association in cells (Figure 4.2B) [104]. PLA analysis showed ~6 foci on average per cell compared with single antibody controls (Figure 4.2B). For comparison, PLA with STN1 and known CST-interacting partners DNA polymerase α-primase and MCM2-7 showed 2.5 and 2.3 foci per cell on average, respectively, suggesting that CST–cohesin association is fairly robust and the number of PLA foci is likely an underrepresentation of their total colocalization in the cell (Figure A.3) [25, 27, 36, 105]. Combined with the co-IP data, these findings reveal an unanticipated association between CST and the cohesin complex.

2.3.3 CST IS NOT REQUIRED FOR SMC3 ACETYLATION, COHESIN LOADING, OR MITOTIC PROGRESSION

A possible explanation for SCC loss after CST depletion is that it stabilizes cohesin loading or establishment [106, 107]. Before genome duplication, cohesin binding is unstable and cohesin molecules quickly associate/dissociate from the DNA [108]. As the genome is duplicated, cohesin is transferred from the unreplicated to the replicated sister chromatids and becomes stably bound. This process is partially facilitated by the acetylation of SMC3 (Ac-SMC3) [60, 61, 109, 110]. Because CST aids in DNA replication, we tested whether Ac-SMC3 or the levels of total or chromatin-bound cohesin were decreased in STN1-depleted cells (Figure 4.3, A–C and Figure A.4 A and B). However, we did not observe any changes in either Ac-SMC3 or chromatin-bound cohesin.

We next investigated whether mitotic progression was altered using live-cell imaging (Figure 4.3, D and E). To visualize mitotic events, an H2B construct fused with red fluorescent protein was stably transduced into STN1-depleted and control cells [111].

Cells were plated and imaged at 5-min intervals over a 3-h period. The time from prophase to the completion of cytokinesis was then measured as a readout of mitotic progression (Figure 4.3D). Mitosis took approximately 1 h in the HeLa cells, consistent with previous studies [112]. On average, shSTN1 cells took ~5 min less to complete mitosis compared with control cells (Figure 4.3E). Further breakdown of the timing from prophase to metaphase or metaphase to cytokinesis did not reveal any significant changes (Figure A.4 C). While there was a slight decrease in overall timing of mitotic progression in shSTN1 cells, these changes are unlikely to explain the increase in SCC loss. Why premature loss of SCC does not lead to defects in mitotic progression in cells lacking CST is not entirely clear. However, work in Drosophila suggests that premature SCC loss is not always sufficient to trigger a robust spindle assembly checkpoint and that mitosis can still occur [113, 114]. Moreover, recent work showed that various cancer cell lines continue to grow despite significant levels of cohesion loss [66, 107]. Accordingly, mitotic progression and cell division may be unaffected despite increased SCC loss in STN1-depleted cells.

4.3.4 CST PROMOTES CHROMOSOME COHESION AFTER REPLICAITON STRESS

Because CST aids in DNA replication restart and SCC loss has been linked to replication stress, we sought to determine whether chemically induced replication stress would increase CST-cohesin association. Cells were treated with hydroxyurea (HU) or aphidicolin (APH) for 2 h or camptothecin (CPT) for 1 h. PLA was then performed with antibodies to endogenous STN1 and SMC3 (Figure 4A). In all cases, we observed an ~2-fold increase in PLA foci, indicating increased association after replication stress

compared with untreated cells. This 2-fold increase is similar to increases observed in replication protein A-bound replication sites by PLA after HU treatment [115]. This suggested to us that CST may prevent SCC loss after replication stress, so we tested SCC levels after treatment with replication inhibitors in shSTN1 cells. After treatment, cells were released into fresh media for 6 h, to allow cells in S phase to reach mitosis. They were then treated with colcemid, collected, and prepared for metaphase spread analysis (Figure 4B and Figure A.5). In agreement with previous findings, SCC loss increased when cells were treated with replication inhibitors [66, 98]. (CPT likely has the greatest effect because it is not reversible like HU and APH.) However, in the STN1-depleted cells, premature SCC loss was greatly increased above shNT cells, consistent with CST promoting SCC after replication stress.

4.4 DISCUSSION

In this study, we present data that CST is involved in chromosome cohesion, potentially through its association with the cohesin complex. Despite significant levels of SCC loss in CST-depleted cells, we did not detect defects in global cohesion levels, SMC3 acetylation, or mitotic progression. Instead, CST appears to be involved in SCC maintenance/remodeling at stalled replication forks. This idea is in line with recent work demonstrating that replication stress, caused by expression of oncogenes or treatment with DNA replication inhibitors, induces SCC loss in human cells [66, 98]. Based on our data, we propose that CST acts at stalled replication forks to maintain or remodel chromosome cohesin after fork stalling or during fork restart (Figure 4.4C). These findings highlight an unexpected function of CST in preserving genome integrity through the maintenance of SCC.

Over a decade ago, depletion of the replication fork stability factors Tipin/Tim and AND1 were shown to increase SCC loss, indirectly associating replication defects with chromatid cohesion [116-119]. Additional studies have implicated other DNA replication and repair factors in chromatid cohesion, and this past year, a pair of studies provided direct evidence that chemically induced replication stress leads to SCC loss in humans [66, 98]. Both of these recent studies suggested that the cohesin antagonist WAPL is involved in cohesion maintenance after replication stress. Benedict et al. propose a model where WAPL removes cohesin to allow replication fork restart through RAD51-dependent mechanisms. Interestingly, CST is proposed to load RAD51 after fork stalling [100]. Therefore, CST could be a key player in cohesin dynamics at stalled forks by facilitating fork restart and cohesion reestablishment. However, other studies suggest that cohesion is reinforced at stalled replication forks and double-strand breaks, in apparent contradiction to the previously mentioned studies [120]. These studies, mostly performed in budding yeast, indicate that cohesin is recruited to stalled or collapsed replication forks for activation of the DNA damage response and homology-based fork restart. How this is reconciled with recent work, including this study, will require molecular characterization of the players involved. However, it likely depends on the fate of the replication fork after initial stalling and what happens to cohesin after the "repair" event. It is also possible that cohesin dynamics at stalled replication forks differs in humans compared with lower eukaryotes, although evidence of cohesion reinforcement has also been observed in human cells after ionizing radiation [65].

Another potential link between CST and cohesion maintenance is that CST interacts with both MCM2-7 and AND-1 [36]. Recent work identified interaction

between the MCM2-7 helicase and ESCO2 as necessary for cohesion establishment [60, 61, 106]. As mentioned above, AND-1 is involved in replication fork stability and helps maintain SCC [118]. Studies in yeast suggest that AND-1 (known as Ctf4 in yeast) stabilizes critical interactions between replisome components and the Chl1 helicase, which is involved in chromatid cohesion [121, 122]. We previously showed that loss of CST leads to decreased chromatin-bound AND-1, which could provide an explanation for increased SCC loss in the absence of CST. CST could also directly interact with cohesin to promote cohesin remodeling or reestablishment. However, our results have not definitively shown whether CST directly interacts with cohesin or is associated with it via interactions with components of the replisome, such as MCM2-7. Future work is needed to define how specific interactions at the replication fork affect chromosome cohesion and fork restart/protection after stalling.

While the function of CST in replication restart/rescue is still unclear, CST is not a general replication factor but rather plays a specialized role in facilitating replication through G-rich regions of the genome (e.g., telomeres, CpG islands) [7, 37, 100]. Because CST promotes replication at specific sites, one might predict that the absence of CST would cause partial versus total loss of chromosome cohesion, as has been previously observed with depletion of the cohesin subunits SA1 or SA2 [103]. Instead, CST depletion leads to complete SCC loss by metaphase spread analysis and mitotic shake-off (Figure 4.1). These findings demonstrate that SCC loss is not restricted to telomeres or specific regions of the genome but instead a complete breakdown of SCC. The reason for complete cohesion loss remains unclear. However, recent studies suggest that complete cohesion loss is common across a variety of cancer cells, which seems to

have little effect on cellular division [66]. It is possible that the gradual accumulation of SCC loss due to replication stress or excessive DNA damage triggers genome-wide cohesin unloading through an unknown mechanism. Perhaps such a pathway is used to induce cell death and prevent the propagation of cells with high levels of genome instability induced by replication stress. In cancer, such pathways could be disengaged to allow cell division and aneuploidy, despite SCC loss. However, future studies are required to fully investigate the connection between replication stress, SCC, and aneuploidy.

4.5 EXPERIMENTAL PROCEDURES

4.5.1 CELL CULTURE

HeLa 1.2.11 cells were cultured in RPMI 1640 media, HEK293T in DMEM, and HCT116 in McCoy's 5A media supplemented with 10% fetal bovine serum and 1% penicillin/streptomycin at 37 °C with 5% CO2. Stable HeLa 1.2.11 shRNA knockdown and HCT116 *CTC1* inducible KO lines have been previously described [37, 44]. Cell lines were regularly checked for Mycoplasma contamination. siRNA experiments were performed using 25 nM ON-TARGETplus siRNA SMARTpool (Dharmacon) to *CTC1* (L-014585-01), *STN1* (L-016208-02), *TEN1* (L-187549-00), or nontargeting control (D-00180-10). siRNAs were transfected into cells with Lipofectamine RNAiMAX (Thermo Fisher Scientific) for 72 h before collection.

4.5.2 METAPHASE SPREADS

Metaphase spreads were prepared as previously described [176] and then stained for 8 to 10 min with Giemsa stain (Ricca Chemical). SCC loss was counted when at least

half of the chromosomes had lost complete cohesion. In most cases, the entire metaphase spread had lost complete cohesion.

4.5.3 WHOLE-CELL LYSATE, CHROMATIN FRACTIONATION, AND WESTERN BLOT ANALYSIS

These techniques were performed, as previously described [36].

4.5.4 ANTIBODIES AND CHEMICAL INHIBITORS

Primary:The primary antibodies used were as follows: SMC1A (Bethyl Laboratories, A300-055A), SMC3 (Bethyl Laboratories, A300-060A), acetylated SMC3 (kindly provided by Dr Prasad Jallepalli), RAD21 (SCC1) (Bethyl Laboratories, A300-080A), SCC-112 (PDS5) (Bethyl Laboratories, A300-089A), OBFC1 (STN1) (Novus Biologicals, NBP2-01006), CTC1 [44], α-tubulin (MilliporeSigma, T-9026), TEN1 [177], MAD2 (Bethyl Laboratories, A300-301A), α-actinin (Santa Cruz Biotechnology, SC17829), H3 (Cell Signaling Technology, 9715), Flag (Thermo Fisher Scientific, MA1-91878, PA1-984B), PolA1 (Bethyl Laboratories, A302-805A), MCM7 (Santa Cruz Biotechnology, sc22782), p53 (Cell Signaling Technology, 2524S), and p21 (Santa Cruz Biotechnology, sc-6246).

Secondary: The secondary antibodies used were from Thermo Fisher Scientific: anti-rabbit-HRP (32460), anti-mouse-HRP (32430), goat anti-rabbit Alexa Fluor 594 (A-11037).

Chemical inhibitors: Cells were treated with APH (1 μM, MilliporeSigma, 178273) or HU (2 mM, MilliporeSigma, 400046) for 2 h or (S)-(+)-CPT (1 μM, MilliporeSigma, C9911) for 1 h.

2.5.5 LIVE-CELL IMAGING

MSCV-H2B-mRFP1 was created by replacing GFP in MSCV-GFP with the H2B-mRFP1 from pCS-H2B-mRFP1, using NotI and XhoI. pCS-H2B-mRFP1 was a gift from Dr Sean Megason (Addgene #53745) and MSCV-GFP a gift from Dr Tannishtha Reya (Addgene #20672). HeLa cells were transduced with retrovirus produced in HEK293T, and RFP-positive cells were selected through two rounds of fluorescence-activated cell sorting. Approximately 3000 cells were plated into 96-well Incucyte ImageLock plates 24 h before imaging. Cells were then imaged at 5-min intervals for 3 h under a 20× objective, using the Incucyte S3 Live-Cell Analysis System.

4.5.6 FISH

After collection, cells were washed with PBS and fixed by dropwise addition of Carnoy's solution (3:1 methanol:acetic acid) with gentle vortexing. Cells were incubated on ice for 10 min and spun down, and the supernatant was removed. Fresh Carnoy's solution was then added and cells stored at 4 °C. Before cytospin, cells were counted and resuspended in fresh Carnoy's solution to a concentration of approximately 500 cells/µl. One hundred microliters of cell suspension was then spun onto slides at 10,000 rpm for 2 min using 3-well adaptors (StatSpin CytoFuge 2). Slides were washed with Carnoy's solution and allowed to dry. Chromosome-specific FISH was then performed with a Texas Red-labeled chromosome 6 alpha satellite probe, following the manufacturer's protocol (Cytocell).

4.5.7 IMMUNOFLOURESCENCE

Cells were pre-extracted with ice-cold 1× CSK buffer (10 mM Hepes, pH 7.4, 0.3 M sucrose, 100 mM NaCl, 3 mM MgCl2) containing 0.1% Triton X-100 for 2 min at

room temperature (RT) and then fixed with ice-cold 100% methanol at −20 °C for 10 min. Immunofluorescence was then performed as previously described [36].

4.5.8 CO-IP

Co-IP was performed as previously described [36]. Plasmids used include pcDNA3.1-Flag-CTC1, pcDNA3.1-Flag-STN1, and pCMV6-TEN1 [36, 37].

2.5.9 PLA

HeLa 1.2.11 cells were fixed for 20 min at RT with 4% formaldehyde in 1× PBS followed by permeabilization with 100% methanol for 20 min at −20 °C. Subsequent steps were performed with the Duolink PLA kit (MilliporeSigma) as previously described [101], except the first wash after primary incubation was performed using wash buffer A, not 5% BSA in 1× PBS. The following primary antibodies were used: 1:100 mouse α-STN1, 1:600 rabbit α-SMC3, 1:100 rabbit α-PolA1, and 1:500 rabbit α-MCM7.

4.5.10 IMAGE ANALYSIS AND STATISTICS

For immunofluorescence, FISH, and PLA, images were taken on an EVOS FL microscope, using a 40× or 60× objective (Thermo Fisher Scientific). At minimum, five images were scored per independent, biological experiment for each condition. Image analysis (Figs. 2B and 3B and Figs. S3 and S4) was performed with CellProfiler. Error bars indicate the ±SEM of at least three independent biological experiments. All p-values were calculated by an unpaired, two-tailed t test.

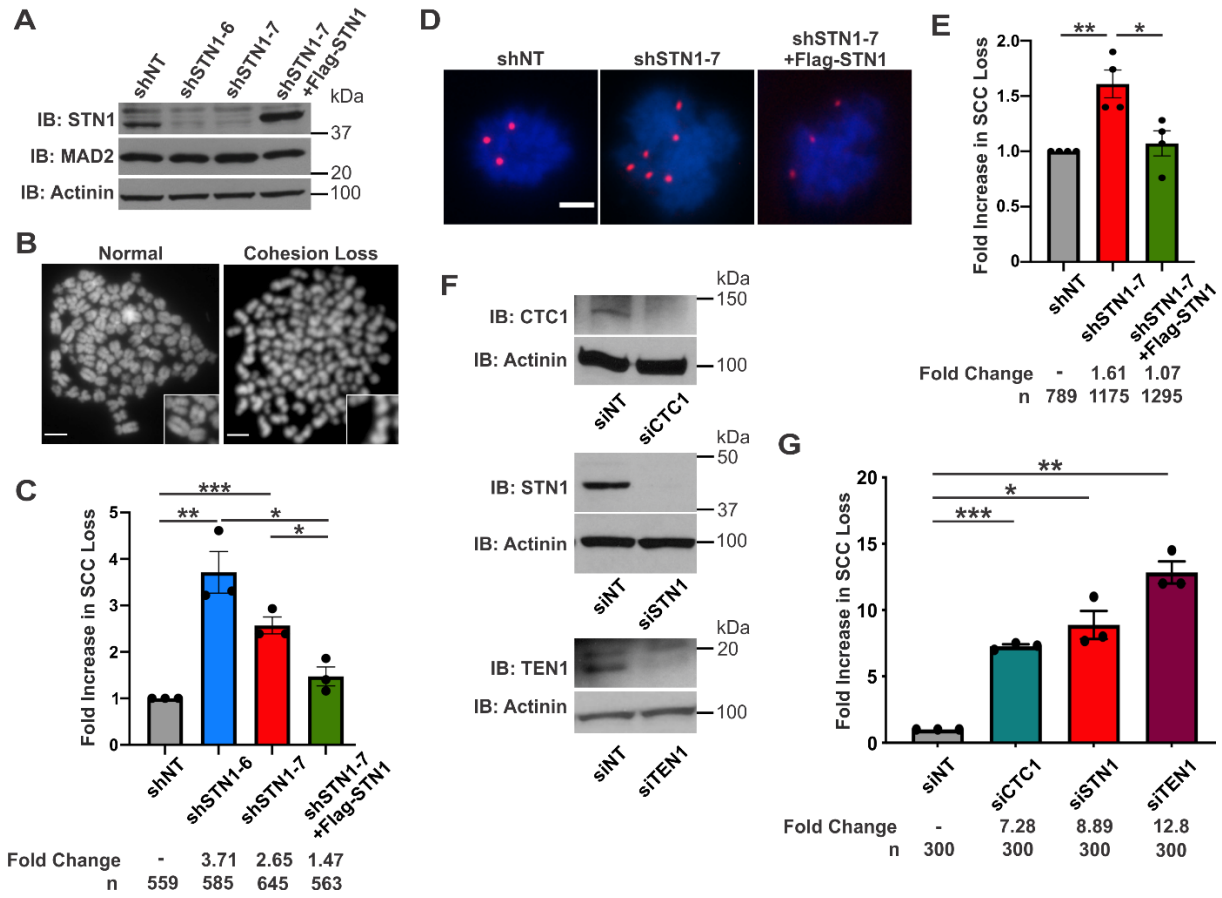

Figure 4.1 ***CST deficiency results in SCC loss.*** A, Western blot of STN1 knockdown and MAD2 levels in HeLa cells. Actinin was used as the loading control. B, example images of metaphase spreads with normal chromosomes or SCC loss. The scale bar represents 5 μm. C, fold increase in cohesion loss after metaphase spread analysis. n = 3 independent, biological replicates. D, representative images of chromosome FISH from cells isolated by mitotic shake-off. Red represents centromere 6 probe; blue represents DAPI. The scale bar represents 5 μm. E, fold increase in nuclei with >4 chromosome 6 foci. n = 4 independent, biological replicates. F, knockdown of CTC1, STN1, or TEN1 by siRNA in HeLa cells. siNT was used as the nontarget control and actinin as the loading control. G, graph of SCC loss after metaphase spread analysis, as indicated. n = 3 independent, biological replicates. (∗p < 0.05, ∗∗p < 0.01, and ∗∗∗p < 0.001). CST, CTC1-STN1-TEN1; SCC, sister chromatid cohesion; shNT, nontargeting shRNA; shSTN1, shRNA knockdown of STN1; shSTN1+Flag-STN1, shSTN1-7 cells plus shRNA-resistant Flag-STN1.

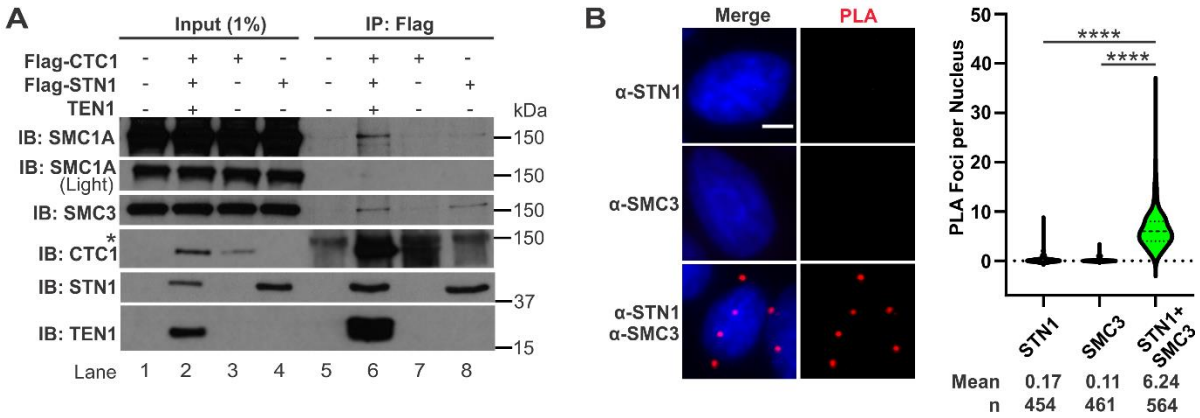

Figure 4.2 ***CST associates with the cohesin complex***. A, co-IP of nuclease-treated lysates from HEK293T cells expressing Flag-tagged CTC1, Flag-tagged STN1, or the full CST complex. The asterisk indicates background band. B, representative images of proximity ligation assay (PLA) performed in HeLa cells with antibodies to STN1 or SMC3 alone or in combination. Red represents PLA foci; blue represents DAPI. The scale bar represents 5 μm. C, violin plot of PLA foci per nucleus. Results are representative of four independent, biological experiments. Bold dashed line represents the median, and dashed lines represent the first and third quartiles. (****$p < 0.0001$). co-IP, coimmunoprecipitation; CST, CTC1-STN1-TEN1.

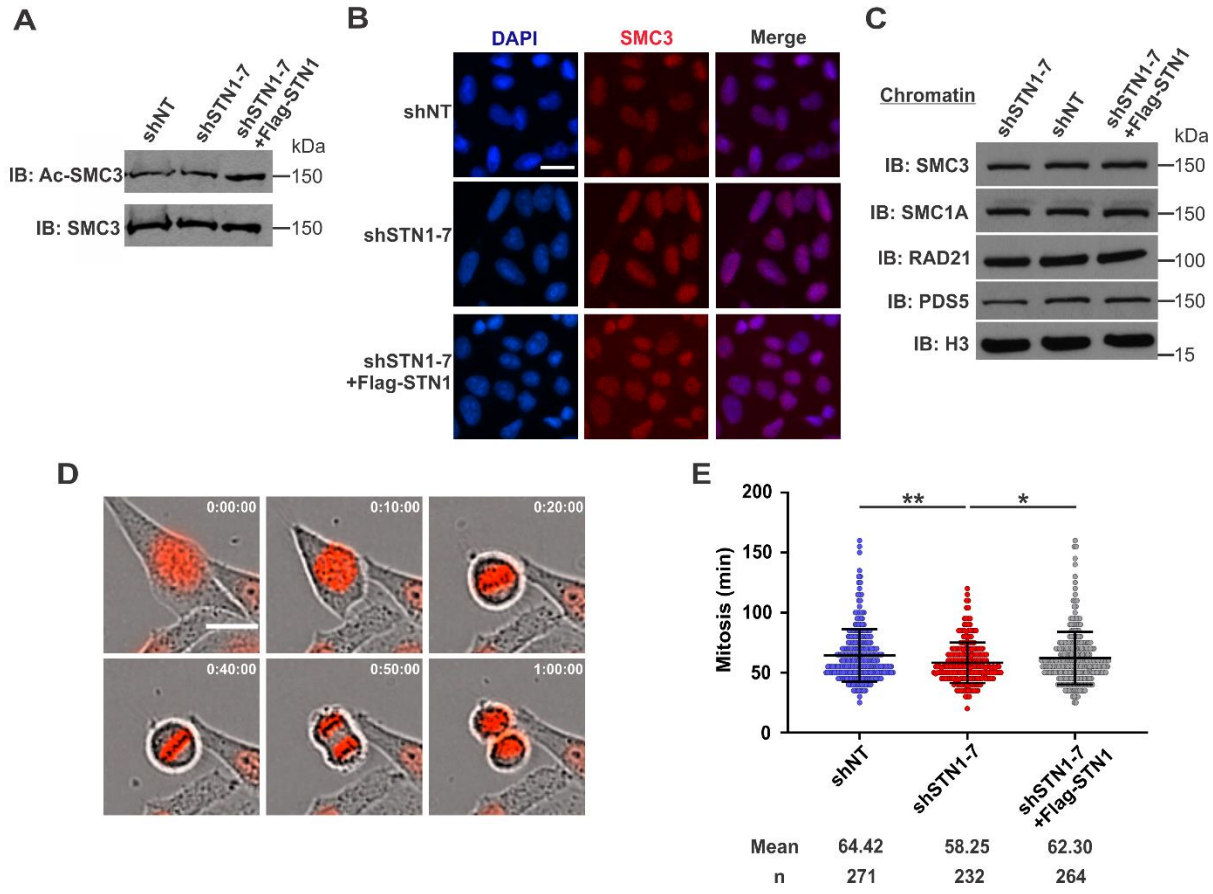

Figure 4.3 ***STN1 depletion does not affect cohesin levels or mitotic timing***. A, Western blot analysis of total SMC and acetylated SMC3 (Ac-SMC3) in HeLa cells, as indicated. B, representative images of SMC3 levels in pre-extracted cells. DAPI is shown in blue and SMC3 in red. The scale bar represents 20 μm. C, Western blot of chromatin-bound cohesin subunits. Histone H3 was used as the loading control. D, HeLa cells stably expressing H2B-RFP were imaged in 5-min intervals for 3 h. The scale bar represents 20 μm. E, dot plot of the time between nuclear envelope breakdown until cytokinesis in individual cells. Black lines and numbers below the graph indicate the average time in minutes to complete mitosis. ($*p < 0.05$ and $**p < 0.01$).

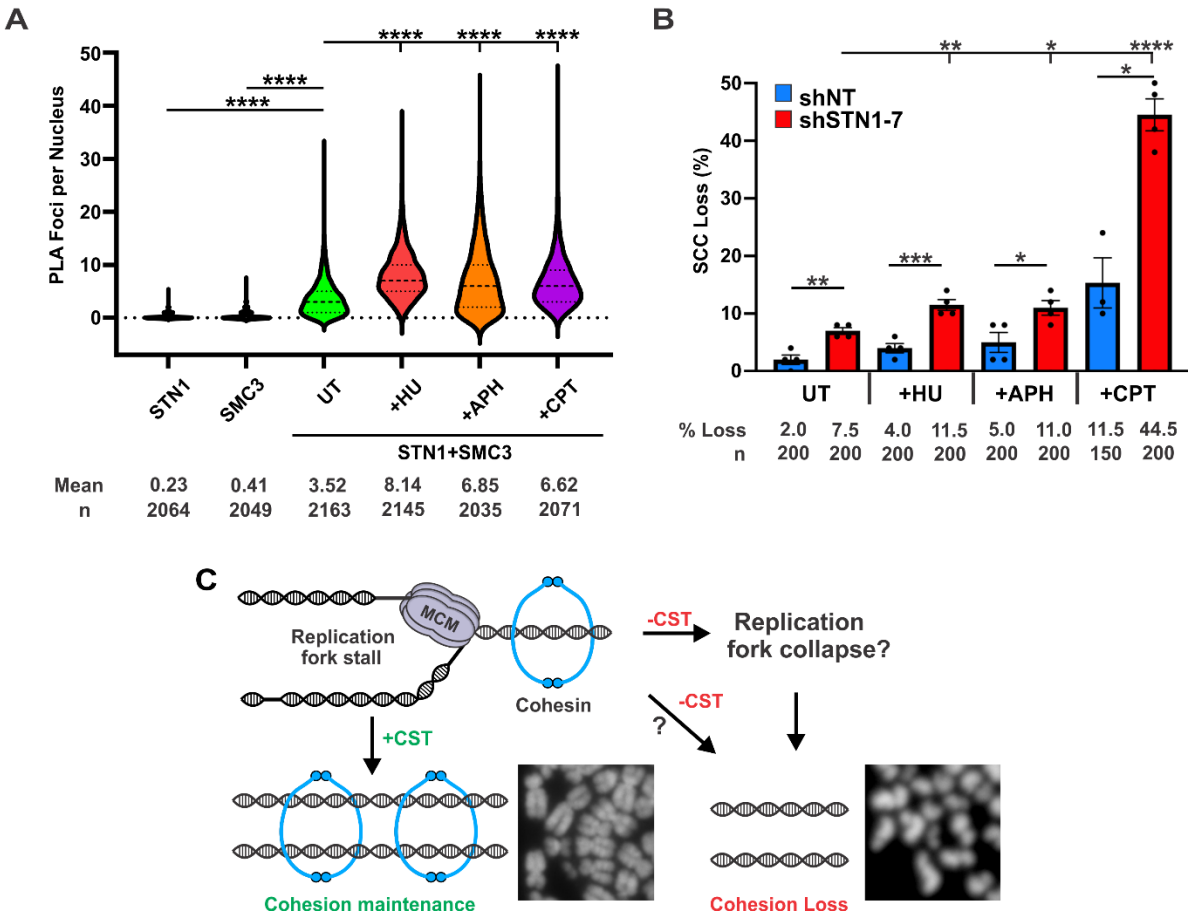

Figure 4.4 ***Replication inhibition increases CST–cohesin association and SCC loss in STN1-depleted cells***. A, violin plot of nuclear PLA foci in HeLa cells after treatment with DNA replication inhibitors. Treatment: hydroxyurea (HU) and aphidicolin (APH) for 2 h and camptothecin (CPT) for 1 h. The bold dashed line represents median and dashed lines the first and third quartiles. n = 3 independent, biological replicates. B, cohesion loss in HeLa shNT and shSTN1 cells after replication stress. Cells were treated with replication inhibitors as in panel A and then released for 8 h before metaphase spread preparation. Colcemid was added 2 h before collection. n = 3 independent, biological replicates. (∗p < 0.05, ∗∗p < 0.01, ∗∗∗p < 0.001, and ∗∗∗∗p < 0.0001). C, model of proposed CST function in cohesin maintenance. Images were cropped from those found in Figure 1B. CST, CTC1-STN1-TEN1; PLA, proximity ligation assay; SCC, sister chromatid cohesion; shSTN1, shRNA knockdown of STN1.

CHAPTER 5

DISCUSSION

5.1 INTRODUCTION

Since its discovery as a Pol α accessory factor, CST has been found to be involved in a number of processes that maintain and preserve genomic DNA. Particularly in DNA replication and repair. Protecting DNA is something CST has in common with the protein it shares the most homology, RPA. As CST is not very abundant it is unlikely it can perform as universal a role as RPA in protecting ssDNA, especially with the ability of RPA to bind shorter substrates, even though they both have similar binding ability on longer substrates [40]. Due to the relatively low amount of CST in the cell its roles when it comes to DNA metabolism must be in response to specific situations. Through the interaction and stimulation of Pol α we know that CST is involved in telomere regulation through C-strand fill in and resection fill-in when it comes to DSBs, whereas RPA mainly protects ssDNA and is excluded from telomeres by POT1 [138, 142, 178-180]. Also, as CST does not have a nuclear localization signal, it has been shown the complex is reliant on its interaction with Pol α to enter the nucleus making this the most important interaction to the function of CST [93]. This is in stark contrast to RPA which enters the nucleus through more traditional means [181]. The CST-Pol α interaction is quite robust as shown in chapter 2, where different replication inhibitors had little effect on the frequency of this interaction occurring in the nucleus. Through our previous work and that of others, CST has been shown to have non-telomere functions through interactions with other replication and repair associated proteins such as MCM2-7, AND1, RAD51 and Shieldin we know that CST plays a role in replication origin licensing, replication fork stalls and DNA repair [5, 36, 40, 138]. While RPA has been shown to enhance PrimPol activity, RPA does not interact with all the factors that CST does and extended

time on ssDNA by RPA elicits a damage response [182, 183]. Our work and others have shown that CST helps cells handle replication stress. In an attempt to better understand the way in which CST responds to replication stress and how this effects the interaction between CST and Pol α we found that the cause of replication stress does have an impact on the interaction between CST and Pol α (Chapter 2). Others have also shown that replication stress negatively impacts SCC establishment which it was interesting to learn that the absence of CST exacerbates this effect (Chapter 4). The specific instances and ways in which CST is recruited to each situation still need to be elucidated. All those CST interactions that help to ensure DNA replication occurs correctly could also impact cohesion establishment. We know that CST has a preference for G-rich DNA like that found at the telomeres and also that it is capable of resolving G4s [5-7]. While RPA has no ssDNA preferences it is also capable of resolving G4s [184]. It is interesting that CST associates with the cohesin complex and that the defects resulting from the absence of CST are not very prominent until the introduction of replication stress. CST being capable of interacting with ssDNA and cohesin could mean it is helping to remodel cohesin at stalled replication forks or CST could be firing other origins and removing replication blocks that may form with inhibitors such as G4s. While CST and RPA can both be involved in the repair of dsDNA breaks it was fascinating to find CST involved in BER (chapter 3). A process that RPA is not involved. This highlights the unique cases in which CST becomes involved. CST aiding in BER and stimulating Pol β while a novel role for CST, is not unexpected with how CST is well known to stimulate Pol α and aid in double strand break repair. It is novel though that CST appears to stimulate every step of

this process. My goal was to better understand the many roles CST plays when it comes to DNA metabolism to which we have learned much but also raised more questions.

5.2 CST BEHIND THE REPLICATION FORK

Interestingly, there is overlap between the novel roles of CST shown in the previous chapters. We showed that the absence of CST leads to worse SCC and that replication stress exacerbates SCC loss in chapter 4. In chapter 2 we showed that the interaction between CST and Pol α are not affected by different replication inhibitors. Together these chapters point to one of the roles CST plays during replication stress mostly likely involves its interaction with Pol α. In Chapter 3 we showed that CST stimulates all parts of the BER pathway which shares some components with DNA replication process. While FEN1 cleavage is stimulated by CST, BER is not the only place that FEN1 plays a role. On the lagging strand during DNA replication, FEN1 is responsible for Okazaki fragment maturation [185-187]. CST in addition to being able to interact with ssDNA and resolve G4s that may form on the lagging strand CST stimulates Pol α which is responsible for Okazaki fragment synthesis. The final step of Okazaki fragment maturation is the ligating of the fragments together which is typically carried about by LIG1, which as shown in chapter 3 is stimulated by CST. Interestingly there is a backup ligation pathway for Okazaki fragment ligation that makes use of LIG3 and XRCC1 [192]. This could mean that some of the PLA foci detected for the interaction between STN1 and XRCC1 could be from Okazaki fragment processing and not BER. While Okazaki fragments can build up behind the replication fork this can lead to genome instability [194]. Only nucleolytic processing and ligation of Okazaki fragments can become uncoupled from replication without major problems [191]. While unlikely it

is possible that CST may play a minor role in Okazaki fragment processing during replication stress. If CST is involved in Okazaki fragment maturation this would most likely be in highly specialized cases as CST is not very abundant. CST has not been found to be associated with the replisome at active, stalled or collapsed replication forks by isolation of proteins on nascent DNA (iPOND) [193]. One group has shown CST playing a role protecting DNA during replication stress at stalled replication forks [40, 158].

CST was shown to colocalize with replication forks on ssDNA in response to HU induced replication stress by PLA [158]. In addition, CST was also shown to colocalize with RPA to recruit RAD51 to prevent nascent strand MRE11 degradation of reversed replication forks [40]. Stalled replication forks can convert to reversed replication forks during replication stress to prevent fork collapse [188]. As we saw treatment with replication inhibitors and the absence of STN1 led to worse SCC. Cohesion establishment occurs behind the replisome with work showing that in order for cohesin to encompass both the daughter DNA strands it must capture the lagging strand in a ssDNA region [64]. CST may aid in cohesion rearrangement during replication stress or in a number of other ways. The cohesion establishment factor, ESCO2 which interacts with MCM2-7 has been shown to be degraded when cells are treated with HU [66]. This means that stalled replication forks can lose their ability to establish SCC. The presence of MCM2-7 at a reversed replication fork is still debatable at this time as it seems the helicase must be moved out of the way for the reversed fork to form. Regardless, as ESCO2 is shown to be degraded with HU treatment even stalled forks may lose the ability to establish SCC. This means that the role CST plays in establishing SCC may be reliant on the ability of

CST to fire dormant replication origins that do not stall so that ESCO2 can be maintained at the replication fork to allow SCC establishment. While ESCO2 is what establishes SCC during DNA replication, SCC can also be aided by ESCO1 and what is termed damage induced cohesion [189]. ESCO1 levels have been found to be elevated in a number of cancers as cancers often experience more replication stress and thus become more reliant on a non-conventional SCC establishment method [190, 191]. Reversed replication forks may trigger damage induced cohesion in the area in which CST could play a part, this would need to be studied. It seems more likely that the role CST plays in SCC has to do with ensuring replication forks proceed smoothly so that ESCO2 can establish SCC. The way in which CST interacts with cohesin still needs to elucidated. CST being involved in a DNA damage induced response is not farfetched though as CST does play a role in DNA repair when it comes to double-strand breaks (DSBs) and BER, as shown in chapter 3, and in chapter 2 it was shown that interaction between CST and cohesin increases with replication inhibitors, many of which can lead to DSBs.

5.3 CST AND DNA DAMAGE

When CST is not present, we know that DNA damage is more prevalent. In chapter 3 this is shown by the elevated 8-oxoG levels present in STN1 KO cells. Damage is worse without CST due to the roles it plays in multiple pathways. Incomplete BER can lead to the need for HR for proper recovery from oxidative damage as repair sites can devolve into DSBs [192]. At DSBs CST recruits and stimulate Pol α to facilitate resection fill in for HR [40, 138]. CST aiding in DNA repair pathways in addition to DNA replication stress is not that surprising as many DNA repair proteins aid in DNA replication. The more interesting aspect of CST is that it aids in different degrees of DNA

damage, BER and DSB repair. This begs the question of how is CST being recruited to each type of DNA damage.

While CST appears to require Pol α in order to enter the nucleus and as shown in chapter 2 this interaction is quite robust, once in the nucleus CST is not always with Pol α [152]. CST has been shown to localize to G-rich regions of the genome, not just the telomeres [8, 39]. G-rich regions of the genome can be prone to the formation of G4s and some G-rich sites are termed fragile sites due to replication fork stalling that can occur at them and lead to DSBs [39]. In the case of DSBS the shielden complex appears to recruit CST to perform strand fill in with Pol α [43, 182]. This information points a few likely mechanisms that are responsible for CST localization within the nucleus in response to DNA damage. The first one is that CST is already present at sites that are prone to DNA damage, G-rich sites or fragile sites. Once Pol α has brought CST into the nucleus, CST may dissolve G4s that form in G-rich regions of the genome allowing it to be associated with these G-rich regions of the genome. It has not been shown if CST is able to remain associated with Pol α while resolving a G4 though it has been shown that CST alone is capable [6, 7]. In the case of DSBs it has been shown that CST is most likely recruited by shielden to DSBs and that Pol α is brought to the site by CST [43, 138]. It is possible the Pol α bound by CST could be recruited somewhere and bring CST but this seems unlikely as Pol α is more abundant than CST and only a small fraction of the Pol α pool is bound by CST [93]. If CST is already associated with G-rich regions of the genome this could explain why it is present at the very first step of BER as shown in Chapter 3. If CST is already present at regions of the genome prone to damage, such as fragile sites,

and is able to be recruited to DSBs it becomes apparent how the absence of CST can contribute to the formation of genetic diseases and cancer.

5.4 ETIOLOGY OF CST RELATED DISEASES

CTC1 and STN1 are both associated with diseases that fall under what are called, telomeropathies or telomere biology disorders. Telomerapothies are characterized by extremely short telomeres which usually leads to premature stem cell failure, especially hematopoietic stem cells [193, 194]. STN1 mutations are associated with Coats plus syndrome [51, 195]. CTC1 mutations are associated with both Coats plus syndrome and dyskeratosis congenita [196]. Coats plus and dyskeratosis congenita result in premature aging symptoms with premature greying hair, intestinal failure and brain calcification [197]. The premature lose of telomeres in CST associated telomeropathies is not the sole cause of these diseases as some patients diagnosed with the Coats plus syndrome displayed normal telomeres [51, 193]. The various roles CST plays in protecting the genome as a whole may better explain how mutations in CTC1 and STN1 lead to disease. The role of CST in BER is a newly discovered function that helps to better understand how CST mutations can contribute to telomeropathies, which as mentioned earlier may not always be caused by short telomeres. While telomere replication is dependent on CST, BER is also needed at telomeres due to their G-rich nature [88, 198]. While the G-rich nature of the telomeres is important to their stability the mutating of guanines to adenines can be quite destructive. In order to combat this shelterin proteins help to augment BER [85]. Improper, partial or even slow BER could lead to a number of DNA defects that result in premature telomere loss as well as genome wide defects. Base substitutions in the telomeres resulting from 8-oxoGs not being repaired would prevent

the shelterin complex from binding and protecting the telomeres and in the genome, mutations could accumulate leading to dysfunctional proteins. If BER is slower without functional CST or reduced levels, this could then lead to abasic sites or ssDNA gaps persisting longer than they should. The longer these damaged states of DNA persist the higher the chance of them devolving into worse damage, double strand breaks. A number of Coats plus and dyskeratosis congenita patients with CTC1 mutations have been shown to display CST that is incapable of localizing to the nucleus [199, 200]. While we know that CST is reliant on Pol α to enter the nucleus we next need to better understand how the different OB-folds of CST dictate functions.

5.5 THE FUTURE OF CST RESEARCH

There are three core interactions CST plays in the cell: CST binds ssDNA, interacts with various proteins and stimulates DNA polymerases. The OB-folds present on CTC1 and STN1 facilitate both DNA and protein binding [91, 201]. One way to better understand the effects of CTC1 and STN1 mutations on patients is to understand how each OB-fold contributes to the many functions of CST. This can be done through single amino acid mutations that are able to disrupt the function of a single OB-fold while leaving the overall CST complex intact. Another way is through the use of OB-fold binding drugs that disrupt their ability to bind DNA or proteins. These have already been developed for RPA and could provide a valuable research tool for understanding CST and have potential therapeutic roles [202].

What determines whether CST interacts or associates with a polymerase, cohesin, or MCM-7 may be dependent on post translational modifications. Both mono- and poly-ADP-ribosylation play a large role in the repair of telomeres and this is carried out by a

number of different ADP-ribose transferases [203]. Some of these ADP-ribose transferases play roles in managing DNA replication stress and DNA repair during replication which is why they are being looked at as cancer treatment targets [204]. The post translational modification of CST or direct interaction partners may be responsible for the localization CST or how it is able to interact and stimulate the different steps of BER. We already know that CST is reliant or at least partially reliant on its interaction with Pol α for nuclear localization [93]. The fission yeast shelterin component Tpz1, a human TPP1 ortholog, when SUMOylated promotes Stn1/Ten1 telomere association in fission yeast [205]. In humans TPP1 and POT1 are responsible for recruiting CST to perform C-strand fill in at the telomeres [138]. In addition, the shielden complex appears to recruit CST to perform strand fill in with Pol α [43, 138]. There is virtually nothing known about the human CST post translational modifications that are most likely facilitating the various roles the protein complex plays in the nucleus. Phosphorylation and ubiquitiniation sites are mapped for CST but the cause and influence of each modification is currently not known. These modifications may promote certain protein-protein interactions with CST and possibly inhibit others. Interestingly the smallest subunit, TEN1, of CST does not appear to contain any ubiquination or phosphorylation sites according to PhosphoSitePlus. While major roles of CST are still being discovered we think the next large research focus for this protein complex is understanding the importance of each post-translational modification.

REFERENCES

1. Miyake, Y., et al., *RPA-like mammalian Ctc1-Stn1-Ten1 complex binds to single-stranded DNA and protects telomeres independently of the Pot1 pathway.* Mol Cell, 2009. **36**(2): p. 193-206.
2. Lim, C.J., et al., *The structure of human CST reveals a decameric assembly bound to telomeric DNA.* Science, 2020. **368**(6495): p. 1081-1085.
3. Stewart, J.A., et al., *Emerging roles of CST in maintaining genome stability and human disease.* Front Biosci (Landmark Ed), 2018. **23**(8): p. 1564-1586.
4. Chen, L.Y., S. Redon, and J. Lingner, *The human CST complex is a terminator of telomerase activity.* Nature, 2012. **488**(7412): p. 540-4.
5. Bhattacharjee, A., et al., *STN1 OB Fold Mutation Alters DNA Binding and Affects Selective Aspects of CST Function.* PLoS Genet, 2016. **12**(9): p. e1006342.
6. Bhattacharjee, A., et al., *Dynamic DNA binding, junction recognition and G4 melting activity underlie the telomeric and genome-wide roles of human CST.* Nucleic Acids Res, 2017. **45**(21): p. 12311-12324.
7. Zhang, M., et al., *Mammalian CST averts replication failure by preventing G-quadruplex accumulation.* Nucleic Acids Res, 2019. **47**(10): p. 5243-5259.
8. Hom, R.A. and D.S. Wuttke, *Human CST Prefers G-Rich but Not Necessarily Telomeric Sequences.* Biochemistry, 2017. **56**(32): p. 4210-4218.
9. Pfeiffer, V. and J. Lingner, *Replication of telomeres and the regulation of telomerase.* Cold Spring Harb Perspect Biol, 2013. **5**(5): p. a010405.
10. Moyzis, R.K., et al., *A highly conserved repetitive DNA sequence, (TTAGGG)n, present at the telomeres of human chromosomes.* Proc Natl Acad Sci U S A, 1988. **85**(18): p. 6622-6.
11. Makarov, V.L., Y. Hirose, and J.P. Langmore, *Long G tails at both ends of human chromosomes suggest a C strand degradation mechanism for telomere shortening.* Cell, 1997. **88**(5): p. 657-66.
12. Lim, C.J. and T.R. Cech, *Shaping human telomeres: from shelterin and CST complexes to telomeric chromatin organization.* Nat Rev Mol Cell Biol, 2021. **22**(4): p. 283-298.
13. Rajavel, M., M.R. Mullins, and D.J. Taylor, *Multiple facets of TPP1 in telomere maintenance.* Biochim Biophys Acta, 2014. **1844**(9): p. 1550-9.
14. Lototska, L., et al., *Human RAP1 specifically protects telomeres of senescent cells from DNA damage.* EMBO Rep, 2020. **21**(4): p. e49076.
15. de Lange, T., *Shelterin-Mediated Telomere Protection.* Annu Rev Genet, 2018. **52**: p. 223-247.
16. Lin, C.G., et al., *The human telomeric proteome during telomere replication.* Nucleic Acids Res, 2021. **49**(21): p. 12119-12135.

17. Blackburn, E.H. and J.G. Gall, *A tandemly repeated sequence at the termini of the extrachromosomal ribosomal RNA genes in Tetrahymena.* J Mol Biol, 1978. **120**(1): p. 33-53.
18. Harley, C.B., A.B. Futcher, and C.W. Greider, *Telomeres shorten during ageing of human fibroblasts.* Nature, 1990. **345**(6274): p. 458-60.
19. Bodnar, A.G., et al., *Extension of life-span by introduction of telomerase into normal human cells.* Science, 1998. **279**(5349): p. 349-52.
20. Xin, H., et al., *TPP1 is a homologue of ciliate TEBP-beta and interacts with POT1 to recruit telomerase.* Nature, 2007. **445**(7127): p. 559-62.
21. Abreu, E., et al., *TIN2-tethered TPP1 recruits human telomerase to telomeres in vivo.* Mol Cell Biol, 2010. **30**(12): p. 2971-82.
22. Tejera, A.M., et al., *TPP1 is required for TERT recruitment, telomere elongation during nuclear reprogramming, and normal skin development in mice.* Dev Cell, 2010. **18**(5): p. 775-89.
23. Zaug, A.J., et al., *CST does not evict elongating telomerase but prevents initiation by ssDNA binding.* Nucleic Acids Res, 2021. **49**(20): p. 11653-11665.
24. Kelleher, C., I. Kurth, and J. Lingner, *Human protection of telomeres 1 (POT1) is a negative regulator of telomerase activity in vitro.* Mol Cell Biol, 2005. **25**(2): p. 808-18.
25. Goulian, M., C.J. Heard, and S.L. Grimm, *Purification and properties of an accessory protein for DNA polymerase alpha/primase.* J Biol Chem, 1990. **265**(22): p. 13221-30.
26. Nakaoka, H., et al., *Xenopus laevis Ctc1-Stn1-Ten1 (xCST) protein complex is involved in priming DNA synthesis on single-stranded DNA template in Xenopus egg extract.* J Biol Chem, 2012. **287**(1): p. 619-627.
27. Ganduri, S. and N.F. Lue, *STN1-POLA2 interaction provides a basis for primase-pol alpha stimulation by human STN1*. Nucleic Acids Res, 2017. **45**(16): p. 9455-9466.
28. Drosopoulos, W.C., S.T. Kosiyatrakul, and C.L. Schildkraut, *BLM helicase facilitates telomere replication during leading strand synthesis of telomeres.* J Cell Biol, 2015. **210**(2): p. 191-208.
29. Sfeir, A., et al., *Mammalian telomeres resemble fragile sites and require TRF1 for efficient replication.* Cell, 2009. **138**(1): p. 90-103.
30. Higa, M., M. Fujita, and K. Yoshida, *DNA Replication Origins and Fork Progression at Mammalian Telomeres.* Genes (Basel), 2017. **8**(4).
31. Spiegel, J., S. Adhikari, and S. Balasubramanian, *The Structure and Function of DNA G-Quadruplexes.* Trends Chem, 2020. **2**(2): p. 123-136.
32. Rhodes, D. and H.J. Lipps, *G-quadruplexes and their regulatory roles in biology.* Nucleic Acids Res, 2015. **43**(18): p. 8627-37.
33. Yang, D., *G-Quadruplex DNA and RNA.* Methods Mol Biol, 2019. **2035**: p. 1-24.
34. Bryan, T.M., *G-Quadruplexes at Telomeres: Friend or Foe?* Molecules, 2020. **25**(16).
35. Paudel, B.P., et al., *A mechanism for the extension and unfolding of parallel telomeric G-quadruplexes by human telomerase at single-molecule resolution.* Elife, 2020. **9**.

36. Wang, Y., et al., *Human CST suppresses origin licensing and promotes AND-1/Ctf4 chromatin association.* Life Sci Alliance, 2019. **2**(2).
37. Stewart, J.A., et al., *Human CST promotes telomere duplex replication and general replication restart after fork stalling.* EMBO J, 2012. **31**(17): p. 3537-49.
38. Wang, F., J. Stewart, and C.M. Price, *Human CST abundance determines recovery from diverse forms of DNA damage and replication stress.* Cell Cycle, 2014. **13**(22): p. 3488-98.
39. Chastain, M., et al., *Human CST Facilitates Genome-wide RAD51 Recruitment to GC-Rich Repetitive Sequences in Response to Replication Stress.* Cell Rep, 2016. **16**(5): p. 1300-1314.
40. Lei, K.H., et al., *Crosstalk between CST and RPA regulates RAD51 activity during replication stress.* Nat Commun, 2021. **12**(1): p. 6412.
41. Ackerson, S.M., C.I. Gable, and J.A. Stewart, *Human CTC1 promotes TopBP1 stability and CHK1 phosphorylation in response to telomere dysfunction and global replication stress.* Cell Cycle, 2020. **19**(24): p. 3491-3507.
42. Barazas, M., et al., *The CST Complex Mediates End Protection at Double-Strand Breaks and Promotes PARP Inhibitor Sensitivity in BRCA1-Deficient Cells.* Cell Rep, 2018. **23**(7): p. 2107-2118.
43. Mirman, Z., et al., *53BP1-shieldin-dependent DSB processing in BRCA1-deficient cells requires CST-Polalpha-primase fill-in synthesis.* Nat Cell Biol, 2022. **24**(1): p. 51-61.
44. Feng, X., et al., *CTC1-mediated C-strand fill-in is an essential step in telomere length maintenance.* Nucleic Acids Res, 2017. **45**(8): p. 4281-4293.
45. Anderson, B.H., et al., *Mutations in CTC1, encoding conserved telomere maintenance component 1, cause Coats plus.* Nat Genet, 2012. **44**(3): p. 338-42.
46. Armanios, M., *An emerging role for the conserved telomere component 1 (CTC1) in human genetic disease.* Pediatr Blood Cancer, 2012. **59**(2): p. 209-10.
47. Keller, R.B., et al., *CTC1 Mutations in a patient with dyskeratosis congenita.* Pediatr Blood Cancer, 2012. **59**(2): p. 311-4.
48. Romaniello, R., et al., *Cerebroretinal microangiopathy with calcifications and cysts associated with CTC1 and NDP mutations.* J Child Neurol, 2013. **28**(12): p. 1702-8.
49. Savage, S.A., *Connecting complex disorders through biology.* Nat Genet, 2012. **44**(3): p. 238-40.
50. Walne, A.J., et al., *Mutations in the telomere capping complex in bone marrow failure and related syndromes.* Haematologica, 2013. **98**(3): p. 334-8.
51. Simon, A.J., et al., *Mutations in STN1 cause Coats plus syndrome and are associated with genomic and telomere defects.* J Exp Med, 2016. **213**(8): p. 1429-40.
52. Gudmundsson, J., et al., *A genome-wide association study yields five novel thyroid cancer risk loci.* Nat Commun, 2017. **8**: p. 14517.
53. Ojha, J., et al., *Genetic Variation Associated with Longer Telomere Length Increases Risk of Chronic Lymphocytic Leukemia.* Cancer Epidemiol Biomarkers Prev, 2016. **25**(7): p. 1043-9.
54. Phelan, C.M., et al., *Identification of 12 new susceptibility loci for different histotypes of epithelial ovarian cancer.* Nat Genet, 2017. **49**(5): p. 680-691.

55. Walsh, K.M., et al., *Common genetic variants associated with telomere length confer risk for neuroblastoma and other childhood cancers.* Carcinogenesis, 2016. **37**(6): p. 576-582.
56. Law, M.H., et al., *Genome-wide meta-analysis identifies five new susceptibility loci for cutaneous malignant melanoma.* Nat Genet, 2015. **47**(9): p. 987-995.
57. Rode, L., B.G. Nordestgaard, and S.E. Bojesen, *Long telomeres and cancer risk among 95 568 individuals from the general population.* Int J Epidemiol, 2016. **45**(5): p. 1634-1643.
58. Gyorffy, B., et al., *Online survival analysis software to assess the prognostic value of biomarkers using transcriptomic data in non-small-cell lung cancer.* PLoS One, 2013. **8**(12): p. e82241.
59. Peters, J.M., A. Tedeschi, and J. Schmitz, *The cohesin complex and its roles in chromosome biology.* Genes Dev, 2008. **22**(22): p. 3089-114.
60. Ivanov, M.P., et al., *The replicative helicase MCM recruits cohesin acetyltransferase ESCO2 to mediate centromeric sister chromatid cohesion.* EMBO J, 2018. **37**(15).
61. Minamino, M., et al., *Temporal Regulation of ESCO2 Degradation by the MCM Complex, the CUL4-DDB1-VPRBP Complex, and the Anaphase-Promoting Complex.* Curr Biol, 2018. **28**(16): p. 2665-2672 e5.
62. Guilliam, T.A., *Mechanisms for Maintaining Eukaryotic Replisome Progression in the Presence of DNA Damage.* Front Mol Biosci, 2021. **8**: p. 712971.
63. Rudra, S. and R.V. Skibbens, *Sister chromatid cohesion establishment occurs in concert with lagging strand synthesis.* Cell Cycle, 2012. **11**(11): p. 2114-21.
64. Murayama, Y., et al., *Establishment of DNA-DNA Interactions by the Cohesin Ring.* Cell, 2018. **172**(3): p. 465-477 e15.
65. Kim, B.J., et al., *Genome-wide reinforcement of cohesin binding at pre-existing cohesin sites in response to ionizing radiation in human cells.* J Biol Chem, 2010. **285**(30): p. 22784-92.
66. Benedict, B., et al., *WAPL-Dependent Repair of Damaged DNA Replication Forks Underlies Oncogene-Induced Loss of Sister Chromatid Cohesion.* Dev Cell, 2020. **52**(6): p. 683-698 e7.
67. Minchell, N.E., A. Keszthelyi, and J. Baxter, *Cohesin Causes Replicative DNA Damage by Trapping DNA Topological Stress.* Mol Cell, 2020. **78**(4): p. 739-751 e8.
68. van Schie, J.J.M. and J. de Lange, *The Interplay of Cohesin and the Replisome at Processive and Stressed DNA Replication Forks.* Cells, 2021. **10**(12).
69. Chan, S.W. and P.C. Dedon, *The biological and metabolic fates of endogenous DNA damage products.* J Nucleic Acids, 2010. **2010**: p. 929047.
70. Limpose, K.L., A.H. Corbett, and P.W. Doetsch, *BERing the burden of damage: Pathway crosstalk and posttranslational modification of base excision repair proteins regulate DNA damage management.* DNA Repair (Amst), 2017. **56**: p. 51-64.
71. Candeias, L.P. and S. Steenken, *Reaction of HO* with guanine derivatives in aqueous solution: formation of two different redox-active OH-adduct radicals and their unimolecular transformation reactions. Properties of G(-H)*.* Chemistry, 2000. **6**(3): p. 475-84.

72. Kobayashi, K. and S. Tagawa, *Direct observation of guanine radical cation deprotonation in duplex DNA using pulse radiolysis.* J Am Chem Soc, 2003. **125**(34): p. 10213-8.
73. Shukla, L.I., et al., *Formation of 8-oxo-7,8-dihydroguanine-radicals in gamma-irradiated DNA by multiple one-electron oxidations.* Nucleic Acids Res, 2004. **32**(22): p. 6565-74.
74. Faucher, F., S. Doublie, and Z. Jia, *8-oxoguanine DNA glycosylases: one lesion, three subfamilies.* Int J Mol Sci, 2012. **13**(6): p. 6711-29.
75. Wallace, S.S., *DNA glycosylases search for and remove oxidized DNA bases.* Environ Mol Mutagen, 2013. **54**(9): p. 691-704.
76. Tell, G., et al., *The many functions of APE1/Ref-1: not only a DNA repair enzyme.* Antioxid Redox Signal, 2009. **11**(3): p. 601-20.
77. Thakur, S., et al., *APE1/Ref-1 as an emerging therapeutic target for various human diseases: phytochemical modulation of its functions.* Exp Mol Med, 2014. **46**: p. e106.
78. Pascucci, B., et al., *Long patch base excision repair with purified human proteins. DNA ligase I as patch size mediator for DNA polymerases delta and epsilon.* J Biol Chem, 1999. **274**(47): p. 33696-702.
79. Sattler, U., et al., *Long-patch DNA repair synthesis during base excision repair in mammalian cells.* EMBO Rep, 2003. **4**(4): p. 363-7.
80. Robertson, A.B., et al., *DNA repair in mammalian cells: Base excision repair: the long and short of it.* Cell Mol Life Sci, 2009. **66**(6): p. 981-93.
81. Hegde, M.L., T.K. Hazra, and S. Mitra, *Early steps in the DNA base excision/single-strand interruption repair pathway in mammalian cells.* Cell Res, 2008. **18**(1): p. 27-47.
82. Krokan, H.E. and M. Bjoras, *Base excision repair.* Cold Spring Harb Perspect Biol, 2013. **5**(4): p. a012583.
83. Hanzlikova, H., et al., *Overlapping roles for PARP1 and PARP2 in the recruitment of endogenous XRCC1 and PNKP into oxidized chromatin.* Nucleic Acids Res, 2017. **45**(5): p. 2546-2557.
84. Vallabhaneni, H., et al., *Defective repair of oxidative base lesions by the DNA glycosylase Nth1 associates with multiple telomere defects.* PLoS Genet, 2013. **9**(7): p. e1003639.
85. Miller, A.S., et al., *Telomere proteins POT1, TRF1 and TRF2 augment long-patch base excision repair in vitro.* Cell Cycle, 2012. **11**(5): p. 998-1007.
86. Wallace, S.S., *Base excision repair: a critical player in many games.* DNA Repair (Amst), 2014. **19**: p. 14-26.
87. Opresko, P.L., et al., *Oxidative damage in telomeric DNA disrupts recognition by TRF1 and TRF2.* Nucleic Acids Res, 2005. **33**(4): p. 1230-9.
88. Barnes, R.P., E. Fouquerel, and P.L. Opresko, *The impact of oxidative DNA damage and stress on telomere homeostasis.* Mech Ageing Dev, 2019. **177**: p. 37-45.
89. Marsden, C.G., et al., *Base Excision Repair Variants in Cancer.* Methods Enzymol, 2017. **591**: p. 119-157.
90. Wallace, S.S., D.L. Murphy, and J.B. Sweasy, *Base excision repair and cancer.* Cancer Lett, 2012. **327**(1-2): p. 73-89.

91. Cai, S.W., et al., *Cryo-EM structure of the human CST-Polalpha/primase complex in a recruitment state.* Nat Struct Mol Biol, 2022.
92. Lue, N.F., et al., *The CDC13-STN1-TEN1 complex stimulates Pol alpha activity by promoting RNA priming and primase-to-polymerase switch.* Nat Commun, 2014. **5**: p. 5762.
93. Kelich, J.M., H. Papaioannou, and E. Skordalakes, *Pol alpha-primase dependent nuclear localization of the mammalian CST complex.* Commun Biol, 2021. **4**(1): p. 349.
94. Schuck, P.L., L.E. Ball, and J.A. Stewart, *The DNA-binding protein CST associates with the cohesin complex and promotes chromosome cohesion.* J Biol Chem, 2021. **297**(3): p. 101026.
95. Ranalli, T.A., M.S. DeMott, and R.A. Bambara, *Mechanism underlying replication protein a stimulation of DNA ligase I.* J Biol Chem, 2002. **277**(3): p. 1719-27.
96. Anantha, R.W., V.M. Vassin, and J.A. Borowiec, *Sequential and synergistic modification of human RPA stimulates chromosomal DNA repair.* J Biol Chem, 2007. **282**(49): p. 35910-23.
97. Vassin, V.M., et al., *Human RPA phosphorylation by ATR stimulates DNA synthesis and prevents ssDNA accumulation during DNA-replication stress.* J Cell Sci, 2009. **122**(Pt 22): p. 4070-80.
98. Qin, Z., et al., *Human RPA activates BLM's bidirectional DNA unwinding from a nick.* Elife, 2020. **9**.
99. Gopalakrishnan, V., C.R. Tan, and S. Li, *Sequential phosphorylation of CST subunits by different cyclin-Cdk1 complexes orchestrate telomere replication.* Cell Cycle, 2017. **16**(13): p. 1271-1287.
100. Calvo, O., et al., *The telomeric Cdc13-Stn1-Ten1 complex regulates RNA polymerase II transcription.* Nucleic Acids Res, 2019. **47**(12): p. 6250-6268.
101. Alam, M.S., *Proximity Ligation Assay (PLA).* Curr Protoc Immunol, 2018. **123**(1): p. e58.
102. McKinley, K.L., et al., *The CENP-L-N Complex Forms a Critical Node in an Integrated Meshwork of Interactions at the Centromere-Kinetochore Interface.* Mol Cell, 2015. **60**(6): p. 886-98.
103. Su, K.C., et al., *CRISPR/Cas9-based gene targeting using synthetic guide RNAs enables robust cell biological analyses.* Mol Biol Cell, 2018. **29**(20): p. 2370-2377.
104. Baranovskiy, A.G., et al., *Structural basis for inhibition of DNA replication by aphidicolin.* Nucleic Acids Res, 2014. **42**(22): p. 14013-21.
105. Marheineke, K. and O. Hyrien, *Aphidicolin triggers a block to replication origin firing in Xenopus egg extracts.* J Biol Chem, 2001. **276**(20): p. 17092-100.
106. Courtot, L., J.S. Hoffmann, and V. Bergoglio, *The Protective Role of Dormant Origins in Response to Replicative Stress.* Int J Mol Sci, 2018. **19**(11).
107. Yeh, Y.C. and I. Tessman, *Differential effect of hydroxyurea on a ribonucleotide reductase system.* J Biol Chem, 1978. **253**(5): p. 1323-4.
108. Bianchi, V., E. Pontis, and P. Reichard, *Changes of deoxyribonucleoside triphosphate pools induced by hydroxyurea and their relation to DNA synthesis.* J Biol Chem, 1986. **261**(34): p. 16037-42.

109. Young, C.W., G. Schochetman, and D.A. Karnofsky, *Hydroxyurea-induced inhibition of deoxyribonucleotide synthesis: studies in intact cells.* Cancer Res, 1967. **27**(3): p. 526-34.
110. Lee, W.T.C., et al., *Single-molecule imaging reveals replication fork coupled formation of G-quadruplex structures hinders local replication stress signaling.* Nat Commun, 2021. **12**(1): p. 2525.
111. Bryan, T.M., *Mechanisms of DNA Replication and Repair: Insights from the Study of G-Quadruplexes.* Molecules, 2019. **24**(19).
112. Sriram, D., et al., *Camptothecin and its analogues: a review on their chemotherapeutic potential.* Nat Prod Res, 2005. **19**(4): p. 393-412.
113. Xu, Y. and C. Her, *Inhibition of Topoisomerase (DNA) I (TOP1): DNA Damage Repair and Anticancer Therapy.* Biomolecules, 2015. **5**(3): p. 1652-70.
114. Diotti, R., et al., *DNA-Directed Polymerase Subunits Play a Vital Role in Human Telomeric Overhang Processing.* Mol Cancer Res, 2015. **13**(3): p. 402-10.
115. Takai, H., et al., *A POT1 mutation implicates defective telomere end fill-in and telomere truncations in Coats plus.* Genes Dev, 2016. **30**(7): p. 812-26.
116. Pinzaru, A.M., et al., *Replication stress conferred by POT1 dysfunction promotes telomere relocalization to the nuclear pore.* Genes Dev, 2020. **34**(23-24): p. 1619-1636.
117. Gu, P., et al., *Distinct functions of POT1 proteins contribute to the regulation of telomerase recruitment to telomeres.* Nat Commun, 2021. **12**(1): p. 5514.
118. Kelich, J., et al., *Telomere dysfunction implicates POT1 in patients with idiopathic pulmonary fibrosis.* J Exp Med, 2022. **219**(5).
119. Wu, P., H. Takai, and T. de Lange, *Telomeric 3' overhangs derive from resection by Exo1 and Apollo and fill-in by POT1b-associated CST.* Cell, 2012. **150**(1): p. 39-52.
120. Aramburu, T., S. Plucinsky, and E. Skordalakes, *POT1-TPP1 telomere length regulation and disease.* Comput Struct Biotechnol J, 2020. **18**: p. 1939-1946.
121. Hahn, A.T., J.T. Jones, and T. Meyer, *Quantitative analysis of cell cycle phase durations and PC12 differentiation using fluorescent biosensors.* Cell Cycle, 2009. **8**(7): p. 1044-52.
122. Posakony, J.W., J.M. England, and G. Attardi, *Mitochondrial growth and division during the cell cycle in HeLa cells.* J Cell Biol, 1977. **74**(2): p. 468-91.
123. McKinley, K.L., *Employing CRISPR/Cas9 genome engineering to dissect the molecular requirements for mitosis.* Methods Cell Biol, 2018. **144**: p. 75-105.
124. Yoshihara, M., et al., *Genome-wide profiling of 8-oxoguanine reveals its association with spatial positioning in nucleus.* DNA Res, 2014. **21**(6): p. 603-12.
125. Lodovici, M. and E. Bigagli, *Oxidative stress and air pollution exposure.* J Toxicol, 2011. **2011**: p. 487074.
126. Salpea, K.D., et al., *Association of telomere length with type 2 diabetes, oxidative stress and UCP2 gene variation.* Atherosclerosis, 2010. **209**(1): p. 42-50.
127. Shen, J., et al., *Telomere length, oxidative damage, antioxidants and breast cancer risk.* Int J Cancer, 2009. **124**(7): p. 1637-43.
128. Beard, W.A., et al., *Eukaryotic Base Excision Repair: New Approaches Shine Light on Mechanism.* Annu Rev Biochem, 2019. **88**: p. 137-162.

129. Nilsen, H. and H.E. Krokan, *Base excision repair in a network of defence and tolerance.* Carcinogenesis, 2001. **22**(7): p. 987-98.
130. Matsumoto, Y. and K. Kim, *Excision of deoxyribose phosphate residues by DNA polymerase beta during DNA repair.* Science, 1995. **269**(5224): p. 699-702.
131. Piersen, C.E., et al., *Evidence for an imino intermediate in the DNA polymerase beta deoxyribose phosphate excision reaction.* J Biol Chem, 1996. **271**(30): p. 17811-5.
132. Wilson, S.H., *Mammalian base excision repair and DNA polymerase beta.* Mutat Res, 1998. **407**(3): p. 203-15.
133. Memisoglu, A. and L. Samson, *Base excision repair in yeast and mammals.* Mutat Res, 2000. **451**(1-2): p. 39-51.
134. Sung, J.S. and B. Demple, *Roles of base excision repair subpathways in correcting oxidized abasic sites in DNA.* FEBS J, 2006. **273**(8): p. 1620-9.
135. Wilson, D.M., 3rd and D. Barsky, *The major human abasic endonuclease: formation, consequences and repair of abasic lesions in DNA.* Mutat Res, 2001. **485**(4): p. 283-307.
136. Muftuoglu, M., et al., *Telomere repeat binding factor 2 interacts with base excision repair proteins and stimulates DNA synthesis by DNA polymerase beta.* Cancer Res, 2006. **66**(1): p. 113-24.
137. Lyu, X., P.B. Sang, and W. Chai, *CST in maintaining genome stability: Beyond telomeres.* DNA Repair (Amst), 2021. **102**: p. 103104.
138. Mirman, Z., et al., *53BP1-RIF1-shieldin counteracts DSB resection through CST- and Polalpha-dependent fill-in.* Nature, 2018. **560**(7716): p. 112-116.
139. Goulian, M. and C.J. Heard, *The mechanism of action of an accessory protein for DNA polymerase alpha/primase.* J Biol Chem, 1990. **265**(22): p. 13231-9.
140. Zaug, A.J., et al., *Reconstitution of a telomeric replicon organized by CST.* Nature, 2022. **608**(7924): p. 819-825.
141. He, Y., et al., *Structure of Tetrahymena telomerase-bound CST with polymerase alpha-primase.* Nature, 2022. **608**(7924): p. 813-818.
142. Feng, X., et al., *CTC1-STN1 terminates telomerase while STN1-TEN1 enables C-strand synthesis during telomere replication in colon cancer cells.* Nat Commun, 2018. **9**(1): p. 2827.
143. Bryan, C., et al., *Structure of the human telomeric Stn1-Ten1 capping complex.* PLoS One, 2013. **8**(6): p. e66756.
144. Otsuka, C., et al., *Difference between deoxyribose- and tetrahydrofuran-type abasic sites in the in vivo mutagenic responses in yeast.* Nucleic Acids Res, 2002. **30**(23): p. 5129-35.
145. Singhal, R.K. and S.H. Wilson, *Short gap-filling synthesis by DNA polymerase beta is processive.* J Biol Chem, 1993. **268**(21): p. 15906-11.
146. Osheroff, W.P., et al., *The fidelity of DNA polymerase beta during distributive and processive DNA synthesis.* J Biol Chem, 1999. **274**(6): p. 3642-50.
147. Ramana, C.V., et al., *Activation of apurinic/apyrimidinic endonuclease in human cells by reactive oxygen species and its correlation with their adaptive response to genotoxicity of free radicals.* Proc Natl Acad Sci U S A, 1998. **95**(9): p. 5061-6.
148. Whitaker, A.M. and B.D. Freudenthal, *APE1: A skilled nucleic acid surgeon.* DNA Repair (Amst), 2018. **71**: p. 93-100.

149. Garcia-Diaz, M., et al., *Identification of an intrinsic 5'-deoxyribose-5-phosphate lyase activity in human DNA polymerase lambda: a possible role in base excision repair.* J Biol Chem, 2001. **276**(37): p. 34659-63.
150. Prasad, R., et al., *Human DNA polymerase beta deoxyribose phosphate lyase. Substrate specificity and catalytic mechanism.* J Biol Chem, 1998. **273**(24): p. 15263-70.
151. Kumar, A., et al., *Interlocking activities of DNA polymerase beta in the base excision repair pathway.* Proc Natl Acad Sci U S A, 2022. **119**(10): p. e2118940119.
152. Kleppa, L., et al., *Kinetics of endogenous mouse FEN1 in base excision repair.* Nucleic Acids Res, 2012. **40**(18): p. 9044-59.
153. Asagoshi, K., et al., *FEN1 functions in long patch base excision repair under conditions of oxidative stress in vertebrate cells.* Mol Cancer Res, 2010. **8**(2): p. 204-15.
154. Kamble, P., et al., *DNA ligase I fidelity mediates the mutagenic ligation of pol beta oxidized and mismatch nucleotide insertion products in base excision repair.* J Biol Chem, 2021. **296**: p. 100427.
155. Balakrishnan, L., et al., *Long patch base excision repair proceeds via coordinated stimulation of the multienzyme DNA repair complex.* J Biol Chem, 2009. **284**(22): p. 15158-72.
156. Collins, A.R., et al., *The comet assay: topical issues.* Mutagenesis, 2008. **23**(3): p. 143-51.
157. Giraud-Panis, M.J., et al., *CST meets shelterin to keep telomeres in check.* Mol Cell, 2010. **39**(5): p. 665-76.
158. Lyu, X., et al., *Human CST complex protects stalled replication forks by directly blocking MRE11 degradation of nascent-strand DNA.* EMBO J, 2021. **40**(2): p. e103654.
159. Fleming, A.M. and C.J. Burrows, *Interplay of Guanine Oxidation and G-Quadruplex Folding in Gene Promoters.* J Am Chem Soc, 2020. **142**(3): p. 1115-1136.
160. Edwards, D.N., et al., *Intramolecular telomeric G-quadruplexes dramatically inhibit DNA synthesis by replicative and translesion polymerases, revealing their potential to lead to genetic change.* PLoS One, 2014. **9**(1): p. e80664.
161. Beard, W.A. and S.H. Wilson, *Purification and domain-mapping of mammalian DNA polymerase beta.* Methods Enzymol, 1995. **262**: p. 98-107.
162. Bornarth, C.J., et al., *Effect of flap modifications on human FEN1 cleavage.* Biochemistry, 1999. **38**(40): p. 13347-54.
163. Tom, S., et al., *Regulatory roles of p21 and apurinic/apyrimidinic endonuclease 1 in base excision repair.* J Biol Chem, 2001. **276**(52): p. 48781-9.
164. Henricksen, L.A., et al., *DNA ligase I competes with FEN1 to expand repetitive DNA sequences in vitro.* J Biol Chem, 2002. **277**(25): p. 22361-9.
165. Gerace, E. and D. Moazed, *Affinity Pull-Down of Proteins Using Anti-FLAG M2 Agarose Beads.* Methods Enzymol, 2015. **559**: p. 99-110.
166. Jhanji, M., et al., *Cis- and trans-resveratrol have opposite effects on histone serine-ADP-ribosylation and tyrosine induced neurodegeneration.* Nat Commun, 2022. **13**(1): p. 3244.

167. Makrantoni, V. and A.L. Marston, *Cohesin and chromosome segregation.* Curr Biol, 2018. **28**(12): p. R688-R693.
168. Haarhuis, J.H., A.M. Elbatsh, and B.D. Rowland, *Cohesin and its regulation: on the logic of X-shaped chromosomes.* Dev Cell, 2014. **31**(1): p. 7-18.
169. Peters, J.M. and T. Nishiyama, *Sister chromatid cohesion.* Cold Spring Harb Perspect Biol, 2012. **4**(11).
170. Uhlmann, F. and K. Nasmyth, *Cohesion between sister chromatids must be established during DNA replication.* Curr Biol, 1998. **8**(20): p. 1095-101.
171. Wutz, G., et al., *Topologically associating domains and chromatin loops depend on cohesin and are regulated by CTCF, WAPL, and PDS5 proteins.* EMBO J, 2017. **36**(24): p. 3573-3599.
172. Morales, C., et al., *PDS5 proteins are required for proper cohesin dynamics and participate in replication fork protection.* J Biol Chem, 2020. **295**(1): p. 146-157.
173. Masamsetti, V.P., et al., *Replication stress induces mitotic death through parallel pathways regulated by WAPL and telomere deprotection.* Nat Commun, 2019. **10**(1): p. 4224.
174. Setiaputra, D. and D. Durocher, *Shieldin - the protector of DNA ends.* EMBO Rep, 2019. **20**(5).
175. Chastain, M., et al., *Human CST Facilitates Genome-wide RAD51 Recruitment to GC-Rich Repetitive Sequences in Response to Replication Stress.* Cell Rep, 2016. **16**(7): p. 2048.
176. Schuck, P.L. and J.A. Stewart, *FISHing for Damage on Metaphase Chromosomes.* Methods Mol Biol, 2019. **1999**: p. 335-347.
177. Kasbek, C., F. Wang, and C.M. Price, *Human TEN1 maintains telomere integrity and functions in genome-wide replication restart.* J Biol Chem, 2013. **288**(42): p. 30139-30150.
178. Wang, F., et al., *Human CST has independent functions during telomere duplex replication and C-strand fill-in.* Cell Rep, 2012. **2**(5): p. 1096-103.
179. Paiano, J., et al., *Role of 53BP1 in end protection and DNA synthesis at DNA breaks.* Genes Dev, 2021. **35**(19-20): p. 1356-1367.
180. Flynn, R.L., S. Chang, and L. Zou, *RPA and POT1: friends or foes at telomeres?* Cell Cycle, 2012. **11**(4): p. 652-7.
181. Jullien, D., et al., *Nuclear import of RPA in Xenopus egg extracts requires a novel protein XRIPalpha but not importin alpha.* EMBO J, 1999. **18**(15): p. 4348-58.
182. Martinez-Jimenez, M.I., A. Lahera, and L. Blanco, *Human PrimPol activity is enhanced by RPA.* Sci Rep, 2017. **7**(1): p. 783.
183. Marechal, A. and L. Zou, *RPA-coated single-stranded DNA as a platform for post-translational modifications in the DNA damage response.* Cell Res, 2015. **25**(1): p. 9-23.
184. Lancrey, A., et al., *The binding efficiency of RPA to telomeric G-strands folded into contiguous G-quadruplexes is independent of the number of G4 units.* Biochimie, 2018. **146**: p. 68-72.
185. Balakrishnan, L., et al., *Acetylation of Dna2 endonuclease/helicase and flap endonuclease 1 by p300 promotes DNA stability by creating long flap intermediates.* J Biol Chem, 2010. **285**(7): p. 4398-404.

186. Zaher, M.S., et al., *Missed cleavage opportunities by FEN1 lead to Okazaki fragment maturation via the long-flap pathway.* Nucleic Acids Res, 2018. **46**(6): p. 2956-2974.
187. Kahli, M., et al., *Processing of eukaryotic Okazaki fragments by redundant nucleases can be uncoupled from ongoing DNA replication in vivo.* Nucleic Acids Res, 2019. **47**(4): p. 1814-1822.
188. Neelsen, K.J. and M. Lopes, *Replication fork reversal in eukaryotes: from dead end to dynamic response.* Nat Rev Mol Cell Biol, 2015. **16**(4): p. 207-20.
189. Strom, L. and C. Sjogren, *DNA damage-induced cohesion.* Cell Cycle, 2005. **4**(4): p. 536-9.
190. Zhang, S., et al., *Increased expression of ESCO1 is correlated with poor patient survival and its role in human bladder cancer.* Tumour Biol, 2016. **37**(4): p. 5165-70.
191. Wang, H., et al., *The correlation of ESCO1 expression with a prognosis of prostate cancer and anti-tumor effect of ESCO1 silencing.* Transl Cancer Res, 2019. **8**(3): p. 950-961.
192. Hayashi, M. and K. Umezu, *Homologous recombination is required for recovery from oxidative DNA damage.* Genes Genet Syst, 2017. **92**(2): p. 73-80.
193. Armando, R.G., et al., *Telomeropathies: Etiology, diagnosis, treatment and follow-up. Ethical and legal considerations.* Clin Genet, 2019. **96**(1): p. 3-16.
194. Grill, S. and J. Nandakumar, *Molecular mechanisms of telomere biology disorders.* J Biol Chem, 2021. **296**: p. 100064.
195. Passi, G.R., et al., *An Indian child with Coats plus syndrome due to mutations in STN1.* Am J Med Genet A, 2020. **182**(9): p. 2139-2144.
196. Han, E., et al., *A unique case of coats plus syndrome and dyskeratosis congenita in a patient with CTC1 mutations.* Ophthalmic Genet, 2020. **41**(4): p. 363-367.
197. Gupta, V. and A. Kumar, *Dyskeratosis congenita.* Adv Exp Med Biol, 2010. **685**: p. 215-9.
198. Jia, P., C. Her, and W. Chai, *DNA excision repair at telomeres.* DNA Repair (Amst), 2015. **36**: p. 137-145.
199. Chen, L.Y., J. Majerska, and J. Lingner, *Molecular basis of telomere syndrome caused by CTC1 mutations.* Genes Dev, 2013. **27**(19): p. 2099-108.
200. Wang, Y. and W. Chai, *Pathogenic CTC1 mutations cause global genome instabilities under replication stress.* Nucleic Acids Res, 2018. **46**(8): p. 3981-3992.
201. He, Q., et al., *Structures of the human CST-Polalpha-primase complex bound to telomere templates.* Nature, 2022. **608**(7924): p. 826-832.
202. Mishra, A.K., et al., *Chemical inhibitor targeting the replication protein A-DNA interaction increases the efficacy of Pt-based chemotherapy in lung and ovarian cancer.* Biochem Pharmacol, 2015. **93**(1): p. 25-33.
203. Muoio, D., N. Laspata, and E. Fouquerel, *Functions of ADP-ribose transferases in the maintenance of telomere integrity.* Cell Mol Life Sci, 2022. **79**(4): p. 215.
204. Poltronieri, P., M. Miwa, and M. Masutani, *ADP-Ribosylation as Post-Translational Modification of Proteins: Use of Inhibitors in Cancer Control.* Int J Mol Sci, 2021. **22**(19).

205. Garg, M., et al., *Tpz1TPP1 SUMOylation reveals evolutionary conservation of SUMO-dependent Stn1 telomere association.* EMBO Rep, 2014. **15**(8): p. 871-7.

APPENDIX A

SUPPORTING INFORMATION

The DNA-binding protein CST associates with the cohesin complex and promotes sister chromosome cohesion

P. Logan Schuck[1], Lauren E. Ball[2] and Jason A. Stewart[1]*

From the [1]Department of Biological Sciences, University of South Carolina, Columbia, SC, USA; [2]Department of Cell and Molecular Pharmacology, Medical University of South Carolina, Charleston, SC, USA

*Corresponding author: jason.stewart@sc.edu

Supporting Experimental Procedures

Flow Cytometry

Samples were prepared as previously described (22). Gating and analysis were performed using FlowJo.

Mass spectrometry

Sample preparation: Three replicate affinity-purifications were performed for CST or a negative control for non-specific binding. Eluates were separated by SDS-PAGE, Coomassie stained, and each lane was cut into three bands. Gel pieces were de-stained and proteins were reduced in 10 mM dithiothreitol (Thermo Scientific, Rockford, IL) at 55°C, and alkylated in 25 mM iodoacetamide (Thermo) for 30 minutes at room temperature in the dark. The protein was digested with trypsin (Sigma) (100 ng) overnight at 37°C. Digestion was quenched by the addition of trifluoroacetic acid (TFA) to a final concentration of 1%, and peptides were extracted from the gel and dried.

LC-MS/MS: Peptides were loaded onto a trap column and separated with a 75 µm x 30 cm analytical column (packed in house, C18-Reprosil-AQ Pur RP 1.9 µm particles, Dr. Maisch, GmbH) at 60°C using a gradient from 5% B to 40% B in 180 min (Solvent A: 0.2% formic acid in 2% acetonitrile; Solvent B: 2% formic acid in 98% acetonitrile) on a U3000 nano LC system. The flow rate was 180 nl/min. Mass spectra were acquired on an Orbitrap Elite (Thermo Scientific) in data dependent mode with one FTMS survey scan, mass range of m/z 400-1700 Th, followed by collisional dissociation of the ten most intense ions and detection in the ion trap. The automatic gain control target value was 10^6 ions for the survey MS scan, the resolution was 60,000 at m/z 400 Th. Ions with a +1 charge were excluded from selection. Dynamic exclusion was enabled with a repeat count of 1, duration of 30 sec, exclusion list size of 50, and exclusion duration of 180 sec. Data were only acquired during the gradient omitting the wash and recalibration time. Chromatography mode was enabled with an expected peak width of 30 sec and a minimum threshold of 1000. Three blanks were run between each sample to avoid carry over.

Protein Identification: Data were searched using MaxQuant v.1.6.1.5 against a Human Uniprot protein database including common contaminants. The false discovery rate, determined using a reversed database strategy, was set at 0.01 at the protein and peptide

level. Fully tryptic peptides with a minimum of 7 residues were required including cleavage between lysine and proline. Two missed cleavages and two modifications were permitted. LC-MS/MS analyses were performed in triplicate for each condition and searched together matching between runs with a 0.7 min window. The fast LFQ feature was disabled. The first search was performed with a 25 ppm mass tolerance, after recalibration a 4.5 ppm tolerance was used for the main search. At least two peptides were required for protein quantification with at least one unique peptide. Parameters included static modification of cysteine with carbamidomethyl, variable N-terminal acetylation, and methionine oxidation. Intensity measurements were quantified and normalized by the MaxQuant LFQ algorithm (49).

Data processing: The protein groups text file was processed in Perseus (Version 1.6.2.1) (50) and matches to the reversed database, contaminants, and proteins only identified by modified peptides were removed. Identified proteins were required to have at least two peptides with at least one unique peptide. The normalized LFQ intensities were log2 transformed. The data were filtered to retain proteins quantified in one of the three biological replicates of the experimental immunoprecipitation. Missing values were replaced by random values imputed from a normal distribution using a width of 0.6, downshift of 1.5, and the total matrix of 3 control and 3 experimental immunoprecipitations. The mean log2 protein intensities were compared between the CST IP and control IP using a Student's t-test. Log2 fold changes in protein intensities and the –log10 pval are shown in the volcano plot.

REFERENCES:

22. Ackerson, S.M., Gable, C.I., and Stewart, J.A. (2020) Human CTC1 promotes TopBP1 stability and CHK1 phosphorylation in response to telomere dysfunction and global replication stress. *Cell Cycle* **19**, 3491-3507

49. Cox, J., Hein, M.Y., Luber, C.A., Paron, I., Nagaraj, N., and Mann, M. (2014) Accurate proteome-wide label-free quantification by delayed normalization and maximal peptide ratio extraction, termed MaxLFQ. *Mol Cell Proteomics.* **13**, 2513-26

50. Tyanova, S., Temu, T., Sinitcyn, P., Carlson, A., Hein, M.Y., Geiger, T., Mann, M., and Cox, J. (2016) The Perseus computational platform for comprehensive analysis of (prote)omics data. *Nat Methods.* **13**, 731-40.

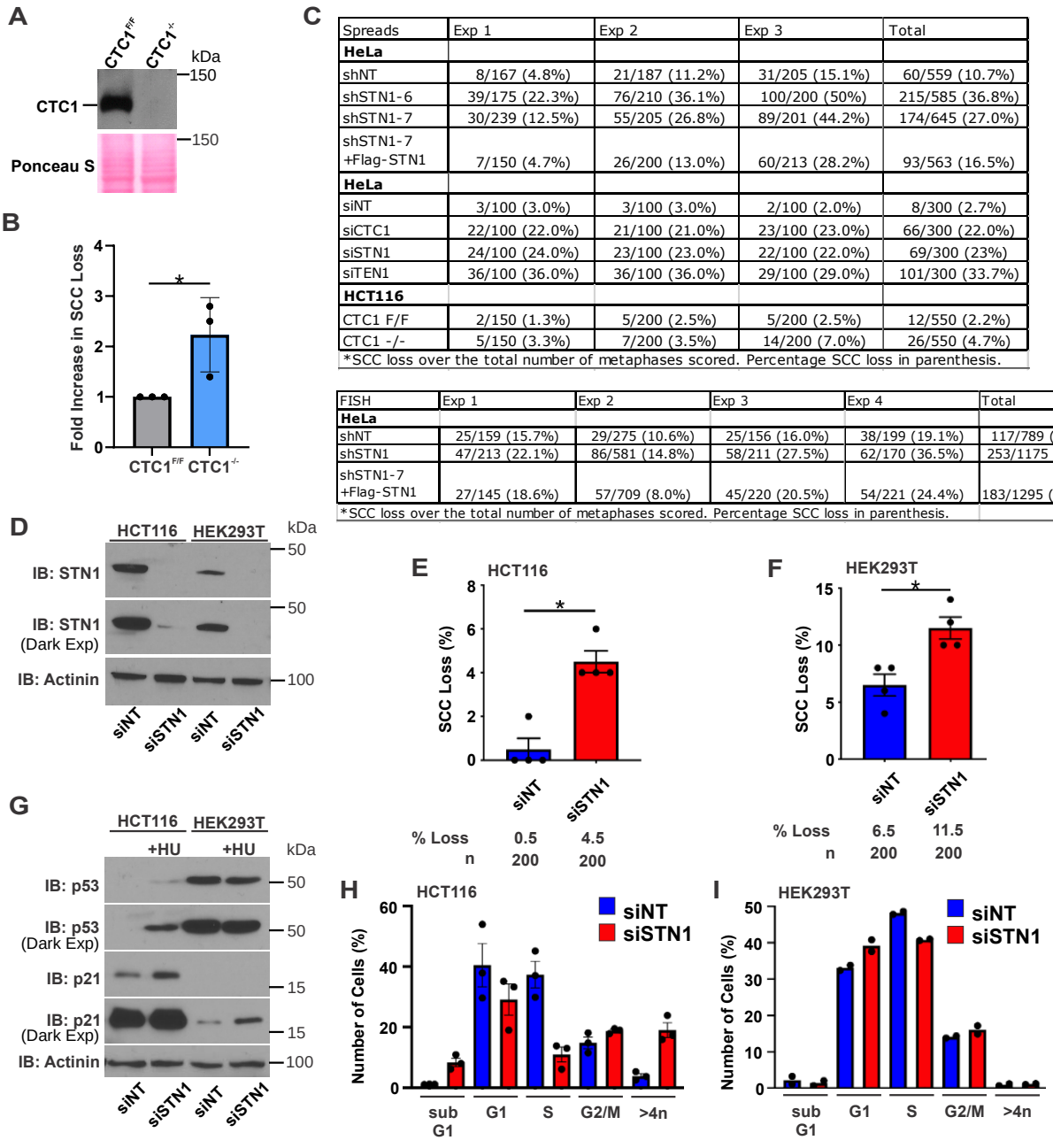

Spreads	Exp 1	Exp 2	Exp 3	Total
HeLa				
shNT	8/167 (4.8%)	21/187 (11.2%)	31/205 (15.1%)	60/559 (10.7%)
shSTN1-6	39/175 (22.3%)	76/210 (36.1%)	100/200 (50%)	215/585 (36.8%)
shSTN1-7	30/239 (12.5%)	55/205 (26.8%)	89/201 (44.2%)	174/645 (27.0%)
shSTN1-7 +Flag-STN1	7/150 (4.7%)	26/200 (13.0%)	60/213 (28.2%)	93/563 (16.5%)
HeLa				
siNT	3/100 (3.0%)	3/100 (3.0%)	2/100 (2.0%)	8/300 (2.7%)
siCTC1	22/100 (22.0%)	21/100 (21.0%)	23/100 (23.0%)	66/300 (22.0%)
siSTN1	24/100 (24.0%)	23/100 (23.0%)	22/100 (22.0%)	69/300 (23%)
siTEN1	36/100 (36.0%)	36/100 (36.0%)	29/100 (29.0%)	101/300 (33.7%)
HCT116				
CTC1 F/F	2/150 (1.3%)	5/200 (2.5%)	5/200 (2.5%)	12/550 (2.2%)
CTC1 -/-	5/150 (3.3%)	7/200 (3.5%)	14/200 (7.0%)	26/550 (4.7%)

*SCC loss over the total number of metaphases scored. Percentage SCC loss in parenthesis.

FISH	Exp 1	Exp 2	Exp 3	Exp 4	Total
HeLa					
shNT	25/159 (15.7%)	29/275 (10.6%)	25/156 (16.0%)	38/199 (19.1%)	117/789 (14.8%)
shSTN1	47/213 (22.1%)	86/581 (14.8%)	58/211 (27.5%)	62/170 (36.5%)	253/1175 (21.5%)
shSTN1-7 +Flag-STN1	27/145 (18.6%)	57/709 (8.0%)	45/220 (20.5%)	54/221 (24.4%)	183/1295 (14.1%)

*SCC loss over the total number of metaphases scored. Percentage SCC loss in parenthesis.

J

	Exp 1	Exp 2	Exp 3	Exp 4	Total
HCT116					
siNT	1/50 (2%)	0/50 (0%)	0/50 (0%)	0/50 (0%)	1/200 (0.5%)
siSTN1	2/50 (4%)	3/50 (6%)	2/50 (4%)	2/50 (4%)	9/200 (4.5%)
HEK 293T					
siNT	2/50 (4%)	4/50 (8%)	3/50 (6%)	4/50 (8%)	13/200 (6.5%)
siSTN1	5/50 (10%)	7/50 (14%)	6/50 (12%)	5/50 (10%)	23/200 (11.5%)

*SCC loss over the total number of metaphases scored. Percentage SCC loss in parenthesis.

Figure A.1. Supporting information related to Figure 1. (A) Western blot of CTC1 in HCT116 cells. Conditional gene disruption of CTC1$^{F/F}$ was induced by the addition of

tamoxifen (TAM) to initiate Cre-induced gene disruption ($CTC1^{-/-}$). Ponceau S: loading control. (B) Metaphase spread analysis of SCC loss in HCT116 cells, as indicated. Samples were collected on day 15 after TAM addition. Replicates were standardized to $CTC1^{F/F}$ cells. (*P < 0.05). (C) Raw numbers and percentages of SCC loss from individual trials in Fig. 1 and S1B. Spreads refers to metaphase spread analysis in Fig. 1C, 1G and S1B, as indicated. FISH refers to analysis of the chromosome specific FISH experiments in Fig. 1E. (D) Western blot of STN1 knockdown by siRNA in HCT116 or HEK293T cells. siNT: non-target control, Actinin: loading control. (E-F) Percent of cohesion loss in HCT116 (E) or HEK293T (F) cells following metaphase spread analysis, as indicated. n=4 independent, biological replicates. (G) Western blot of p53 and p21 levels. +HU: 2mM HU treatment for 24 h. Dark Exp: extended exposure time. Actinin: loading control. (H-I) Percentage of cells in different phases of the cell cycle in HCT116 (H) or HEK293T cells (I) cells. (J) Raw numbers and percentages of SCC loss from individual trials in Fig. S1E-F. (*P < 0.05)

A mber of Peptides

	Trial 1		Trial 2		Trial 3	
	Mock	CST IP	Mock	CST IP	Mock	CST IP
STN1	14	446	1	738	12	629
CTC1	1	30	0	41	1	47
TEN1	0	3	0	4	0	4
POLA1	3	19	1	23	0	22
POLA2	0	12	0	25	0	22
PRIM1	0	7	0	4	0	9
SMC1A	0	5	0	2	1	3
SMC3	0	3	1	3	1	3

B

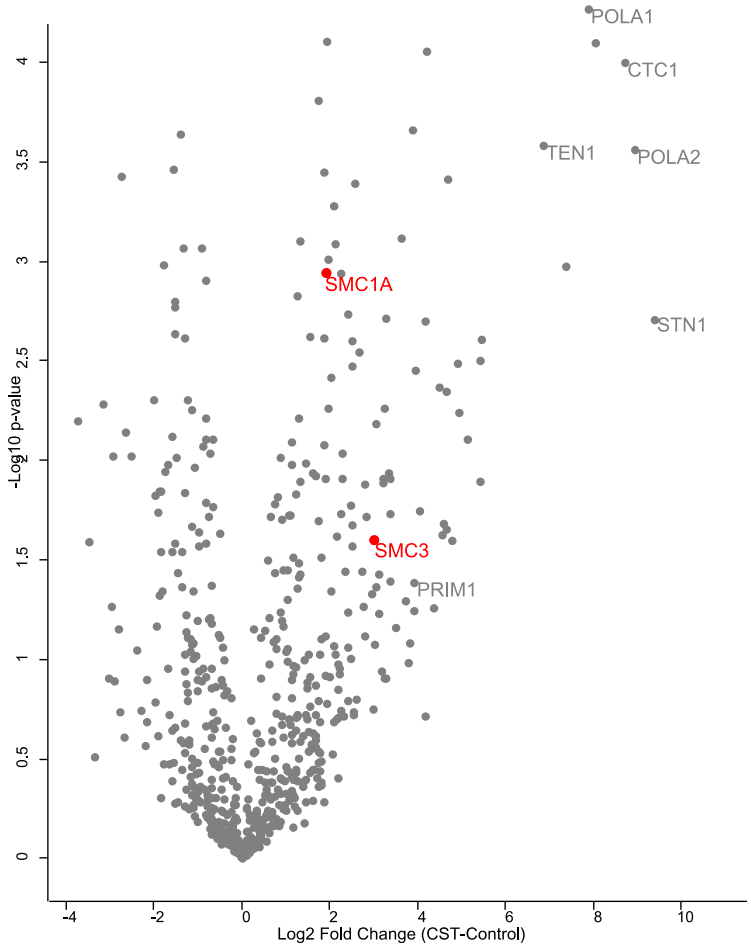

Figure A.2. CST interacts with the cohesin complex. (A) Total number of peptides identified in three independent replicates of mass spectrometry to identify CST interacting partners. All three CST subunits were overexpressed in HEK 293T cells.

Flag-tagged STN1 was pulled down and samples sent for analysis by mass spectrometry. (B) Volcano plot showing the log2 fold changes in protein intensity from CST immunoprecipitation as compared to control versus the log10 Student's t-test p value.

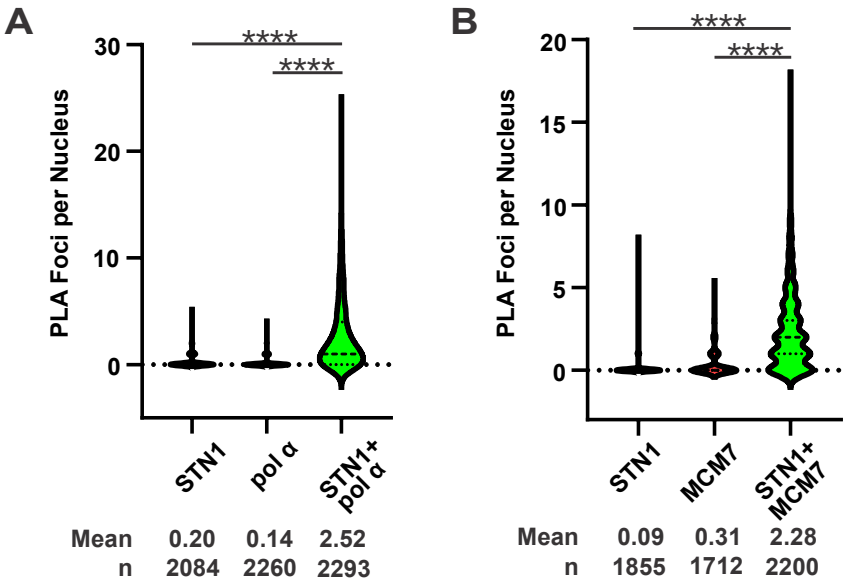

Figure A.3. PLA demonstrating STN1 interaction with pol α and MCM2-7. (A) Proximity ligation assay (PLA) performed in HeLa cells with antibodies to STN1, the pol α subunit PolA1 or in combination (STN1+ pol α). (B) PLA was performed in HeLa cells as in (A) with antibodies to STN1 and MCM7 (STN1+MCM7). Violin plots of PLA foci per nucleus. Results for (A) and (B) are representative of two independent, biological experiments. Bold dashed line: median, dashed lines: first and third quartiles. (****P < 0.0001).

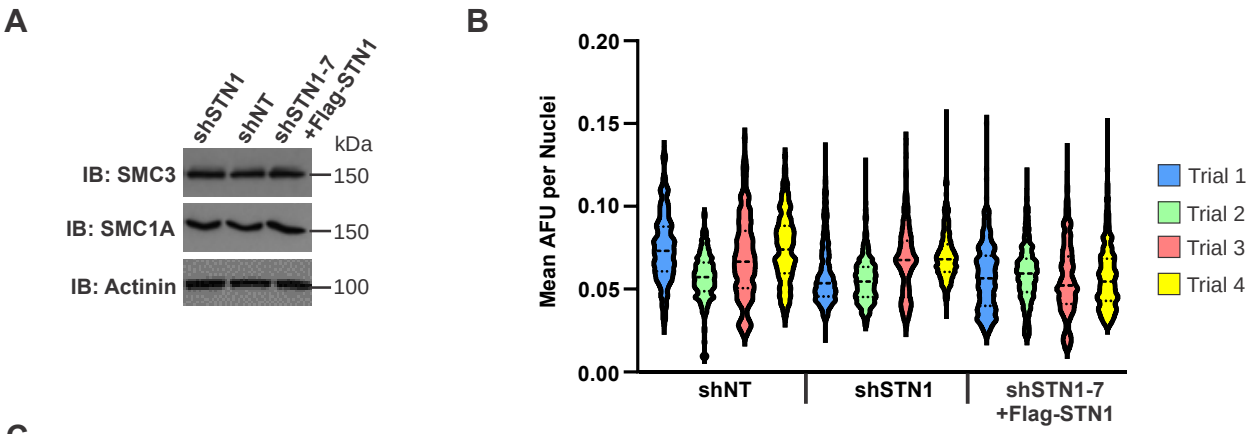

C

Prophase to Metaphase

	Trial 1	Trial 2	Trial 3	Average	SD
shSTN1	0:17:12	0:18:24	0:23:54	0:19:50	0:03:34
shNT	0:19:15	0:17:48	0:30:40	0:22:34	0:07:03
Res	0:14:46	0:16:34	0:24:53	0:18:44	0:05:24

Metaphase to Cytokinesis

	Trial 1	Trial 2	Trial 3	Average	SD
shSTN1	0:42:39	0:42:59	0:33:34	0:39:44	0:05:21
shNT	0:34:28	0:39:24	0:40:30	0:38:07	0:03:13
Res	0:38:22	0:46:58	0:39:45	0:41:42	0:04:37

Figure A.4. CST deficiency does not affect cohesin levels or mitotic timing. (A) Western blot analysis of total cohesin levels in HeLa shSTN1 knockdown cells using whole cell extracts. Actinin serves as a loading control. (B) Nuclear SMC3 immunofluorescence intensity was measured in 4 independent trials (see Fig 3B). Violin plots of each trial, which shows no significant changes in SMC3 levels in shSTN1 cells versus controls. (C) Top, time between nuclear envelope breakdown to metaphase plate formation was measured in HeLa shSTN1 cells expressing H2B-RFP (see Fig 3D). Bottom, time between metaphase plate formation to cytokinesis was measured for each mitotic cell. n=3 independent biological experiments. SD: standard deviation. Time represented in hours: minutes: seconds.

	Exp 1	Exp 2	Exp 3	Exp 4	Total
HeLa					
shNT	2/50 (4%)	0/50 (0%)	1/50 (2%)	1/50 (2%)	4/200 (2%)
shSTN1	4/50 (8%)	3/50 (6%)	4/50 (8%)	4/50 (8%)	15/200 (7.5%)
shNT +HU	2/50 (4%)	2/50 (4%)	1/50 (2%)	3/50 (6%)	8/200 (4%)
shSTN1 +HU	5/50 (10%)	7/50 (14%)	5/50 (10%)	6/50 (12%)	23/200 (11.5%)
shNT +APH	4/50 (8%)	4/50 (8%)	1/50 (2%)	1/50 (2%)	10/200 (5%)
shSTN1 +APH	7/50 (14%)	6/50 (12%)	5/50 (10%)	4/50 (8%)	22/200 (11%)
shNT +CPT	12/50 (24%)	5/50 (10%)		6/50 (12%)	23/150 (11.5%)
shSTN1 +CPT	21/50 (42%)	25/50 (50%)	19/50 (38%)	24/50 (48%)	89/200 (44.5%)

Figure A.5. Supporting information for Figure 4B. Raw numbers and percentages of SCC loss from individual trials. Exp 3 shNT +CPT was not included due to technical issues that led to low cells counts and an insufficient numbers of metaphase spreads for analysis.